



**institute of  
telecommunications**

## **DISSERTATION**

# **System Level Investigations for Mobile and Indoor Users in Future Cellular Networks**

**ausgeführt zum Zwecke der Erlangung des akademischen Grades  
eines Doktors der technischen Wissenschaften**

**Dipl.-Ing. Martin Klaus Müller**

geboren am 23. März 1986

Matrikelnummer: 1026943

**Juli 2018**

eingereicht an der Technischen Universität Wien  
Fakultät für Elektrotechnik und Informationstechnik



**Betreuer:**

**Univ. Prof. Dr.-Ing. Markus Rupp**

Institute of Telecommunications  
Technische Universität Wien  
Österreich

**Begutachter:**

**Ph.D., H.D.R., Marco Di Renzo**

Signals & Systems Laboratory  
Paris-Saclay University  
France

**Prof. Dr. Luis Castedo Ribas**

Department of Computer Engineering  
University of A Coruña  
Spain





## Abstract

Operators of cellular networks are hard pressed to provide a seamless wireless connection to their users. Due to the expanded demand not only for coverage but also for increased network capacity, the network architecture needs to be adapted and evolve beyond the classical hexagonal grid. The globally ongoing trend of urbanization leads to more and more users utilizing their wireless devices indoors or in mobile scenarios, when commuting or traveling. These scenarios pose particular challenges to implementing a suitable network in terms of propagation conditions as well as optimal base station (BS) deployment. Therefore, in this thesis, I investigate the potential network-wide average performance of wireless cellular networks particularly in high speed train (HST) environments, as well as of network deployments indoors.

An investigation on network scale requires to limit the complexity of the applied system models. This is necessary in order to still obtain mathematically tractable formulations as well as to be able to perform simulations with finite duration. Since the scenarios under investigation are in themselves rather specific and also in comparison fundamentally different for some aspects, I first introduce available models for signal propagation and interferer geometry. I then justify the chosen models and introduce the different approaches for evaluating performance metrics in both scenarios.

Wireless cellular networks in HST scenarios exhibit several specific aspects of technical and non-technical nature that need to be taken into account in the system design. Especially the decision between direct communication or relay aided communication has to be made. To justify the utilization of system level (SL) simulations, that include various abstractions, throughput results are compared to more detailed link level (LL) simulations, parameterizing both simulations with reference values from real-world measurements. Additionally, I present a framework for investigating the performance improvement of remote unit collaboration schemes.

Signal propagation in indoor scenarios is dominated by wall blockages. Initial investigations focus on the influence of the distribution of blockage objects. Therefore, four different wall generation methods are introduced, which are parametrized such that the created spatial scenarios remain comparable. Based on these methods, expressions for the average attenuation of a link and for the signal to interference ratio (SIR) are derived. Subsequently, the effect of the BS placement is considered, by placing BSs randomly or by arranging them in a regular grid. Here, additionally the area spectral efficiency (ASE) is utilized to identify the dependency of the network capacity on the BS density.

---

## Kurzfassung

Betreiber zellulärer Netze stehen unter großem Druck ihren Nutzern eine störungsfreie drahtlose Verbindung zur Verfügung zu stellen. Aufgrund des erhöhten Bedarfs, nicht nur für Abdeckung sondern auch für eine erhöhte Netzkapazität, muss die Netzarchitektur angepasst werden und über das klassische hexagonale Grid hinaus verbessert werden. Der weltweit stattfindende Trend der Urbanisierung führt dazu, dass mehr und mehr Nutzer ihre drahtlosen Endgeräte in Gebäuden oder in mobilen Szenarien, wenn sie reisen oder pendeln, benutzen. Diese Szenarien stellen besondere Anforderungen an die Realisierung eines passenden Netzes sowohl im Bezug auf Ausbreitungsbedingungen als auch auf optimale Basisstationsplatzierung dar. Deshalb untersuche ich in meiner Dissertation die potentielle netzweite Durchschnittsperformanz von drahtlosen, zellulären Netzen insbesondere im Hochgeschwindigkeitszug (HGZ) Umfeld als auch von Netzinstallationen innerhalb von Gebäuden.

Eine Untersuchung auf Netzebene verlangt die Komplexität des verwendeten Systemmodells zu beschränken. Dies ist notwendig sowohl um noch mathematisch lösbare Formulierungen zu erhalten als auch um Simulationen in endlicher Dauer durchführen zu können. Da die untersuchten Szenarien an sich recht spezifisch sind und sich auch im Vergleich zueinander in einigen Aspekten fundamental unterscheiden, erläutere ich zuerst verfügbare Signalausbreitungsmodelle und Modelle für Interferer Geometrie. Ich rechtfertige dann die gewählten Modelle und stelle die verschiedenen Ansätze zur Auswertung der Leistungsmetriken in beiden Szenarien vor.

Drahtlose zelluläre Netze in HGZ Szenarien weisen mehrere spezifische Aspekte technischer und nicht-technischer Natur auf, die beim Systementwurf in Betracht gezogen werden müssen. Insbesondere die Entscheidung zwischen direkter oder Relay unterstützter Kommunikation muss getroffen werden. Um die Verwendung von Simulationen auf „System Level“ zu rechtfertigen, die unterschiedliche Abstraktionen beinhalten, werden Durchsatzergebnisse mit detaillierteren „Link Level“ Simulationen verglichen, wobei beide Simulationen mit Referenzwerten von realen Messdaten parametrisiert werden. Zusätzlich präsentiere ich ein Framework zur Untersuchung der Leistungsverbesserung durch die Zusammenarbeit von abgesetzten Übertragungseinheiten.

Signalausbreitung innerhalb von Gebäuden wird durch die Blockierung durch Wänden dominiert. Erste Untersuchungen sind auf den Einfluss der Verteilung solcher blockierender Objekte fokussiert. Hierfür werden vier unterschiedliche Wandgenerierungsmethoden eingeführt, die so parametrisiert sind, dass die erzeugten räumlichen Szenarien vergleichbar bleiben. Basierend auf diesen Methoden werden Ausdrücke für die durchschnittliche Dämpfung eines Verbindungspfades und für das Signal-zu-Interferenz Verhältnis hergeleitet. Nachfolgend wird der Einfluss der Basisstationsplatzierung betrachtet, indem Basisstationen zufällig oder in einem regulären Grid angeordnet werden. Hier wird zusätzlich die räumliche spektrale Effizienz verwendet um die Abhängigkeit der Netzkapazität von der Basisstationsdichte zu identifizieren.

---

## Acknowledgements

My first words of gratitude extend to Prof. Markus Rupp. Under his guidance, and by sharing his knowledge and expertise, I was able to pursue my research with the necessary freedom but also with the certainty of being on the right path.

Next, I want to thank Dr. Marco Di Renzo, who agreed to review my thesis, and who gave many inspiring talks in the context of stochastic geometry in wireless networks that I was fortunate to attend.

Similarly, I want to thank Prof. Luis Castedo, who also agreed to review my thesis, and furthermore welcomed me with the greatest hospitality at his institute in A Coruña during my stay there. In this context I also want to thank José García-Naya and Tomás Domínguez-Bolaño, with whom I had a productive collaboration and many interesting exchanges of ideas.

I especially value the support and input from our Institute's industry partners, who gave practical relevance to sometimes rather theoretical research questions. Special thanks go to Waltraud Müllner, Georg Schell and Gerd Saala.

During my time at the Institute of Telecommunications, I was surrounded by a great team of students and researchers and I consider myself grateful that I could share my time with them. There are too many names to mention, but I want to specifically thank Martin Taranetz, who sparked many ideas and contributed immensely to my work. The same goes for Stefan Schwarz, who was always up for discussing even the slightest detail. With Martin Mayer and Fjolla Ademaj I shared the pleasure to assist for a lecture and we spent many hours preparing and correcting together. Furthermore, I want to thank Gabor Hannak and Osman Musa for their company, and in particular Michael Meidlinger, whose friendship I value dearly.

Through the continuous support and encouragement of my friends and through countless hours spent together, they provided the much needed balance outside of work. In particular I want to thank Geetha, Marta, Jovan, Sina and Nikola and the FFB crew for allowing me to lean on them whenever necessary.

Abschließend möchte ich mich von ganzem Herzen bei meinem Bruder und bei meinen Eltern bedanken, die mich immer bedingungslos unterstützt haben und mir die Gewissheit gegeben haben, immer auf sie bauen zu können.

---

# Contents

<b>1. Introduction</b>	<b>1</b>
1.1. Motivation and Scope of this Thesis . . . . .	1
1.2. Outline and Contributions . . . . .	4
1.3. Notation . . . . .	7
<b>2. Preliminaries</b>	<b>9</b>
2.1. Aggregate Interference Evaluation . . . . .	9
2.2. Propagation Effects . . . . .	10
2.3. Propagation Models . . . . .	11
2.3.1. Small Scale Models . . . . .	12
2.3.2. Classic Large Scale Models . . . . .	13
2.3.3. Stochastic Blockage Models . . . . .	13
2.4. Interference Geometry . . . . .	14
2.4.1. Deterministic Node Locations . . . . .	15
2.4.2. Stochastic Node Locations . . . . .	16
2.5. Base Station Types . . . . .	17
<b>3. Context and Methodology</b>	<b>19</b>
3.1. Scenario Context . . . . .	19
3.2. Performance Evaluation Methods . . . . .	20
3.3. Comparison of Approaches for Train and Indoor Scenarios . . . . .	20
<b>4. Performance Evaluation in High Speed Train Scenarios</b>	<b>23</b>
4.1. Design Aspects for Supplying Wireless Connections in High Speed Train Scenarios	24
4.1.1. Particularities of High Speed Train Scenarios . . . . .	24
4.1.2. Advantages of Remote Radio Units . . . . .	26
4.1.3. Comparison of Relay and Direct Link Approach . . . . .	27
4.1.4. Further Technical Aspects and Operator View . . . . .	31
4.2. Parameter Calibration of Simulations through Channel Measurements . . . . .	33
4.2.1. Measurement Environment and Procedure . . . . .	33
4.2.2. Necessary Adaptations of the Simulator . . . . .	35
4.2.3. Comparison of Results . . . . .	36

4.3.	Performance Improvement of Remote Unit Collaboration Schemes . . . . .	43
4.3.1.	System Model . . . . .	43
4.3.2.	Theoretical Model for SIR Calculation . . . . .	44
4.3.3.	Simulation Results and Necessary Approximations . . . . .	47
4.3.4.	Simulation Results for Relay and Direct Link Setup . . . . .	52
4.4.	Summary . . . . .	53
<b>5.</b>	<b>Performance Evaluation of Indoor Cellular Networks</b>	<b>55</b>
5.1.	Introduction . . . . .	56
5.2.	Impact of Wall Generation Methods on Indoor Network Performance . . . . .	56
5.2.1.	System Model . . . . .	56
5.2.2.	Wall Generation Methods . . . . .	59
5.2.3.	Comparability of Scenarios in Terms of Wall Volume . . . . .	61
5.2.4.	Average Number of Wall Blockages . . . . .	63
5.2.5.	Performance Evaluation . . . . .	66
5.2.6.	SIR Approximations by Utilizing the Average Wall Attenuation . . . . .	69
5.2.7.	Numerical Evaluation . . . . .	72
5.3.	Sector Size and Area Spectral Efficiency . . . . .	80
5.3.1.	System Model Adaptations . . . . .	81
5.3.2.	Analytical Description . . . . .	82
5.3.3.	Results for Coverage Probability and Area Spectral Efficiency . . . . .	86
5.3.4.	Discussion of Results . . . . .	88
5.4.	Summary . . . . .	89
<b>6.</b>	<b>Conclusions</b>	<b>93</b>
6.1.	Summary of Contributions . . . . .	93
6.2.	Open Issues for Future Research . . . . .	95
<b>A.</b>	<b>List of Abbreviations</b>	<b>97</b>
	<b>Bibliography</b>	<b>99</b>



# Chapter 1.

## Introduction

### 1.1. Motivation and Scope of this Thesis

Since the first definition of mobile cellular network standards, the technical capabilities and the available services of said networks, but also the demands of the mobile users have evolved drastically. While analog first generation (1G) and digital second generation (2G) cellular networks were designed for voice transmissions, the following third generation (3G) and fourth generation (4G) networks shifted the focus to data transmission with increasing high data rates. Alongside with the improving network proficiency also the network architectures changed significantly, also due to growing subscriber numbers as well as demanding services and increased expectations of customers.

Classical network deployments following a hexagonal grid (cf. [39]), are mostly designed for coverage and can satisfy the needs of customers with moderate service demands. The trend of improved network capacity goes hand in hand with intensified usage behavior (users that are "always online") and the development of applications and services with ever increasing data rate demand. Thus, in 4G wireless networks, represented by the Long Term Evolution (LTE) and the LTE advanced (LTE-A) standard [5] of the Third Generation Partnership Project (3GPP), the concept of heterogeneous networks (HetNets) [41, 66] emerged. Following the aforementioned trends, HetNet deployments do not only provide coverage, but also adhere to the increased data rate demand by utilizing appropriate base station (BS) types, such as pico or femto cells [11].

Nevertheless, it is by far not only classical outdoor users that demand a reliable supply of broadband wireless access. Due to the worldwide ongoing trend of urbanization [23] and the increased mobility of users, e.g., commuting to and from work [81], indoor and mobile scenarios will be the predominant environment of users in future networks. Therefore, wireless network providers have to adapt their network design to fit the characteristics of these specific environments that exhibit unique features for signal propagation and user behavior.

In order to better understand these scenarios, I investigate the performance of wireless networks for high speed trains (HSTs) (exemplary for mobile users) as well as indoor deployments in my thesis.

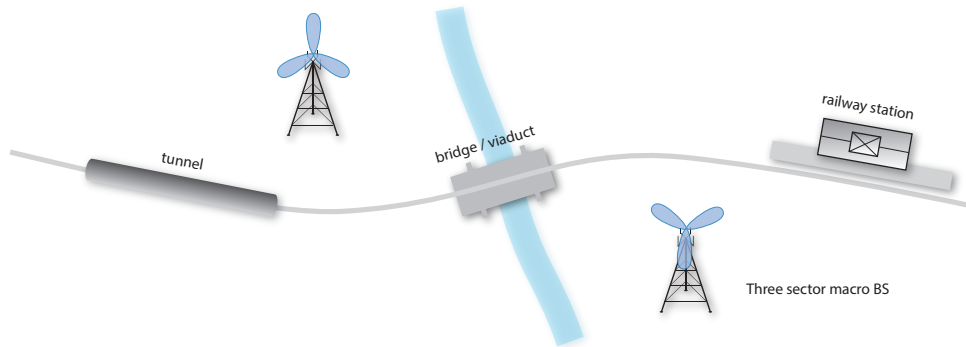


**Figure 1.1.:** Diverse environment along a railroad track. Wireless access is supplied by macroscopic BSs, which makes a connection in tunnels or railway stations problematic.

## Performance Investigation for High Speed Train Scenarios

Wireless communications standards have been utilized in HST train scenarios as a derivation of the Global System for Mobile Communications (GSM) standard, namely GSM - Rail(way) (GSM-R) [92]. There also exist initiatives to define an equivalent LTE for Railway (LTE-R) standard [49, 90]. This however is intended purely for the task of conveying train control information, not for providing a wireless connection to passengers. Doing so is a more demanding task, since not necessarily dedicated antennas on the carriage are available. Additionally, the sum capacity, that is demanded by the passengers can be substantial. The aforementioned “always online” attitude of users also means for railway operators, that a wireless connection has to be provided to their passengers on board, not the least in order to increase the attractiveness compared to competitors or other means of transportation.

HST scenarios exhibit particularities that result in potential complications for wireless networks. Next to the large user density (confined within the train carriage) that travel at high speed, also the diverse environment poses a challenge (cf. Fig. 1.1). Especially tunnels and viaducts require special consideration [8, 43, 50]. Due to these scenario particularities, a promising solution is dedicated hardware in form of remote radio units (RRUs) along the tracks, potentially connected via fiber to a common BS, which alleviates the problem of frequent handovers and large distances from the tracks, when macro BSs are used. Another important network design decision results from the high penetration loss of the signal through the metal chassis or (usually metal coated) windows. The opposing approaches are either a direct communication between a BS and the passengers (and thus having to deal with the penetration loss), or to install relays on the train carriages [19], which comes with increased delays and also legal issues when crossing national borders.

In my thesis, I thus focus on these scenario particularities and take the specific propagation conditions and user and BS positioning into account in order to highlight critical aspects and predict the performance for cellular networks in HST environments.

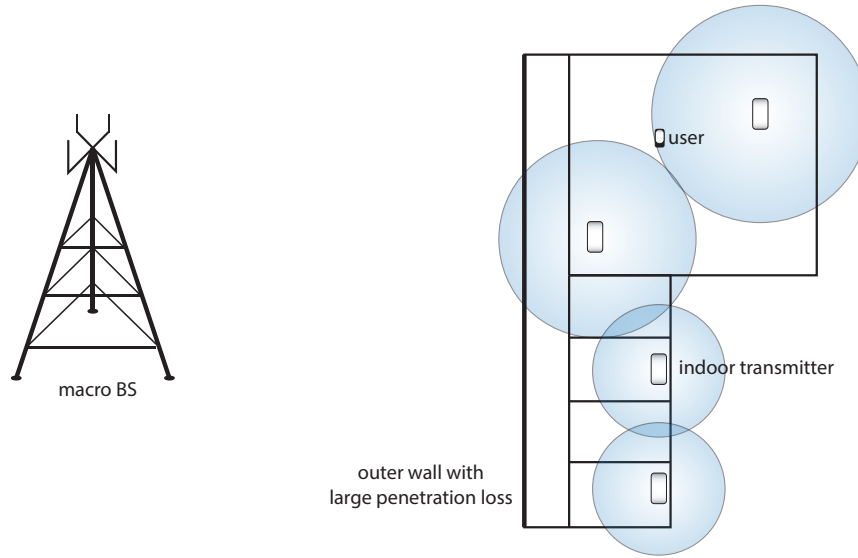


**Figure 1.2.:** Example of a wireless indoor network. Supplying coverage with a macro BS from outside is problematic due to the large penetration loss of outer walls and difficult penetration deeper into the building.

## Performance Investigation for Indoor Scenarios

As mentioned before, more and more users of mobile networks are located *indoors*. Providing coverage to such users from outside with macro BSs comes with the disadvantage of relatively large penetration losses stemming from outer walls and windows [27]. This becomes even more severe when users are located further inside of the building (cf. Fig. 1.2). Additionally, the aforementioned trend of urbanization, with up to 80 % of global data traffic generated and consumed indoors [55], more capacity is necessary than it can be provided by a macro BSs from the outside. To overcome these issues, distributed antenna systems (DASs) are promoted to be used in indoor scenarios [78].

Also for such systems, the propagation conditions are still dominated by the indoor walls that introduce reflections as well as penetration losses among other effects. The placement of indoor BSs (of whichever form - pico cells or RRUs) thus has to be adapted to the given wall configuration. The room layout can vary greatly, when, e.g., comparing a shopping mall or an office building. Furthermore, due to moving users<sup>1</sup>, the user concentration will shift its location during the day. This makes a flexibly configurable system necessary, as it is provided by, e.g., [57].

Most investigations on indoor wireless networks are performed via measurements or focus on the individual link quality [29], as well as investigating floors with explicit wall configurations [89], which however does not provide insights in terms of average network performance. Thus, I focus on system level investigations of said networks in my thesis.

<sup>1</sup>Mind that it is not a "mobile" scenario w.r.t. network time scales, but rather a "quasi-static" scenario.

## 1.2. Outline and Contributions

### Chapter 2: Preliminaries

In Chapter 2, I provide an overview on aggregate interference evaluation techniques as a basis for performance evaluation on network scale. Therefore, I discuss the basic propagation effects and resulting abstractions in form of propagation models as one of the main interference shaping factors. The other aspect is given by the interference geometry for which I discuss modeling options and concepts, especially from stochastic geometry. In the last part of the chapter I discuss different BS types that are prevalent in different environments. Major parts of this chapter were published in the following co-authored survey:

- [i] M. Taranetz and M. K. Müller, “A survey on modeling interference and blockage in urban heterogeneous cellular networks”, *EURASIP Journal on Wireless Communications and Networking*, vol. 2016, no. 1, pp. 1–20, Oct. 2016

### Chapter 3: Context and Methodology

The following Chapter 3 defines the scenario context, namely indoor and HST environments under the general assumption of utilization of the LTE-A standard and the resulting implications for my investigations.

Furthermore, I introduce here the performance evaluation methods that are applicable for these two scenarios under investigation, especially in order to obtain average performance results for a complete network. I compare my chosen approach of system level (SL) considerations to other available techniques and discuss how performance results can be obtained subsequently.

Finally, I discuss how the aforementioned propagation and interference geometry models fit to the environment specifics and highlight important aspects to consider in modeling HST and indoor scenarios.

### Chapter 4: Performance Evaluation of High Speed Train Scenarios

In Chapter 4, I present my results obtained for HST scenarios. In the first part of the chapter, I discuss in detail various design aspects of cellular networks in combination with HSTs and especially focus on the comparison of direct passenger-BS communication with relay aided communication, as well as suggestions on how to combat scenario specific issues, such as frequent handovers. Also aspects that are not of pure technical nature are discussed, such as economical and legal considerations of network and railways operators.

The next part of this chapter constitutes a comparison of throughput results based on measurements, which constitutes of results obtained by detailed link level (LL) simulations versus results obtained by SL simulations that require substantial approximations. This has the purpose of verifying the applicability of SL simulations for HST scenarios and to demonstrate that the introduced abstractions still lead to reliable performance estimations. Additionally, I discuss further aspects that could not easily be introduced in the LL simulations, but are available through SL simulations, due to the considerably lower computational complexity.

Performance improvements of remote unit collaboration schemes are discussed in the last part of this chapter. For a generic setup with RRUs placed alongside the tracks I discuss three schemes, namely a baseline scheme with no collaboration, a cooperation scheme, where the second-closest RRU does not transmit in order to avoid unnecessary interference, and a cooperation scheme, where the two closest RRUs are connected to form a common sector. Results are obtained by an analytical model based on maximum ratio transmission (MRT) and Gamma fading and by SL simulations from the Vienna LTE-A SL Simulator [77]. Necessary approximations to account for the discrepancy between MRT and codebook based precoding (CBP) (which is applied in the simulator) are also included in the analytical model. Finally, I provide simulation results for the comparison of direct and relay-aided communication to show the influence of the penetration loss as well as the scheduling gain.

The contributions of this chapter are published in the following papers<sup>2</sup>:

- [ii] M. K. Müller, S. Schwarz, and M. Rupp, “QoS investigation of proportional fair scheduling in LTE networks”, in *Proc. of the Wireless Days Conference*, Valencia, Spain, Nov. 2013
- [iii] M. K. Müller, M. Taranetz, and M. Rupp, “Performance of remote unit collaboration schemes in high speed train scenarios”, in *Proc. of the 82nd Vehicular Technology Conference (VTC2015-Fall)*, Boston, US, Sep. 2015
- [iv] M. K. Müller, M. Taranetz, and M. Rupp, “Providing current and future cellular services to high speed trains”, *IEEE Communications Magazine*, Oct. 2015

## Chapter 5: Performance Evaluation of Indoor Cellular Networks

Chapter 5 deals with the performance evaluation in indoor environments. I discuss the influence of wall generation methods and therefore establish conditions for comparability among different generation methods with according parameter sets. I introduce three mathematically tractable methods, that vary in randomness of their geometric wall placement strategy. Additionally, I consider a generic floor plan generator, as a more realistic reference for my analytical methods. For the mathematically tractable approaches, I derive the average number of walls blocking a link as well as expressions for the signal to interference ratio (SIR) performance. Due to the complexity of

---

<sup>2</sup>The results for the comparison of LL and SL simulations were obtained during my research stay at the Department of Computer Engineering (GTEC) at the University of A Coruña and are so far unpublished.

the mathematical expressions, I first introduce simplifying assumptions and then take measures for increasing the accuracy of these approximations. In terms of BS placement, I consider a regular grid and compare results for different BS grid orientations and different number of BS tiers. For the resulting parameter combinations I provide analytical results (where available) along with SL results based on Monte-Carlo simulations. The resulting average values are obtained from temporal and spatial realizations.

The second set of results then revolves around the comparison of random and regular BS placement and their influence on the coverage probability and the area spectral efficiency (ASE) performance. Following the pioneering results in [12], I derive expressions for the aforementioned metrics while including wall blockages in the system model. I specifically address the influence of the individual wall penetration value as well as the average sector size. The ASE is chosen as metric, since it reflects the available network capacity and thus indicates how many users can be served by a given network and BS density.

The contributions in this chapter are published in the following papers:

- [v] M. K. Müller, M. Taranetz, and M. Rupp, “Effects of wall-angle distributions in indoor wireless communications”, in *IEEE 17th International Workshop on Signal Processing Advances in Wireless Communications (SPAWC 2016)*, Jul. 2016, pp. 1–5
- [vi] M. K. Müller, M. Taranetz, V. Stoyanov, and M. Rupp, “Abstracting indoor signal propagations: Stochastic vs. regular”, in *International Symposium ELMAR 2016*, Sep. 2016, pp. 249–252
- [vii] M. K. Müller, M. Taranetz, and M. Rupp, “Analyzing wireless indoor communications by blockage models”, *IEEE Access*, vol. 5, pp. 2172–2186, Dec. 2016
- [viii] M. K. Müller, S. Schwarz, and M. Rupp, “Investigation of area spectral efficiency in indoor wireless communications by blockage models”, in *Workshop on Spatial Stochastic Models for Wireless Networks (SpaSWiN)*, May 2018, pp. 1–6

## 1.3. Notation

The following notation is used throughout this dissertation:

---

$f_X(\cdot)$	Probability density function of $X$
$\mathbb{E}[X]$	Expected value of $X$
$\bar{x}$	Empirical mean of $x$
$\mathbb{P}[\cdot]$	Probability
$\mathcal{U}[x, y]$	Uniform distribution with support $[x, y]$
$\exp(\mu)$	Exponential distribution with mean $\mu$
$\delta(x)$	Dirac delta distribution
$\Gamma(k, \theta)$	Gamma distribution with shape $k$ and scale $\theta$
$\mathcal{L}_X(s)$	Laplace transform of $X$ evaluated at $s$
$\text{mod}(\cdot, \cdot)$	Modulo operator
$\lfloor \cdot \rfloor$	Floor operator

---





## Chapter 2.

### Preliminaries

While the propagation of an electromagnetic signal from a transmitter to a receiver can in theory be exactly evaluated by determining Maxwell's equations, it is a task way too complex to solve for a large scale propagation environment. Thus, the occurring propagation effects are usually described by models with varying degrees of abstraction. Applying these models then allows to assess, e.g., the received signal strength without the necessity for an infinitely accurate description of the environment. When considering the link from the desired transmitter as well as links from interfering transmitters, the signal to interference ratio (SIR) can be utilized as metric for describing the performance of mobile networks. These aspects, including path loss modeling, interference geometry, as well as the influence of different base station (BS) types, are discussed in this chapter. A more exhaustive survey of this matter can be found in [87].

#### 2.1. Aggregate Interference Evaluation

The signal at the receiver is usually comprised of a desired signal (attenuated and distorted on the transmission path), interference from other transmitters that utilize the same frequency band, as well as noise. When considering larger networks and when the impact of the network geometry is of interest, the noise is modeled rather coarsely through a noise power spectral density (given in [Watt/Hz]) and sometimes a receiver noise figure. This results in a specific average noise power for a given transmission bandwidth. In the presence of many interferers with considerable interference power at the receiver, the influence of the noise becomes negligible. Such networks are called *interference limited*. This is mostly true for currently deployed Long Term Evolution (LTE) networks.

The interference can be categorized as *own-cell interference*, comprised of, e.g., inter-carrier, inter-symbol or inter-layer interference, and as *aggregate co-channel interference* which stems from other cells in the same network. The influence of the network geometry is not captured by the own-cell interference - which is also true for the noise - why I focus on the characterization of the aggregate co-channel interference in my work.

From the above we gather that the description of the aggregate co-channel interference (simply referred to as *aggregate interference* in the remainder of this thesis) for dense networks needs to be done accurately, since it has a significant influence on the network performance [12, 14, 46]. A generic formulation of the path loss attenuation of each link in decibel is given as

$$PL = P_t - P_r + G_t + G_r, \quad (2.1)$$

where  $P_t$  and  $P_r$  represent the transmit- and receive power levels, and  $G_t$  and  $G_r$  refer to the transmit- and receive antenna gains. Building the ratio of the desired signal strength and the aggregate interference, yields the SIR that forms the basis for performance evaluation and prediction on network scale. Expressed in the linear domain, the SIR  $\gamma$  is

$$\gamma = \frac{P_{r,d}}{\sum_i P_{r,int}^{(i)}}, \quad (2.2)$$

where  $P_{r,d}$  is the received power of the desired signal and  $P_{r,int}^{(i)}$  is the interference power at the receiver of interferer  $i$ . Based on the SIR, further performance metrics can then be derived, such as the coverage probability, throughput or area spectral efficiency (ASE), as I will do in Chapters 4 and 5.

Since the aggregate interference term in the denominator of Eq. (2.2) changes with receiver location and time, it can be described as a stochastic process [35]. Optimally, the interference statistics can be described by relatively few parameters. This is true for the well known abstractions of the hexagonal grid model [39] or the Wyner model [96]. Nevertheless, mathematical tractability of the interference statistics is not easily obtained. When aggregating a large number of interferes without a dominating term, a *Gaussian random process* can be used to approximate the interference probability density function (pdf) since in this case, the central limit theorem can be applied [9]. This is however not necessarily true in reality and the pdfs deviate from those obtained by the Gaussian approach [28, 46]. An alternative lies in the characterizing the interference by using the Laplace transform (LT) of the pdf, or equivalently its characteristic function (CF) or moment generating function (MGF). This approach is specifically suitable in combination with stochastic geometry since it allows for systematically identifying LT, CF or MGF for the interference pdf [45]. I discuss important concepts in this context in Section 2.4 and utilize them then in Chapter 5.

## 2.2. Propagation Effects

The transmitted signal (irrespective of desired or interfering) is influenced by the environment on its way to the receiver. This attenuation and distortion of the signal is caused by four basic mechanisms<sup>1</sup> [10]:

---

<sup>1</sup>Note that the antenna gains introduced in Eq. (2.1) are usually treated separately from the other propagation effects and are also not included in the models discussed in the following section.

- free-space path loss: the distance-dependent loss along a line of sight (LOS) link
- reflections: waves are reflected by objects that are substantially larger than the wavelength
- diffraction: based on Huygen's principle, secondary waves form behind large impenetrable blockages
- scattering: energy is dispersed in various directions by objects that are small relative to the wavelength

Dependent on the environment, the original signal can arrive at the receiver over several links with different delays (i.e., multi-path propagation), which can then interfere with each other. Moving reflectors (also relative to the transmitter or the receiver when they are moving) leads to Doppler shifts.

As already indicated above, the occurring effects depend on the carrier frequency and the material or structure of objects that are in the environment. Additionally, geometric location and distances play an important role, why, e.g., indoor propagation behaves differently than transmission in a rural area over long distances. Due to all these interdependencies and overlapping effects, there is the need for finding abstract yet accurate models that capture the most prominent effects of the investigated scenario and if possible still assure mathematical tractability. Thus in the next chapter, I introduce particular categories of propagation models, that capture different behavioral aspects of the wireless transmission and discuss prominent representatives in each category.

## 2.3. Propagation Models

Commonly, the path loss attenuation is formulated as

$$\text{PL} = \underbrace{L(d, f) + X_\sigma}_{\text{large-scale path loss}} + \underbrace{F}_{\text{small-scale path loss}}, \quad (2.3)$$

where  $L(d, f)$  refers to the mean path loss,  $X_\sigma$  is the shadowing and  $F$  denotes the small-scale fading. The term  $L(d, f)$  is mainly based on the effect of free-space path loss, which depends on the distance  $d$  between transmitter and receiver as well as the carrier frequency  $f$ . Note that it is independent of the node locations within the scenario. The random variable (RV)  $X_\sigma$  corresponds to the shadowing caused by blockages. The RV  $F$  primarily captures the effects of the multi path propagation. It is important to note that Eq. (2.3) does not model each of the four basic propagation mechanism, as presented in Section 2.2, separately. Each of the three terms rather incorporates *all* mechanisms to a certain extent.

The terms in Eq. (2.3) can be grouped into *large-scale path loss*, including the mean path loss and the shadowing, and *small-scale path loss* referring to  $F$ . This terminology is derived from the scale

in space and time, where severe variations are expected to occur. A taxonomy of propagation models is presented in Fig. 2.1.

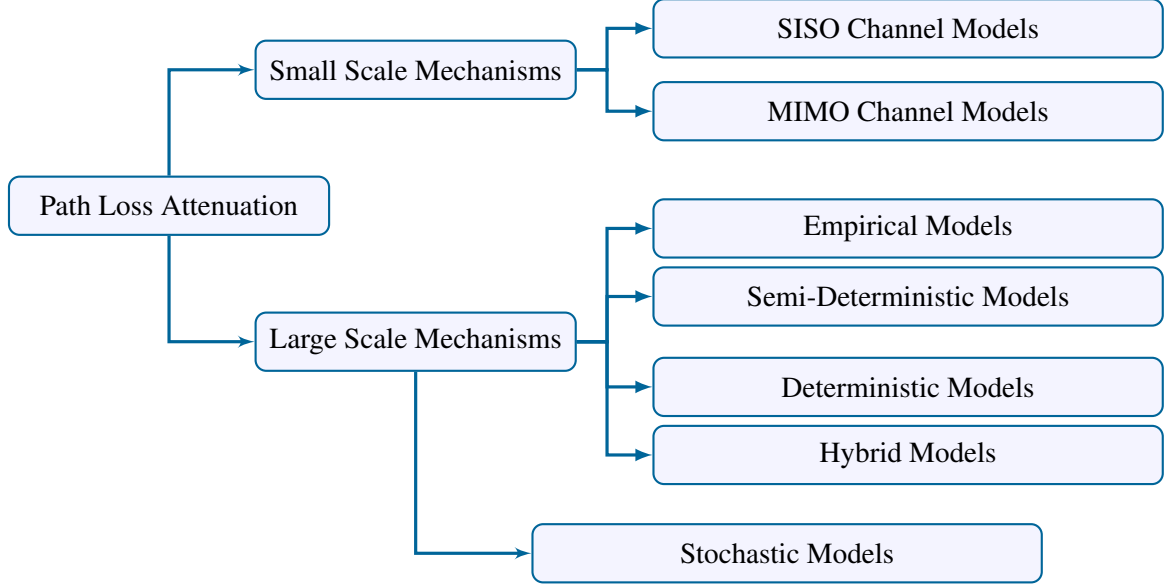


**Figure 2.1.:** Overview on models for abstracting small-scale- and large-scale signal propagation mechanisms. Approaches for large-scale mechanisms include conventional and stochastic models. ©2016 EURASIP, [87].

### 2.3.1. Small Scale Models

The *small-scale component* describes the fluctuation around the respective mean which is given by the large-scale components. This fluctuation can be substantial within a short period of time as well as within few wavelengths distance and results from multi-path propagation, moving receivers and transmitters as well as scattering objects, and the resulting positive or negative interference of different paths at the receiver location. The corresponding models are commonly denoted as *channel models* [6, 24, 40, 54, 95]. They incorporate the effects of single-input single-output (SISO) and multiple-input multiple-output (MIMO) transmissions and may include correlations over time and frequency. Furthermore, these models can be distinguished by considering a 2D propagation, such as classical power delay profile (PDP) based channel models, e.g., the VehA channel model [56] or the Typical Urban channel model [1], or 3D propagation modeling [6]. These variations on a short temporal and spatial scale are of interest when instantaneous transmission characteristics are investigated. For long-term average trends of a whole network, it is infeasible to model these fluctuations in all detail, while I restrict myself to utilizing channel models with a large degree of abstraction. This also allows to include these small-scale components in analytical models,

which is not possible with a highly sophisticated model such as the Third Generation Partnership Project (3GPP) 3D channel model TR 36.873 [6].

### 2.3.2. Classic Large Scale Models

In literature, a substantial number of large-scale path loss models have been reported. They can be categorized into four groups: *empirical models*, *deterministic models*, *semi-deterministic models* and *hybrid models* (cf. Fig. 2.1). The main distinctive characteristic of these models is the trade-off between accuracy and complexity. While these models aim at representing the large-scale component in Eq. (2.3), they do not necessarily distinguish mean path loss and shadowing. The advantage of empirical path loss models is the ability to characterize them with only a few parameters and describe the signal propagation either by a deterministic law or by some RV. A classical example is the log-distance dependent path loss model [75] with some path loss exponent that depends on the considered environment and the link condition, such as LOS or non line of sight (NLOS). It is commonly defined as

$$\text{PL} = \text{PL}(d_0) + 10\alpha \log_{10} \frac{d}{d_0} + X_\sigma, \quad (2.4)$$

where  $\text{PL}(d_0)$  is the path loss at a reference distance  $d_0$ ,  $\alpha$  is the path loss exponent and  $d$  is the link length. This model also includes *random* shadow fading as *log-normal shadowing* in the term  $X_\sigma$ , where the effect of blockages is combined into a log-normally distributed RV. The variance  $\sigma$  of the distribution depends on the environment and has to be determined by measurements. Thus, the model is only valid for a specific scenario and requires an empirical calibration step. In real-world scenarios, the locations of large objects will be highly correlated, which has to be included in the model [84].

### 2.3.3. Stochastic Blockage Models

Intuitively, a longer link increases the likelihood of buildings to intersect with it, which is not taken into account by log-normal shadowing. This has also been the result of recent studies [17, 18]. This can be included either by generating correlated LOS maps (cf. [7]) or by explicitly modeling building objects and checking for obstructed links. To do so, there emerged the class of stochastic path loss models that describe attenuation due to blockages by statistical parameters, and as a consequence, e.g., the probability for a link to be in LOS. Their formulation is based on concepts from *random shape theory*, which represents the formal framework around random objects in space [22].

Let  $\mathcal{O}$  denote a set of objects on  $\mathbb{R}^n$ , which are closed and bounded, i.e., have finite area and perimeter. For instance,  $\mathcal{O}$  could be a collection of lines, circles or rectangles on  $\mathbb{R}^2$  (conf. Fig. 2.2), or a combination of cubes in  $\mathbb{R}^3$ . For each object in  $\mathcal{O}$ , a *center point* is determined, which has to be

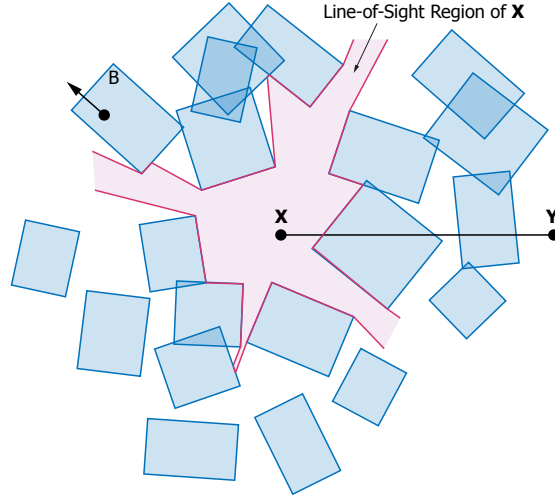


**Figure 2.2.:** Snapshot of a ROP with rectangular objects. Object centers are distributed according to a PPP. Size and orientation of the objects are determined from some distribution. Center and orientation of a generic building  $B$  are indicated in the upper left corner of the figure. Shaded area around  $X$  shows its LOS region. ©2016 EURASIP, [87].

well-defined but does not necessarily relate to the object's center of gravity. Non-symmetric objects additionally require to specify the orientation in space by a directional unit vector. In the analysis of mobile cellular networks, the objects in  $\mathcal{O}$  represent blockages such as buildings and walls, as will become apparent in Chapter 5. A random object process (ROP) is constructed by randomly sampling objects from  $\mathcal{O}$  and placing their corresponding center points at the samples of some point process (PP). The orientation of each object is independently determined according to some probability distribution.

In general, a ROP is difficult to analyze, particularly when there are correlations between sampling, location and orientation of the objects. For the sake of tractability, a *Boolean scheme* is commonly applied in literature [16, 18, 86]. It satisfies the following properties: (i) the center points form a Poisson point process (PPP), (ii) the attributes of the objects such as orientation, shape and size are mutually independent, and (iii) for each object, sampling, location and orientation are also independent. These assumptions of independence enable the tractability of the analysis. On the other hand, they omit correlations among blockages, as observed in practical scenarios.

## 2.4. Interference Geometry

Next to the path loss, the interference geometry has the largest influence on the aggregate interference. Also here, abstractions to some baseline model are necessary. The previously mentioned hexagonal

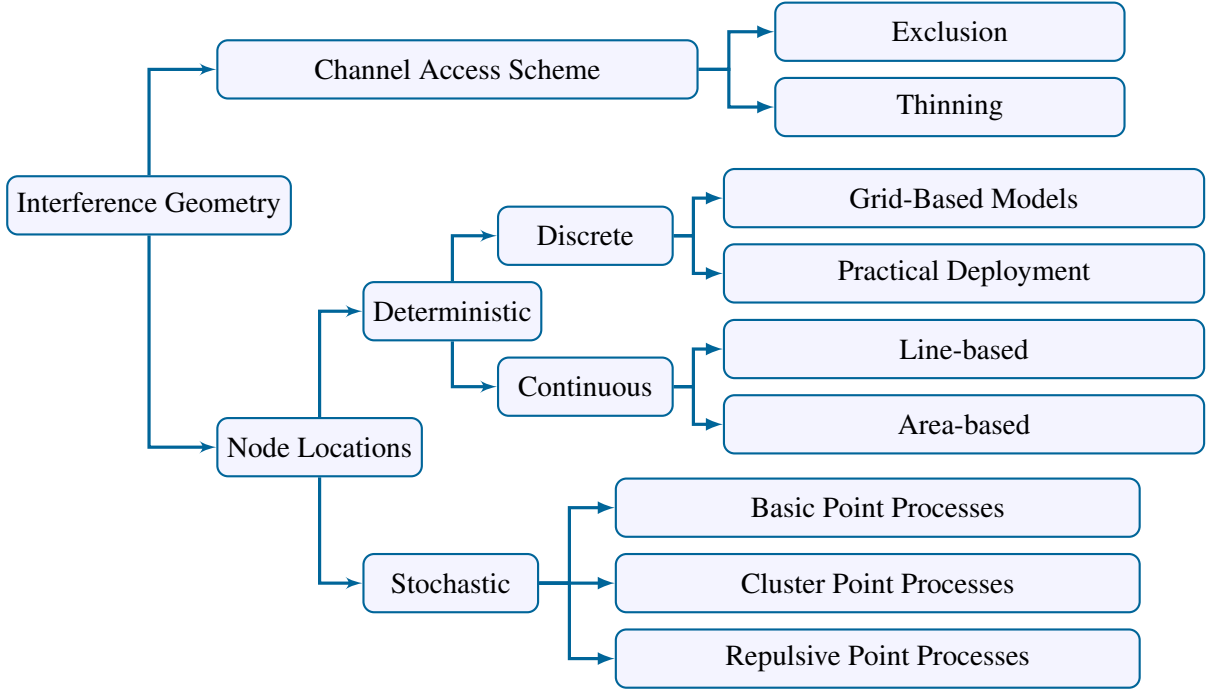


**Figure 2.3.:** Models for abstracting interference geometry. The interference geometry is affected by both the node locations as well as the channel access scheme. ©2016 EURASIP, [87].

grid model has for several decades been a widely accepted and useful model for homogeneous network deployments, usually of macro BSs. With the emergence of more heterogeneous networks, including several tiers of different BS types and especially with the unplanned deployment of femto cells (cf. Section 2.5), networks exhibit a more random and heterogeneous topology [11, 13]. These opposing approaches are also manifested in the available models for interference geometries (cf. Fig. 2.3). Next to deterministic and stochastic node locations, which will be described in some more detail in the following, there exist the approaches that include the channel access scheme, leading to thinning of interferers or an exclusion region around the transmitter-receiver pair. This however considerably complicates the analysis and is therefore frequently neglected and I also do not consider this in my work.

### 2.4.1. Deterministic Node Locations

The deterministic approaches can broadly be categorized into *discrete* and *continuous* models, with either individually modeled node locations or distributed interference power over a certain area. For my purposes I focus on discrete models. Combining the relative distance between receiver

and interferer with an appropriate path loss model leads to a weighted sum of random variables. Certain fading distributions, such as Rayleigh, log-normal or Gamma enable to exploit techniques that make use of variants of the CF or the MGF [24, 54]. This will be utilized in Chapter 4. The main point of criticism for these models is the lack of spatial randomness which means that SIR distributions are more concentrated than they would be for spatial realizations of realistic, more irregular deployments.

### 2.4.2. Stochastic Node Locations

The basis of stochastic geometry was already laid in the early 19th century [21, 79]. Its application for characterizing interference in wireless networks is a rather recent development [14, 15]. When BS locations are abstracted to some PP, *spatial averages* over network realizations can be obtained. Closed-form expressions for the aggregate interference pdf are however not available (only in one special case). What makes stochastic geometry viable though is the fact that it provides means for systematically evaluating the Laplace transform of the aggregate interference. The enabling identity is the probability generating functional (PGFL) [22]: Let  $\Psi$  denote an arbitrary PP. Then, its PGFL formulates as

$$\mathcal{G}[g] = \mathbb{E} \prod_{x \in \Psi} g(x), \quad (2.5)$$

where  $g(x) : \mathbb{R}^d \rightarrow [0, \infty)$  is measurable.

It proves particularly useful to evaluate the LT of the sum  $\sum_{x \in \Psi} f(x)$ :

$$\begin{aligned} \mathbb{E} \left[ \exp \left( -s \sum_{x \in \Psi} f(x) \right) \right] &= \mathbb{E} \left[ \prod_{x \in \Psi} \exp(-s f(x)) \right] \\ &= \mathcal{G}[\exp(-s f(\cdot))], \end{aligned} \quad (2.6)$$

which characteristically appears in the analysis of aggregate interference with *discrete* node location models. The function  $f(\cdot)$  represents the received power from an individual interferer at location  $x$ . Consequently,  $I = \sum_{x \in \Psi} f(x)$ . Since  $I$  is a RV that is strictly positive, its LT always exists.

The most well studied point process is the PPP, which comes with the benefit of simplified analysis. For a stationary PPP  $\Psi$  of intensity  $\lambda$ , the number of points in any set  $B \subset \mathbb{R}^d$  is a Poisson RV with distribution

$$\mathbb{P}[\Psi(B) = k] = \exp \left( -\lambda |B| \frac{(\lambda |B|)^k}{k!} \right), \quad (2.7)$$



and the number of points in disjoint sets are independent RVs. Another advantage of the PPP is that an exact expression of the PGFL is known:

$$\mathcal{G}[g] = \exp \left( - \int_{\mathbb{R}^d} (1 - g(x)) \Lambda(dx) \right), \quad (2.8)$$

where  $\Lambda$  corresponds to the intensity measure of  $\Psi$ , which describes the average number of points in a given subset. In combination with Eq. (2.6), this allows to transform the (infinite) sum of interference powers into a spatial integral, which is easier to handle mathematically.

Still, to obtain a closed form aggregate interference pdf, further measures have to be taken, as summarized in [35]. A convenient technique, which is also used in [12], is to resort to Rayleigh fading, which simplifies the analysis.

The main limitation of stochastic modeling of interference locations is that the obtained results are averages over an ensemble of spatial realizations. This means that only first order statistics are investigated and variations within individual spatial network realizations, that can be substantial, are hidden. Especially when using a PPP, spatial correlation is not included in the model, as it would be by models taking into account the channel access scheme, or for PPs with repulsion.

As a conclusion, the spatial randomness of stochastic models and the complete regularity of, e.g., a hexagonal grid model are intrinsically opposite approaches, each with their own simplifying assumptions, but yield lower and upper performance bounds for wireless network deployments [11].

## 2.5. Base Station Types

With more complex environments and distinct situations in which coverage should be provided by a cellular network, more than the standard macro BS is required in order to fulfill the task. This can be done by adding pico or femto cells [11, 26] or utilizing distributed antenna systems (DASs) [59]. While pico cells are usually deployed at traffic hot-spots to increase the network capacity at dedicated locations and are located both outdoors and indoors, femto cells are typically installed by the consumer inside their flats. This leads to a more heterogeneous and less regular network. A DAS can be described as a BS with spatially separated antennas. This allows to radiate the signal in an optimal location in scenarios, where radio propagation is problematic or where otherwise many BSs would have to be installed to achieve the same coverage without the need for increased capacity. This makes them well suited for indoor environments [78], but also for train environments along the tracks or in tunnels [94].

These different types of BSs all vary in their characteristics, such as transmit power, installation height, deployment mode or antenna types. These differences have to be taken into account in the modeling of the respective scenario and also have an impact on the choice of the propagation models (cf. Section 2.2) that are suitable for the individual BS types.



## Chapter 3.

### Context and Methodology

In order to set the context for the investigations in Chapters 4 and 5, I narrow down the scenario specifics in this chapter, explain available methods for performance evaluation and substantiate my chosen approach.

#### 3.1. Scenario Context

Since the first utilization of the hexagonal grid model, there has been abundant research on networks with this underlying topology. Also the emerging heterogeneous networks, that arise from the diversified needs and increased demand for wireless connections of users within a cellular network, have already been investigated thoroughly [30, 31, 34, 35]. As introduced in Chapter 1, I do not go in the direction of classical outdoor users, but focus however on the investigation of wireless networks in high speed train (HST) and indoor scenarios in my work. These environments cover the predominant cases of wireless communications in future wireless networks [23, 81], but exhibit specific propagation conditions and network deployment considerations.

While my conclusions are not only true for a specific transmission standard, it has to be noted that the general background of this work is the Third Generation Partnership Project (3GPP) LTE advanced (LTE-A) standard [3]. This has several implications for the system model of the investigated scenarios as well as partially on the performance results. First of all, LTE-A uses a carrier frequency below 6 GHz which has an influence on the choice of propagation models. Additionally, the penetration loss values of indoor walls or train chassis are different for this frequency range as for, e.g., transmissions in the mmWave band. Throughput results acquired by simulations then are also objected to the parameter-set given by the standard, i.e., a predefined set of modulation and coding schemes (MCSs) or typical carrier frequency and transmission power. More details on this can be found in the description of the corresponding system model in Chapters 4 and 5.

## 3.2. Performance Evaluation Methods

There exist various approaches to investigate the performance of cellular networks. While measurements of course come with the advantage of not having to model or abstract the environment, they are usually tedious to perform, do not easily allow for repeatability and are limited in scale - commonly only one or rarely a few transmission links are included in one measurement. Additionally, it is difficult to conclude from a set of measurements to an entire scenario. With link level (LL) simulations, this situation is improved with a more controlled setup and still provides a detailed reproduction of realistic propagation and transmission aspects, but again the focus is only on a few number of links due to complexity issues. In order to predict and estimate the network-wide performance on a larger scale, the scenario has to be abstracted further by, e.g., the aforementioned propagation models (cf. Section 2.3). This then allows to perform system level (SL) simulations with large numbers of network nodes, but is also necessary for any analytical considerations to obtain a mathematical description of the problem that is still tractable.

An often used technique to simulate wireless networks is ray-tracing, which is also utilized for the investigation of train and indoor environments [47, 63, 64]. This technique relies on well defined objects in the environment, with which geometric rays then interact. Thus, also paths that contain several reflections are included in the investigation. It is however difficult to draw general conclusions from the obtained results, due to the fundamental dependency on site-specific information. Take for example the same wagon but with a different arrangement of the interior (e.g., seats or doors), and you may already obtain a substantially different result.

In my work, I apply rather abstract propagation models and derive analytical expressions for performance metrics as well as performing SL simulations. Due to the complex underlying scenarios, I employ approximations in the analytical models where necessary, to maintain mathematical tractability. For SL simulations, I perform Monte-Carlo simulations to average over temporal as well as spatial realizations and either use a standalone code or utilize the Vienna LTE-A SL Simulator [77]. This simulator is fully standard compliant and allows to simulate networks with several users and base stations (BSs) with arbitrary locations, while providing a vast number of propagation models, that can also be adapted to the scenario under investigation.

## 3.3. Comparison of Approaches for Train and Indoor Scenarios

While I discussed the similarities of how to approach the investigation of the network performance in train and indoor scenarios up to here, I now clarify the differences among both scenarios.

The passengers as mobile users in train scenarios are concentrated in a confined space within the train, that travels at high speed. BSs are deployed along the tracks in regular distances. Therefore,

modeling their positions as deterministic node locations (cf. Section 2.4) is an obvious fit. The deployment of remote radio units (RRUs) is beneficial in such scenarios, because the system can be flexibly adapted to the train position, as I will explain in Chapter 4. A very specific effect that has to be taken into account is the (usually substantial) penetration loss that is experienced by the signal when entering the carriage.

Signal propagation in indoor scenarios is mostly dominated by the signal blockage through walls. Therefore, I employ different wall generation methods (cf. Section 2.3) to include the wall penetration loss in the system model. I consider both regular and random BS positions and compare the results for both options. Reflections are not included explicitly, but are rather accounted for in the path loss and in the channel model.



## Chapter 4.

# Performance Evaluation in High Speed Train Scenarios

The availability of a broadband wireless connection even in non-stationary scenarios, e.g., while commuting and traveling, is nowadays expected by the majority of user. In order to provide such connectivity to their passengers, there exist combined efforts from railway operators as well as mobile network operators. Especially in high speed train (HST) scenarios, a number of unique aspects w.r.t. signal propagation and technical issues are encountered, that make this task particularly demanding. Especially the high concentration of fast moving users, the resulting need for frequent handovers and large penetration losses into the train carriage are challenging.

This chapter is mainly based on my work in [69, 70] and yet unpublished results from my research stay at GTEC and contains the following contributions:

- In Section 4.1, particularities of wireless communications in HST scenarios are presented. This includes a discussion of specific aspects for the transmission of wireless signals as well as a comparison of the benefits and advantages of direct communication between user and base station (BS) and communication via relays, installed in the train. Further technical and economical aspects are discussed in the last part of this section.
- In Section 4.2, I present a comparison of link level (LL) and system level (SL) simulations with input from real-world measurements. This comparison acts as proof of concept to demonstrate that, for an appropriate calibration of propagation models, the large degree of abstraction in SL simulations still allows results with good accordance to real world measurements.
- In Section 4.3, I investigate the potential of remote radio unit (RRU) collaboration schemes in HST scenarios. Knowing the position of the train along the tracks allows for coordination and cooperation, thus either avoiding interference from close RRUs or even combining the signals from these RRUs. I compare theoretical results to those from simulations, explain the major discrepancies in the model and also provide results for the aforementioned comparison of direct passenger-BS communication and relay-aided communication.

## 4.1. Design Aspects for Supplying Wireless Connections in High Speed Train Scenarios

In the current market of train services, the provision of mobile broadband access to costumers has become a distinguishing feature for choosing this means of transportation or among competitors. Due to the ubiquitous use of the Internet and the rapid adoption of novel devices such as smart phones and tablet computers, most passengers have become accustomed to experiencing high data rates and having the service following them no matter where they go. With the number of commuters being expected to increase, the high user mobility is also one of the most emphasized scenarios in the initiative for the fifth generation (5G) of wireless communications. LTE advanced (LTE-A), the contemporary standard for wireless communications, is not optimized for the challenges of HST scenarios. Hence, many railway operators - mostly in collaboration with mobile operators - have increased efforts to satisfy the ever increasing requirements. There also exist international collaborations on a broad level to push for higher data rates and shorter latencies, for example the Shift2Rail initiative by the European Union [83]. Additionally, LTE for Railway (LTE-R) has been proposed in [90] as an evolution of GSM - Rail(way) (GSM-R), addressing required performance parameters and necessary adaptations on the architecture of the system. Nevertheless, LTE-R has not been standardized yet. Furthermore, the main concern of LTE-R is not the passenger communication, which however is the scope of my work. Therefore, I mostly focus on LTE-A.

Wireless communication in HST scenarios is confronted with unique conditions, which have a considerable impact on network planning. In particular, the scenarios are characterized by users being densely packed inside of the train and moving at high speed, as well as the specific propagation effects in a broad variety of different environments. Most publications on this topic assume a relay-based approach, assuming additional hardware installed on the train, that communicates with the BS as well as with users without them communicating directly ([74, 101]). However, the direct communication between users and BSs has its own advantages, but has not been given enough attention in literature. In the following, I discuss various aspects that are peculiar for HST scenarios and provide an extensive comparison between the relay approach and the less studied direct link approach. In Section 4.3 I then present simulation results for both, direct and relay aided communication.

### 4.1.1. Particularities of High Speed Train Scenarios

Wireless communications in HST scenarios exhibit several key differences to the traditional considerations of a coverage oriented network. What is more, there is not the same amount of extensive experience with such scenarios as with classical networks. Thus, many effects have not been fully understood and it is not clear which are the most significant in HST scenarios. The state of the art is discussed in the following, along with the aspects that are currently identified as most important.



Following [25], newly built tracks for HSTs should support at least 250 km/h and many operational systems exceed this value. These speeds lead to a high Doppler shift, which causes several transceiver impairments such as channel estimation errors and inter carrier interference (ICI) in orthogonal frequency division multiplexing (OFDM) systems. It also leads to rapidly changing channel conditions, as it can be seen from the throughput and channel quality indicator (CQI) results in Section 4.2.

Moreover, the channel characteristics along the tracks vary greatly. The surroundings show several distinct categories, which encompass certain different features that influence the signal propagation. Among those are tunnels, trenches, cuttings, stations, viaduct-like structures or bridges. An example for such a diverse environment is shown in Fig. 4.1. An extensive description of such categories is described in [8]. In addition to the onerous propagation conditions, a large part of the signal may be shielded by the metal chassis and the metal coated windows of the carriage. If the signal is first received by a relay, this can lead to a very strong multi-path component additionally to the line of sight (LOS) path.

Another peculiarity of HST scenarios is the user distribution and user movement. Opposed to classical assumptions of random user placement, all users are concentrated within the train. Their location and movement is approximately deterministic and strongly correlated among users, as it is predefined by the course of the tracks and the speed of the train. This implicates a certain a priori knowledge that can be exploited to compensate for some of the above mentioned issues.

The high user concentration results in pulse-like traffic in the cells along the tracks. This leads to BSs being either completely idle or confronted with a high load (in case the hardware is dedicated to serving the train) or to large performance fluctuations in a cell (in case also the surrounding environment is covered by the respective BS). From the high speed of the train it follows that small cells are traversed in a very short time, thus leading to a frequent necessity for handovers. When all users aboard a train simultaneously require a handover to the next cell, the control channel easily gets congested and suspends users from associating with the neighboring cell. As indicated above, the deterministic user behavior may provide a considerable advantage for implementing elaborated handover schemes.

Due to the diversity of environments, the modeling of the fast fading channel becomes a complex task. Many considerations regarding wireless communication in HST scenarios are based on simulations applying the Winner channel model [53]. Even though the model is highly adjustable, it was originally not intended to represent the characteristics of an HST scenario. Furthermore, it does not reflect the dynamic changes in the channel characteristics from one category to another. Thus, such simulations only yield first order statements that may considerably deviate from reality and may not appropriately reflect the specifics of the environment. 3GPP has recently introduced a 3D channel model in [6]. However, specific aspects for train communications are not yet included and have to be determined.

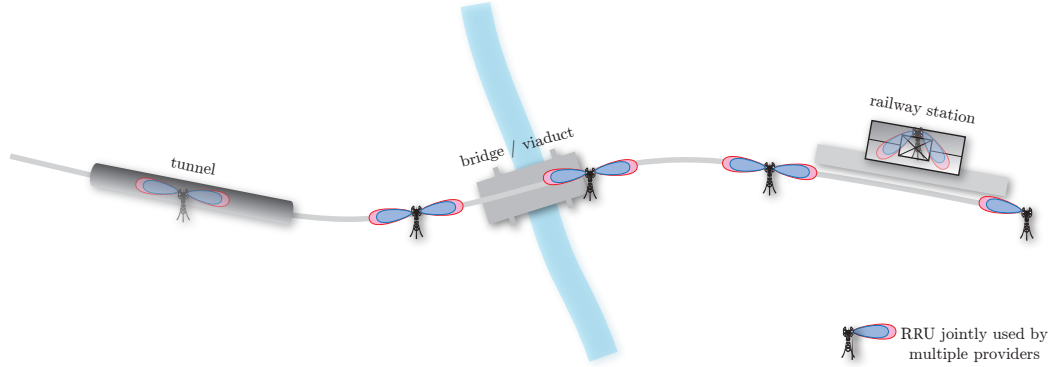


**Figure 4.1.:** Various environments along a railroad track. The track is supplied by RRUs that can be used by multiple network operators. ©2015 IEEE, [70].

#### 4.1.2. Advantages of Remote Radio Units

It is commonly agreed that a satisfactory quality of service can only be achieved by employing dedicated hardware in an HST scenario, especially in the form of RRUs. Due to their smaller size and cost compared to classical BSs, it is possible to install them close to the tracks and in great numbers. Several RRUs can be connected to one BS via radio over fiber (RoF). This allows for very flexible routing options as explained in the subsequent section. An example for an RRU installation along the tracks is presented in Fig. 4.1.

Supplying passengers of HSTs with mobile broadband access by a cellular LTE-A network is a demanding task. The majority of the railway tracks runs through rural areas and is not adequately covered by the already deployed BSs. Hence, it is necessary to install dedicated equipment that is capable of handling the pulse-like traffic characteristics of the passing trains. Since the users are concentrated in a very limited space, the usage of RRUs promises to be beneficial. Connected by optical fiber links, they can be powered-up on demand and dynamically associate with a BS, thus even allowing a cell to "travel" with the train and avoiding the problem of frequent handovers [38, 74, 101].

Applying RRUs inherently imposes the question of their optimal locations along the railroad track and the type of collaboration among them. In scenarios, where the main radiation directions of the RRUs are aligned along the tracks, mutual interference becomes the performance limiting factor. Therefore, it is imperative to determine which RRUs to use simultaneously and how to group them for BS association. The performance improvement of RRU collaboration schemes is discussed in more detail in Section 4.3.

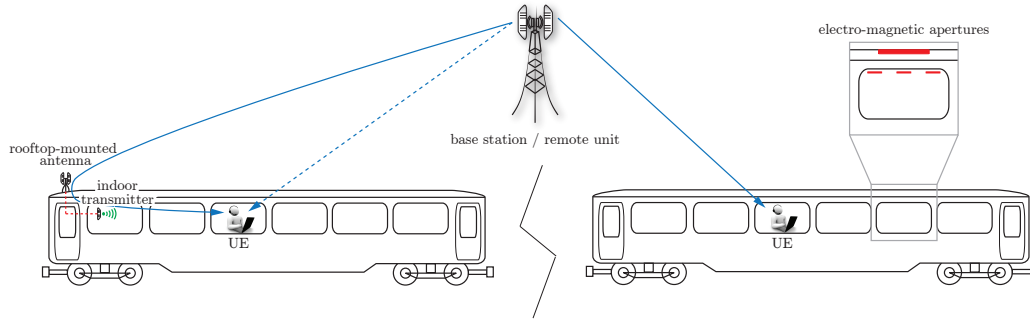


**Figure 4.2.:** Signal reception with relay- and direct-link approach. Zoomed view indicates possibilities for applying electro-magnetic apertures. ©2015 IEEE, [70].

#### 4.1.3. Comparison of Relay and Direct Link Approach

Generally speaking, there exist two opposing approaches to provide wireless communications to passengers of an HST. In the first case, the UE directly associates with the BSs along the tracks, while in the second case this link is established via a relay, as shown in Fig. 4.2. Subsequently, a comparison between these two approaches is drawn and advantages and drawbacks on both sides are discussed.

##### Relay Approach

In the relay scenario, one or several antennas are mounted on the outside of the train. These are connected to one or more relays which are then distributing the signal inside the train. This approach has the major advantage that the signal is not attenuated by the chassis and the windows of the carriage. Moreover, this setup allows to configure the relay such that it appears as a single user to the BS, thus significantly reducing the number of handovers. Therefore, all traffic is aggregated by the relays and then distributed to the users. It is also widely discussed in literature [82, 85, 97], often assuming that the train moves on a railroad viaduct, which allows to define favorable geometrical problems [8, 37, 51]. An example, where the capacity for distributed antenna systems is discussed, is presented in [74].

While the quality of the experienced link might considerably be improved, the employment of relays does not come without cost. Firstly, relays have to be licensed for the specific band they are operating on. This is of minor consequence when no borders are crossed. In smaller countries such as, e.g., in most European, one train connection can easily span three or more countries. For each country, the relays have to be registered individually or have to be switched off when crossing the border, which leaves the system in a direct-link state. Another consequence is, that the employment of

carriages becomes restricted to the countries/routes for which the relays on board are licensed and thus becomes less flexible.

A second issue appears with the choice of the frequencies for the RRU-to-relay and the relay-to-user connection. If the same frequency is used on both link-sections, thus only bypassing the penetration loss of the carriage, the user might still receive a considerable amount of the desired signal by a direct link through the window. The relative receive power of these two links depends on the individual position of the user and the actual penetration loss. Due to the latency caused by the relay, the signal might be perceived via several multi-path components that cannot be equalized, given that the attenuation of the direct signal is not large enough<sup>1</sup>.

The aforementioned problem is completely avoided when two different frequencies are used on both sections of the link. For example, a dedicated frequency of a mobile operator is used from RRU to the relay and a second frequency, e.g., in the Industrial, Scientific and Medical (ISM) band, for the supply with WiFi inside. This setup is frequently referred to in literature [101]. Nonetheless, it only provides a data connection for the passengers. Since only the relay is visible as a single user for the BS, the passengers are not accessible for mobility management. Additionally, this only partially avoids the problem of frequent handovers, but does not overcome issues such as the low average load in the sector when no train is present. Using frequencies in the ISM band comes with a strict constraint on the equivalent isotropically radiated power (EIRP), which may be a limiting factor for distributing the signal inside of the carriage.

The performance of this setup may also considerably depend on the number of antennas and relays per train/carriage. It has to be scrutinized whether the relays should work individually (e.g., one per carriage) or if the received signals should be combined. This is also affected by the possibility to connect all relays to all carriages. Since a cable connection will not be feasible in practice, near field communication standards at higher frequencies than the traditional 6 GHz band (e.g., in the upper mmWave band) may be considered for this task.

### **Direct-Link Approach**

The direct-link approach assumes a direct connection between RRU and user. In comparison to the above scenario, the signal does experience a severe penetration loss into the carriage in this case. As the chassis of the carriages is usually made of metal, the signal enters the train mainly through the windows. However, the penetration loss may greatly vary among window types, as they are mostly metal coated themselves. Attenuation values range from 20 dB to 40 dB for metal coated windows of a German ICE-train [91], but other train-types exhibit different values as observed, e.g., in [98] with a combined range of 10 dB to 40 dB.

---

<sup>1</sup>It can however still come to problematic situations even then, e.g., in a train-station with open doors.

Note that these values reflect the situation for current carriages in use. Since the interest among railway operators is increasing to provide best quality of experience to their customers, the design of future trains is likely to be adapted to the demands of the wireless link. Among various options is the possibility to introduce windows with small penetration loss (omitting the metal coating). Another option is to include apertures in the chassis or the window itself, by incorporating materials that are more permeable for electromagnetic waves, for example carbon fiber materials. Examples for such apertures are indicated in Fig. 4.2. To illustrate the different performance for both approaches, simulation results, comparing direct and relay aided communication are displayed in Fig. 4.18.

### Handover Issues

While it is possible in the relay approach to let the whole train appear as the equivalent of one or two users (given the proper frequency setup), this option is not available for the direct-link approach. Each active passenger appears as an individual user. Therefore, many handovers have to be executed when the train moves from one cell to another. Considering the high speeds and that even "inactive" passengers, not actively transmitting data, have to be handed over to the next cell, this can lead to a considerable amount of traffic on the control channel and might in extreme cases lead to blocking of users.

As mentioned above, the deterministic location of the train and the semi-deterministic location of the UEs (confined inside of the train, but not known in particular) enables new concepts of handover and cell extension, including

- Moving cell
- Smart handover schemes
- Sliding handover

The moving cell concept is shown in Fig. 4.3. For both approaches, relay and direct-link, it increases the cell length from around 1 km to a maximum of up to 50 km. Commercial systems with the necessary capabilities for that task are already available, e.g., with systems similar to [57]. The working principle is that many RRUs are associated with a central control entity via RoF. When the train leaves the range of one RRU, the central unit will reroute the data-stream towards the next RRU along the tracks. In that manner, the cell 'travels' with the train (in an abstract sense, this can be interpreted as a semi-static beamforming scheme), enabling a transparent and smooth transition, without the need for handovers over longer distances. Considering a speed of 250 km/h, the transition of a cell of 1 km length takes approximately 15 seconds and a handover becomes necessary. With the moving cell concept, the period of reoccurring handovers is enhanced to 12 minutes. The concept is further detailed in [38].

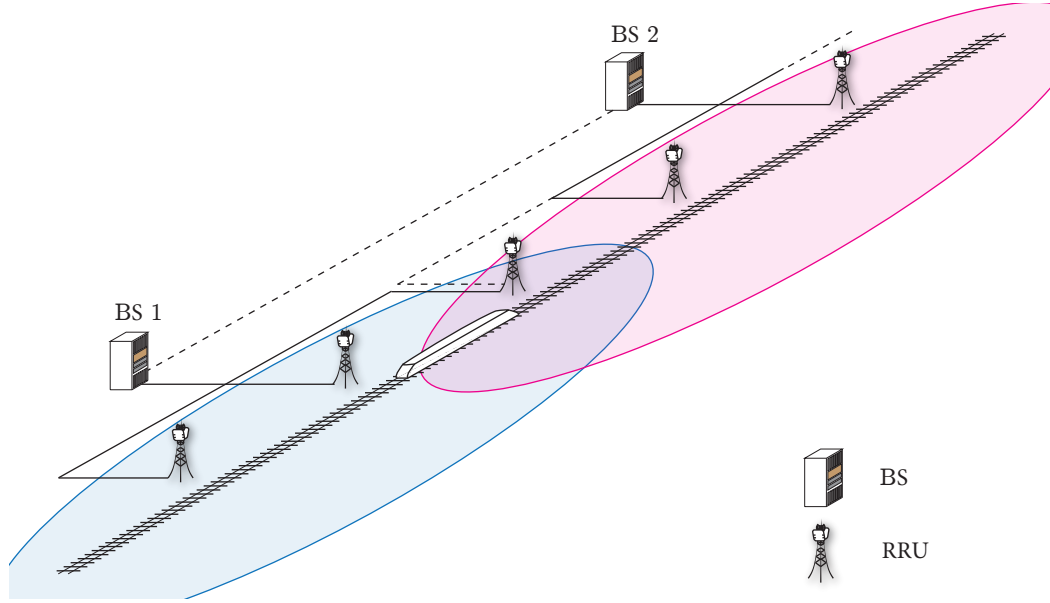


**Figure 4.3.:** RRU deployment along railroad tracks. Figure indicates moving cell- and sliding handover concept. ©2015 IEEE, [70].

Smart handover schemes were reported, e.g., in [65]. Such schemes improve the handover performance, but assume cells simply touching each other on the outer cell borders. Nonetheless, they do not omit the issue that many handovers have to be handled simultaneously when transitioning from one cell to the next. To further alleviate this issue, a possible solution would be to spread out the handover region wider than just between the two RRUs at the cell borders. I call this a *sliding handover*. It is conceptually illustrated in Fig. 4.3. In the figure, it is observed that the cell overlap spans three RRUs. When the train enters the handover zone, the control entity signals to a fraction of the users to perform a handover, while the others remain in the current cell. To find the optimal point for initializing the handover, the knowledge of the exact train position and the predefined trajectory (given by the tracks) can be exploited. In order to generate such an overlap region, the RRU in the middle of the handover region is shared by both cell control centers<sup>2</sup>. It can also transmit on different frequency bands and exploit coordinated multi-point (CoMP) schemes in order to avoid excessive interference in the handover zone. Fraction-wise handover avoids the overload of the control channel. To further smoothen the handover situation, the handover zone can be extended arbitrarily. This effectively leads to a reduction of the total cell length (because of the longer overlap), which is however only a small fraction compared to the total length.

<sup>2</sup>Cell control center basically describes a more intelligent BS

#### 4.1.4. Further Technical Aspects and Operator View

The aspects of wireless communications in HST scenarios that have been discussed in the previous sections considerably affect many design choices for an actual system. The choice between relay- and direct link approach is aggravated by the fact that many of the presented aspects are interdependent, thus influencing each other. In this section, these dependencies are discussed from the train- and the mobile-operators' point of view.

##### Technical Aspects

The interior of a train is characterized by many objects such as seats and baggage racks as well as passengers that reflect or absorb electro-magnetic waves. For a direct-link as well as for the relay approach, this has to be taken into account. The actual position of the user might have an even greater impact than the characteristics of the outdoor link. In the relay approach, only the characteristics of the interior of the carriage have to be considered for the second part of the link. For the direct-link, a possible loss due to penetration through compartment walls needs to be considered. Such path can even be dominant over one passing directly through the window closest to the user, since the penetration through windows might show a strong dependence on the angle of incidence. This has to be considered in the modeling of the direct-link channel. Possible shadowing of a train passing by in the opposite direction constitutes a further issue, that might be included as a possible environment scenario, which occurs with a certain probability.

The selection of the carrier frequency also considerably impacts the overall system-performance. The most relevant options are:

- Licensed bands (i.e., LTE-A frequencies)
- Unlicensed bands (ISM bands)
- Free bands in mmWaves

On the one hand, licensed bands allow the access to mobility management. On the other, distinct bands might experience a considerably different interference environment. In rural scenarios, the interference from neighboring BSs can become a major issue, while for ISM bands, due to the limited EIRP, and due to the lack of close interferers, the interference will be smaller. The limitation of the radiated power could be compensated with the deployment of very cost efficient RRUs along the tracks, being spaced at very short distances. The application of mmWave is currently a hot topic for dense static deployment scenarios, however their applicability for high mobility scenarios has yet to be scrutinized<sup>3</sup>. A possible application could be to radiate mmWaves from the tracks (i.e., from surface level) to the train base (assuming antennas being installed there).

---

<sup>3</sup>An example for an initiative, discussing the usage of mmWave in train scenarios, is IEEE 802.15 IG HRRRC

The choice of a relay- or a direct-link approach also strongly impacts the optimal placement and antenna orientation of the RRUs. While aligning the transmitter radiation directions along the tracks work well in combination with relays, a positioning off the tracks with an antenna orientation perpendicular to the track-orientation can be beneficial for the direct-link approach, as it may overcome issues with a shallow angle of incidence, causing high penetration loss through the windows.

### **Operator View**

Besides all the technical aspects, mobile operators will also take economical factors such as capital expenditure (CAPEX) and operational expenditure (OPEX), political issues, necessary cooperations and complexity of implementation into consideration. The two key players in an HST scenario are the railway operators and the mobile operators, whose perspectives might considerably deviate from each other.

For a mobile operator, the direct-link comes with the benefit of not having to rely on additional hardware being installed on the train. Thus, their system for supplying wireless access becomes more independent. The train-types only have to grant the expected penetration characteristics. Additionally, the mobile operator has all options for mobility management as opposed to a relay scenario with WiFi on the second part of the link. A railway operator might also favor the direct approach, once for not being obligated to install and maintain additional hardware, but more importantly for not having to deal with any legal issues when trains are crossing borders. For both sides this approach comes with the benefit of a reduced necessity for synchronizing with each other.

Along with this first decision comes the question of average performance, that should be supplied to the passengers. Most importantly this affects the optimal placement and distance of the RRUs. The total amount of RRUs and connected hardware along the tracks (e.g. control entities, acquired sites) defines the CAPEX and OPEX of the whole system. Thus, the RRU spacing needs to be optimized for granting the required performance while minimizing the cost. Modifying the carriages might therefore change the cost picture completely, but thereby offloading some of the cost to the railway operator. For example, installing windows with a low penetration loss or carriages with electro-magnetic apertures (as demonstrated in Fig. 4.2) and employing the direct-link approach will enable to significantly increase the spacing of the RRUs, thus reducing CAPEX and OPEX substantially.

An interesting question for mobile operators is whether the deployed hardware should also be used to supply the vicinity of the train tracks. From a cost perspective, this can be profitable but, simultaneously, it increases the complexity of network planning.

For railway operators, it is beneficial to keep control over mobile communications which is the case when the task for supplying wireless access for their trains is not completely handed off to



a mobile operator. For one, the target of mobile operators is mostly to achieve a good coverage with minimal effort. Thus, they will concentrate on lucrative parts of highly frequented routes. The railway operator on the other hand has the goal to provide coverage for the whole rail network, with a minimum performance guaranteed everywhere. Thereby, the competitiveness of the railway operator is consistently increased, as the additional service is provided comprehensively. Currently, interest among railway operators is increasing to employ the hardware for mobile communications also for conveying control data for the trains. Since this aspect will be critical for the security of the system, it will be the operators desire to ensure the *dependability* of the communication system including aspects such as stringent latency constraints. From this perspective, many aforementioned arguments need to be reevaluated. For example, railway operators typically do not buy their own licensed frequency bands. On the other hand, freely accessible bands such as the ISM bands come with the disadvantage of unpredictable interference, which is not feasible for security relevant systems.

## 4.2. Parameter Calibration of Simulations through Channel Measurements

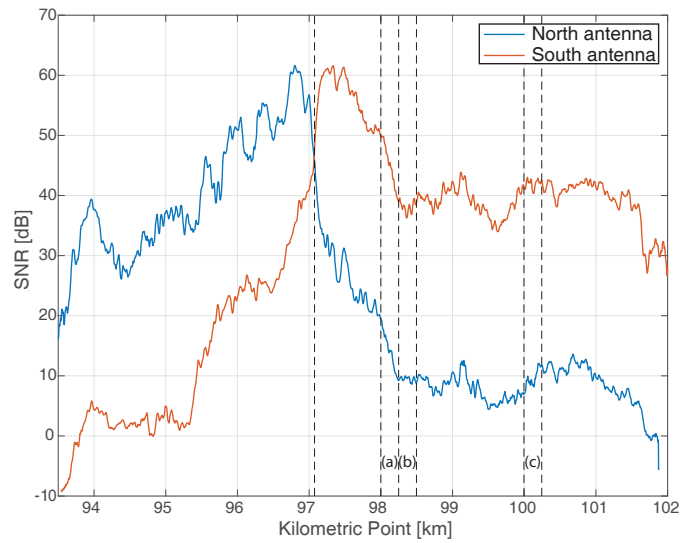
Following these general considerations for wireless communications in HST scenarios, I now discuss the feasibility of SL simulations for investigating the performance in said scenarios. Therefore, I present a comparison of performance results directly based on measured channels by the research group of the Department of Computer Engineering (GTEC) at the University of A Coruña and presented in [33] with results obtained with the Vienna LTE-A System Level Simulator (SLS). This comparison acts as a proof of concept, that SL simulations yield relevant results when investigating HST scenarios, even though the aforementioned abstractions in form of propagation models (cf. Chapter 2) and further link abstractions for simulating the transmission in a SL simulator are applied.

### 4.2.1. Measurement Environment and Procedure

I will give a brief introduction of the measurements, discussing the most important details for my comparison in the following. For a more detailed description please refer to [33]. The measurements were carried out in the south of Spain on a segment between KP 93.0 and 102.0, with a two-sector BS located at KP 97.075. A map of this train segment can be found in Fig. 4.4a. Each sector antenna was installed on 20 m height and radiated along the tracks and they were facing in exactly opposite directions in azimuth. The carrier frequency was set to 2.6 GHz and the BS transmitted a Long Term Evolution (LTE) signal of 10 MHz bandwidth. The transmit power was 46 dBm, but I am only interested in relative received power values, as it will be explained later. The receive antenna was mounted on top of the train roof, which means the signal does not experience penetration loss for



(a) Map of the measurement environment  
- BS position indicated with a green dot.



(b) Measured SNR for both sector antennas for the whole track.  
The BS is located at KP 97.075

**Figure 4.4.:** The two figures show the measurement track utilized in [33] and the corresponding measured SNR for the northern and southern sector antenna. It can be observed that even in back-fire direction of the respective sector antenna, the SNR is still considerably high. Map Image by ©2017 DigitalGlobe, Cartography Institute of Andalucía, Map Data by ©2017 Google, National Geographic Institute of Spain.

entering the carriage. The measurements were carried out at different speeds, whereas I only consider results for a train speed<sup>4</sup> of 200 km/h.

As of the time of the measurement, the used frequency band was otherwise unoccupied. Thus, the only source of interference was of one sector on the other, stemming from the back-fire direction of the transmit antenna. This can be seen in Fig. 4.4b, where the SNR of one receive antenna is shown for the full stretch of the measurement segment. The blue curve shows the SNR when using the transmit antenna facing north, the red curve using the transmit antenna facing south. As it can be seen, the SNR is considerably higher when the train is in the main radiation direction of the respective transmit antenna, but the difference between the SNR from northern and southern antenna is rather constant with 30 dB.

Due to the high SNR larger than 20 dB, the LTE frames could be correctly synchronized which is a necessity for accurately estimating the wireless channel response. For this estimation, the pilot symbols in the LTE transmit frame were utilized. Due to continuous transmission, the wireless channel was estimated along the whole train path.

The thus obtained channel traces are then used in a post-processing step to acquire corresponding CQI and throughput values. Note that throughput results were not obtained directly from the measurements since the transmit data were not known a priori, but only afterwards, using the channel traces. Therefore, the GTEC 5th generation of mobile networks (5G) Simulator was used [32]. The simulator creates a simpler OFDM signal but with almost similar characteristics as LTE regarding, e.g., fast Fourier transform (FFT) size or resource grid structure. To avoid saturation of the CQI, the interference power is boosted artificially by 15 dB (channel variations are left unchanged). All possible CQIs are transmitted and the largest successful transmission is regarded as actual transmission, which mimics perfect feedback without any feedback delay. I consider single-input single-output (SISO) transmission, i.e., one transmit and one receive antenna.

### 4.2.2. Necessary Adaptations of the Simulator

Several adaptations have to be performed in order to simulate the measurement scenario in the Vienna LTE-A SLS. Firstly the geometry has to be included in the simulation setup. Therefore, I place a user at the according distance and let it move away from the BS with a speed of 200 km/h. Usually, the noise power spectral density and the transmit power for all BSs is an input parameter for the simulator. Since I want to set the simulator parameters such that I obtain the SNR and signal to interference ratio (SIR) at the receiver - which are the values known from the measurement (cf. Fig. 4.4b) - I have to set these values relatively to each other. For a given position and a given path loss exponent and offset (w.r.t. the desired sector antenna), I then set the noise power spectral density and the path loss offset for the link of the interfering sector to the user in such a way, that the desired SNR and SIR

---

<sup>4</sup>Note that only measurement points with constant speed are considered.

values are obtained at the initial user position. These values have to be set differently for each user position.

The path loss exponent can be calculated *globally* (for the whole trace), as it was done in [33]. There, the simplified distance dependent path loss is defined as

$$\widetilde{\text{PL}}(d) = b + 10\gamma \log_{10}(d) + X_{\sigma} \quad (4.1)$$

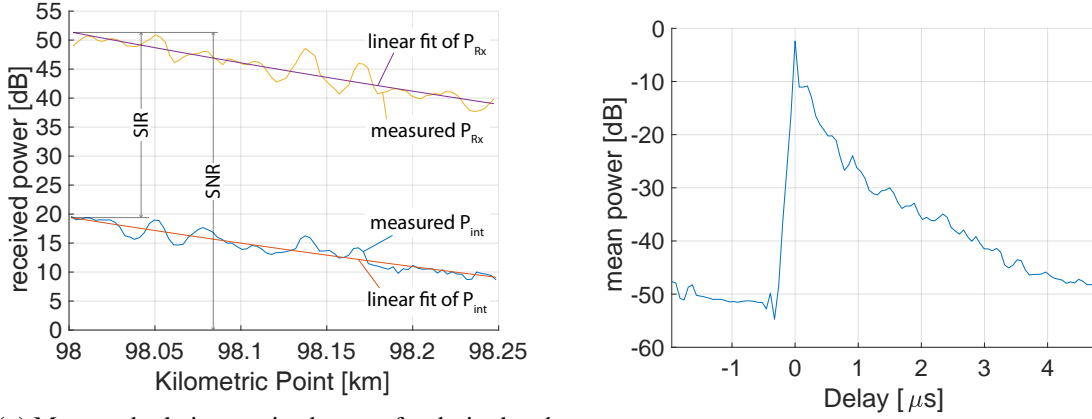
where  $d$  is the link length,  $\gamma$  the path loss exponent and  $b$  corresponds to the path loss at breakpoint distance. The shadow fading is combined in  $X_{\sigma}$ , but is omitted for my further considerations. We take the values for  $\gamma$  and  $b$  from the estimation in the reference for desired and interfering link and adjust both values for  $b$  (one for desired and one for interfering link) according to SIR and SNR at the respective train segment. This can also be done *locally*, only fitting the specific segment of the measurement. An example for this is shown in Fig. 4.5a where the SNR for the transmit antenna of the southern sector (upper curve) and the northern sector (lower curve) is shown, including a linear fit. Since the fit is performed in a logarithmic scale, the slope of the curve directly corresponds to the path loss exponent of the log-distance path loss model. The offset is determined at the first point of the trace.

The channel traces, in form of wireless channel taps for each quasi-LTE symbol, need to be adapted as well, in order to be imported into the simulation. Since the time-frequency granularity of the simulator is on resource block (RB) basis, I utilize every 12th subframe (with a random offset) and average seven symbols in time, to represent the channel for one RB. When brought in this form, the channel traces can directly be used in the simulation for the desired sector and the interfering sector. Next to this direct input, there is also the option to generate new channels with similar characteristics. Therefore, I use the average power delay profile (PDP) of the particular trace and utilize this in the channel factory of the simulator, which is based on [100].

### 4.2.3. Comparison of Results

The results obtained through LL simulations and through SL simulations are compared in terms of throughput for three different positions:

- (a)  $\triangleq$  KP 98.00 - 98.25 km: Strong change in SNR
- (b)  $\triangleq$  KP 98.25 - 98.50 km: Strong channel variations
- (c)  $\triangleq$  KP 100.25 - 100.50 km: Almost constant SNR, small channel variation



(a) Measured relative received power for desired and interfering sector for position (a), including linear fit; SNR and SIR at first point used for simulator-parametrization.

(b) Average PDP for position (a). It is averaged over all subcarriers and the delay is normalized to the maximum value.

**Figure 4.5.:** These two figures show the extracted values from the channel traces for (a) setting the path loss exponent and (b) the simulator's channel factory, that is based on the PDP.

These positions are also indicated in Fig. 4.4b. For the SL simulations, several combinations are utilized to show the influence of the individual aspects. The following options are considered:

- Path loss exponent estimated from
  - (a) the whole trace
  - (b) the considered segment of the trace
- Feedback delay of
  - (a) 0 ms (no feedback delay)
  - (b) 1 ms
- Channel traces directly imported or generated from PDP

I do not however consider all permutations of these parameter options, but only show the result for five sets. The corresponding outcome for the LL simulations and the SL simulations are shown in Figs. 4.7 to 4.12.

In Fig. 4.7 throughput results from LL simulations with the GTEC 5G Simulator are displayed. Note that the temporal resolution per point is 10 ms for these results. The blue curves show throughput over train location (in KP), the red curve indicates the average throughput for the corresponding segment.

Due to the assumption of perfect channel knowledge and CQI choice, there are only successful transmissions.

The first set of SL simulations is shown in Fig. 4.8. These results resemble the LL setup most accurately, since they use the measured channel traces, do not impose any feedback delay and use the path loss exponent estimated from the actual segment. It can be seen that (1) throughput trends over distance are preserved (especially visible for location (a)) and (2) that the average throughput results are in good accordance (only 5%-8% difference).

Results for using the path loss exponent estimated globally, as done in the reference, are shown in Fig. 4.9. The decreasing trend of the throughput is then no longer visible, which is especially obvious in Figs. 4.9a and 4.9c.

The effect of increasing the feedback delay to 1 ms is quite drastic, as it can be seen in Fig. 4.10 and especially in Fig. 4.10b which corresponds to a segment with large channel variations. From the overestimation of CQI values, an increased amount of failed transmissions, and on the other hand a reduced throughput when using a lower CQI than the channel would support. To visualize this, I show in Fig. 4.6 the throughput for position (b) with the corresponding CQI offset with the utilized CQI for transmission and the actually estimated CQI for the corresponding channel access. It can be seen that the used CQI is up to 4 values too high and six values too low. Comparing the two figures, it clearly shows that more failed transmissions occur where the CQI difference is large. Even though there is a drop in average throughput compared to the LL results, it is not as drastic as it may seem (mostly because of the 1 ms resolution of the results) - the relative amount of failed transmissions is below 10%. The more critical issue here is the increased jitter, which may lead to problems for protocols or applications on a higher layer, that require a reliable connection and a constant packet delay.

Generating channels from the averaged PDP with the simulator's channel factory function leads to even larger variations of the throughput results, while the average remains almost unchanged, when no feedback delay is assumed (cf. Fig. 4.11), and a corresponding severe reduction of average throughput for a feedback delay of 1 ms (cf. Fig. 4.12). The difference here is the fact that channels in the simulator are assumed to be Rayleigh which is clearly not the case in the considered measurement scenario. It can still be seen however, that the average throughput remains the same since the channel fluctuates around the same mean as before.

Regarding the simulation complexity, it can be said that the direct simulations are very detailed and require even for such a simplistic scenario (one desired and one interfering BS and a single user) a considerable amount of simulation time, in the range of hours. The SL simulations on the other hand only require around 1.5 minutes simulation time.

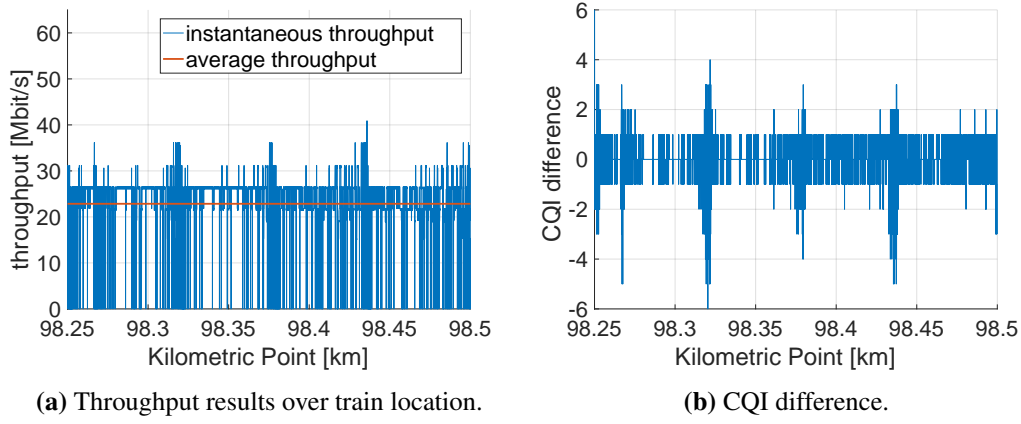


**Figure 4.6.:** Throughput (left) and CQI difference (right) for Position (b). Transmission has 371 failed transmissions from 4 430 total; Corresponding CQI difference calculated by subtracting CQI used for transmission and actually estimated CQI for the corresponding time instance.

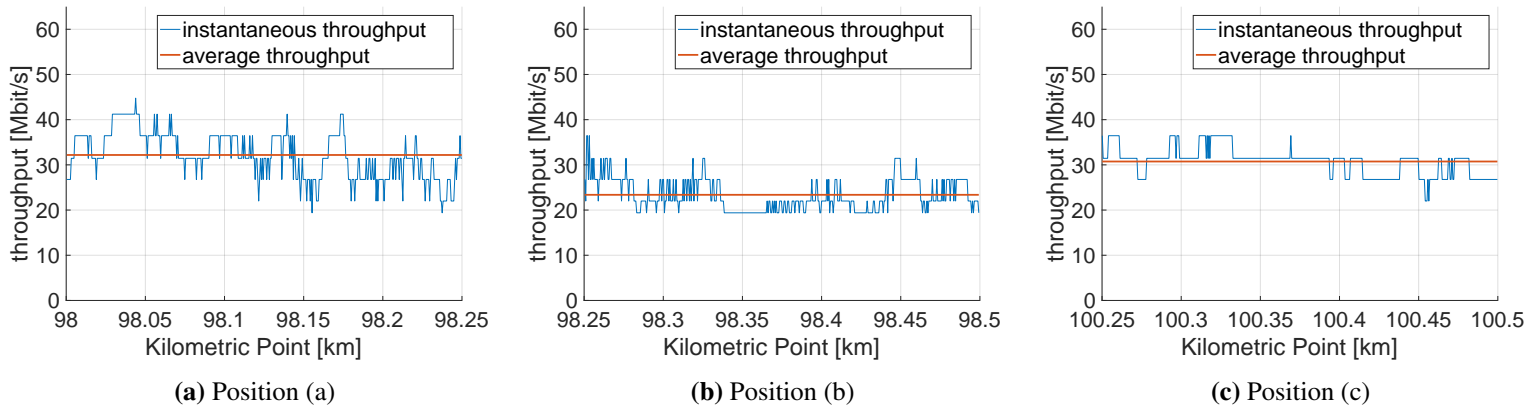


**Figure 4.7.:** Throughput results obtained from LL simulations for all three considered positions.

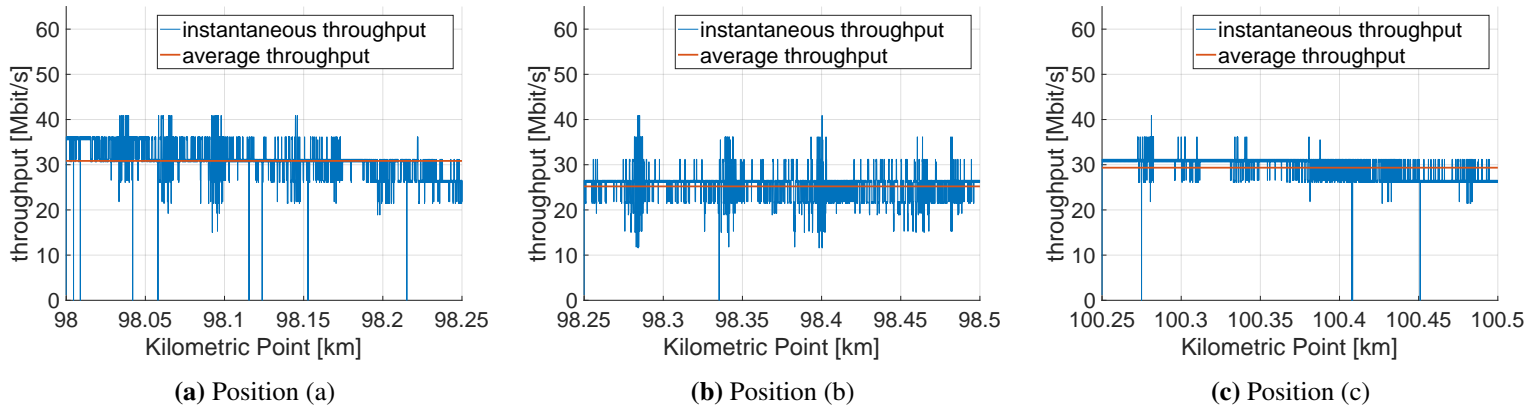


**Figure 4.8.:** Throughput results obtained from SL simulations for all three considered positions, with locally fitted path loss exponent, no feedback delay and direct channel trace input.



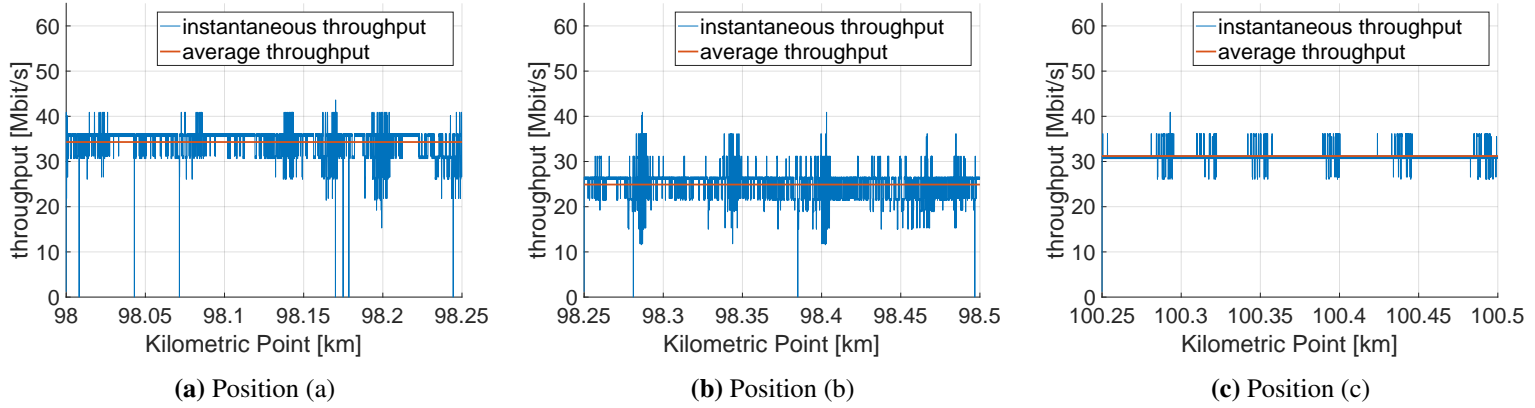


**Figure 4.9.:** Throughput results obtained from SL simulations for all three considered positions, with globally fitted path loss exponent, no feedback delay and direct channel trace input.

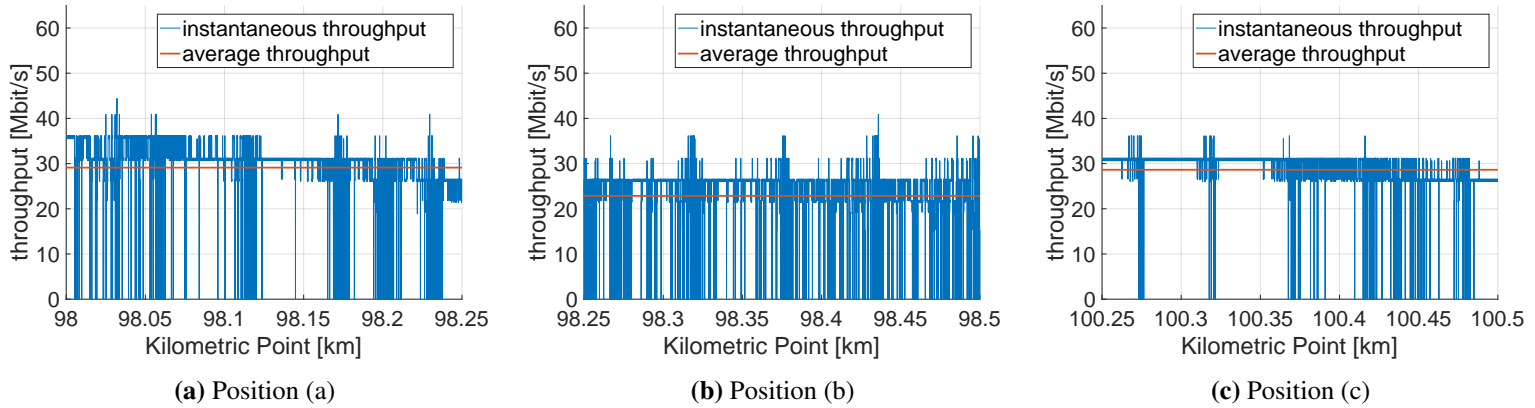


**Figure 4.10.:** Throughput results obtained from SL simulations for all three considered positions, with locally fitted path loss exponent, 1 ms feedback delay and direct channel trace input.

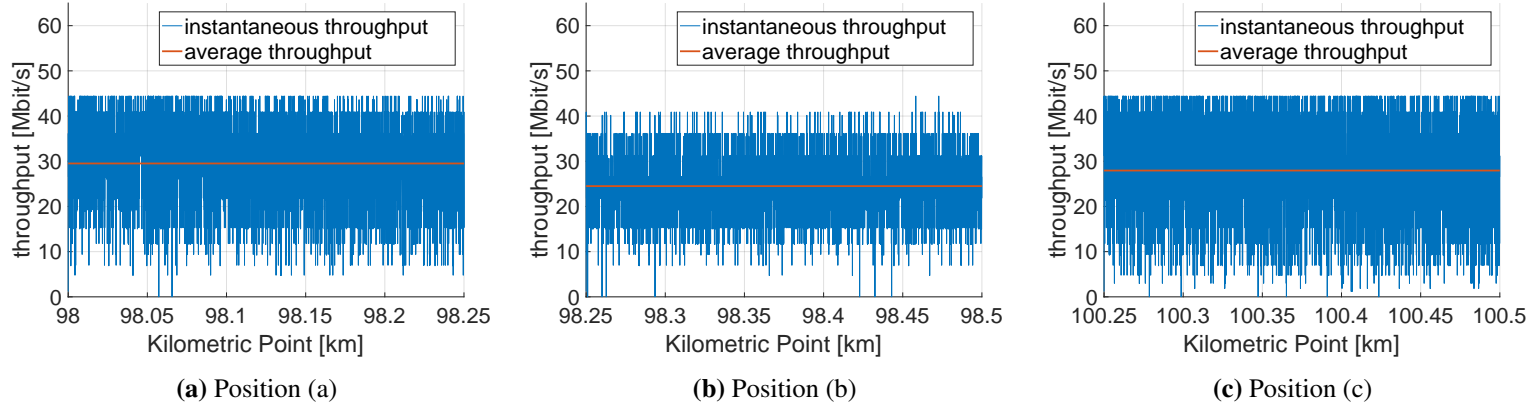


**Figure 4.11.:** Throughput results obtained from SL simulations for all three considered positions, with locally fitted path loss exponent, no feedback delay and channel generated based on PDP.

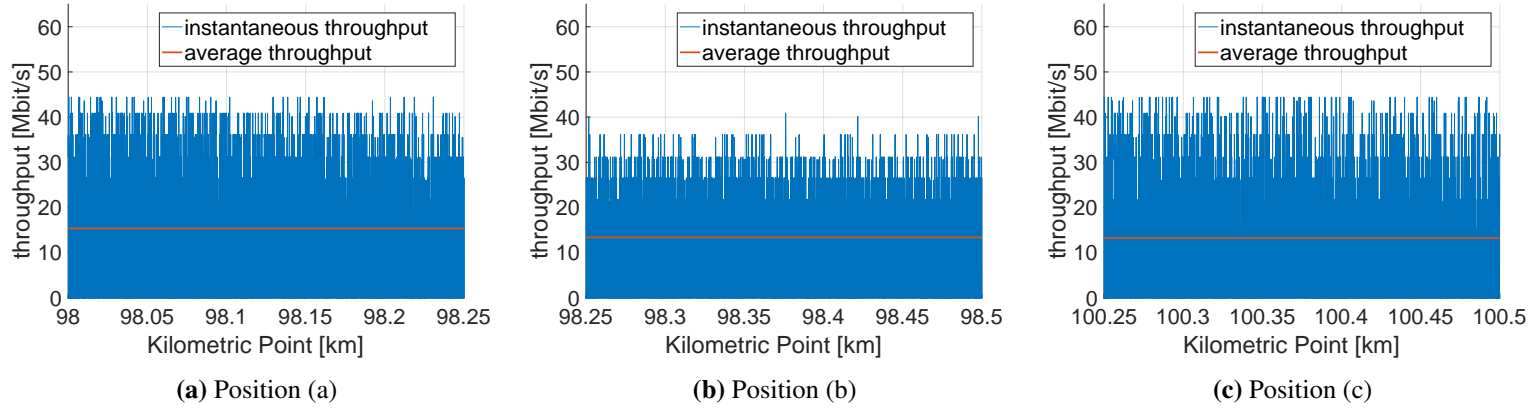


**Figure 4.12.:** Throughput results obtained from SL simulations for all three considered positions, with locally fitted path loss exponent, 1 ms feedback delay and channel generated based on PDP.

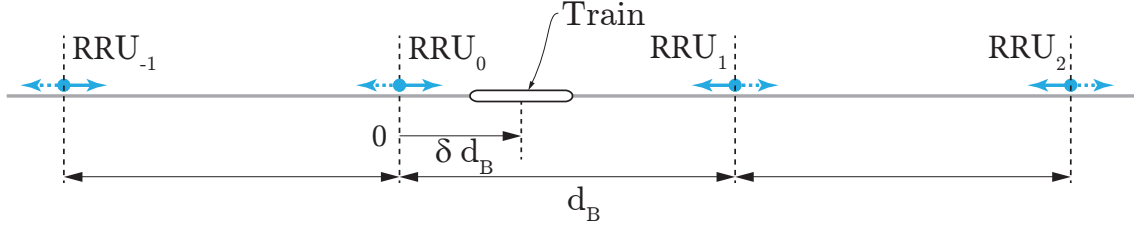


**Figure 4.13.:** Representative segment of a railroad track with four equidistantly spaced sites. Each site employs two RRUs pointing in opposite directions. RRUs depicted as dashed lines are omitted in the analysis. The user is located at position  $\delta d_B$  relative to  $RRU_0$ . ©2015 IEEE, [69].

### 4.3. Performance Improvement of Remote Unit Collaboration Schemes

Installing an additional relay on the train, to facilitate the communication, is an approach that has already been extensively discussed in literature [82, 85, 97]. The possibility of a direct communication between the base station and the passenger on the other hand has been neglected until now, despite it having numerous advantages (cf. Section 4.1).

Therefore, in this section, I first examine the impact of various RRU collaboration schemes on the user receiver performance when moving in HSTs without relay nodes. I consider an RRU deployment along the rail-road track and compare the schemes in terms of average spectral efficiency. To do so, my contribution is twofold: First, I propose a theoretical model to investigate the performance of RRU coordination and -cooperation. It is based on the sum of Gamma random variables and leads to convenient mathematical expressions. Secondly, I evaluate the performance under realistic conditions with the Vienna LTE-A System Level Simulator [77].

In the last part of this section, I then present simulation results for a comparison between the relay and the direct link approach.

#### 4.3.1. System Model

Consider a representative segment of an RRU deployment along a railroad track, which comprises four equidistantly spaced sites, each equipped with two RRUs, pointing in opposite directions, as shown in Fig. 4.13. The train is assumed to move between  $RRU_0$  and  $RRU_1$ , and its center position is expressed relative to  $RRU_0$  as  $\delta d_B$ , with  $0 < \delta < 1$ . The nodes  $RRU_{-1}$  and  $RRU_2$  serve as dominant interferers. For simplicity, all other sources of interference are neglected. Due to antenna directivity, some RRUs are ignored in the analysis, as indicated by dashed arrows in Fig. 4.13.

There are several ways to associate BSs with the RRUs. In this work, I investigate three schemes:

1. **Baseline.** All RRUs employ different cell IDs, i.e., are attached to different BSs. Then,

$$\begin{aligned} \mathcal{S} &= \{\text{RRU}_0\}; \mathcal{I} = \{\text{RRU}_{-1}, \text{RRU}_1, \text{RRU}_2\} \quad , 0 < \delta < 0.5 \\ \mathcal{S} &= \{\text{RRU}_1\}; \mathcal{I} = \{\text{RRU}_{-1}, \text{RRU}_0, \text{RRU}_2\} \quad , 0.5 < \delta < 1. \end{aligned} \quad (4.2)$$

2. **Coordination.**  $\text{RRU}_0$  and  $\text{RRU}_1$  are attached to different BSs and coordinate their transmission such that they do not interfere each other. Then,

$$\begin{aligned} \mathcal{S} &= \{\text{RRU}_0\}; \mathcal{I} = \{\text{RRU}_{-1}, \text{RRU}_2\} \quad , 0 < \delta < 0.5 \\ \mathcal{S} &= \{\text{RRU}_1\}; \mathcal{I} = \{\text{RRU}_{-1}, \text{RRU}_2\} \quad , 0.5 < \delta < 1. \end{aligned} \quad (4.3)$$

3. **Cooperation.**  $\text{RRU}_0$  and  $\text{RRU}_1$  are associated with the same BS and coordinate their transmission such that both can be exploited as useful signal. Then,

$$\begin{aligned} \mathcal{S} &= \{\text{RRU}_0, \text{RRU}_1\}; \mathcal{I} = \{\text{RRU}_{-1}, \text{RRU}_2\} \quad , 0 < \delta < 0.5 \\ \mathcal{S} &= \{\text{RRU}_0, \text{RRU}_1\}; \mathcal{I} = \{\text{RRU}_{-1}, \text{RRU}_2\} \quad , 0.5 < \delta < 1. \end{aligned} \quad (4.4)$$

To make a fair comparison, it is assumed that the transmit power per BS is limited to  $P_T$ , i.e.,

$$\sum_{\{i | \text{RRU}_i \in \mathcal{S}\}} P_i^{\text{Tx}} \leq P_T. \quad (4.5)$$

In order to clarify the impact of the RRU deployment on the performance, no sophisticated power allocation techniques are applied. In the *cooperation* scheme, associated- and interfering RRUs transmit with half power in each direction.

#### 4.3.2. Theoretical Model for SIR Calculation

For the analysis, the signal from  $\text{RRU}_i$  is assumed to experience a log-distance dependent path loss law  $\ell_i(\delta)$  with exponent  $\alpha = 2$  (i.e., free space propagation) and Gamma distributed small-scale fading,  $G \sim \Gamma[N_{\text{Tx}}, \theta]$ , which corresponds to maximum ratio transmission (MRT) with  $N_{\text{Tx}}$  transmit antennas and  $\theta$  as scale parameter of the fading distribution. The relevance of the Gamma distribution is explained by the facts that it includes several important channel models such as Rayleigh and Nakagami-m as special cases and further allows to accurately approximate composite fading distributions such as Rayleigh-Lognormal [52].

The received power from  $\text{RRU}_i$  at a user at relative position  $\delta$  is expressed as

$$P_i^{\text{Rx}}(\delta) = P_i^{\text{Tx}} G_i \ell_i(\delta), \quad (4.6)$$

where  $P_i^{\text{Tx}}$  denotes the transmit power of  $\text{RRU}_i$ . Assuming that the penetration loss into the train carriage is constant, it can be omitted in the analysis since the scenario is considered interference limited and signal and interference are attenuated equivalently.

Applying MRT corresponds to a best case scenario in terms of desired signal power and a worst case in terms of interference. The corresponding aggregate received powers are

$$S(\delta) = \sum_{\{i|\text{RRU}_i \in \mathcal{S}\}} P_i^{\text{Rx}}(\delta), \quad (4.7)$$

$$I(\delta) = \sum_{\{i|\text{RRU}_i \in \mathcal{I}\}} P_i^{\text{Rx}}(\delta), \quad (4.8)$$

where  $\mathcal{S}$  and  $\mathcal{I}$  refer to the set of desired and interfering RRUs as obtained from Eqs. (4.2) to (4.4), respectively. These expressions correspond to weighted sums of Gamma random variables (RVs). Sticking to integer-valued shape parameters, which correspond, e.g., to the number of antennas per RRU under the assumptions of MRT and Rayleigh fading, allows to employ the generalized integer gamma (GIG) distribution [24, 88]. It yields expressions of the form  $\sum_k a_k x^{b_k} e^{c_k x}$  for both desired signal- and aggregate interference distributions, respectively. Then, the distribution of the SIR  $\gamma(\delta) = S(\delta)/I(\delta)$  generically formulates as

$$f_\gamma(\gamma; r) = \sum_s \sum_i a_s a_i \gamma^{b_s} (c_i + c_s \gamma)^{-i-b_s-b_i} \Gamma(i + b_s + b_i). \quad (4.9)$$

*Proof.* Assume that the fading is distributed according to a Gamma RV with integer shape parameter. Then, the distributions of Eqs. (4.7) and (4.8) can be evaluated by applying the GIG distribution. We obtain sums of elementary functions of the form  $a x^b e^{-c x}$ , where the auxiliary parameters  $a, b$  and  $c$  fulfill  $a \in \mathbb{R}$ ,  $b \in \mathbb{N}^+$  and  $c > 0$ . Thus,  $f_S(\gamma; r)$  and  $f_I(\gamma; r)$  can generically be written as

$$f_S(\gamma; r) = \sum_s a_s \gamma^{b_s} e^{-c_s \gamma}, \quad (4.10)$$

$$f_I(\gamma; r) = \sum_i a_i \gamma^{b_i} e^{-c_i \gamma}, \quad (4.11)$$

and allow to straightforwardly evaluate

$$f_\gamma(\gamma; r) = \int_0^\infty z f_S(z \gamma; r) f_I(z; r) dz, \quad (4.12)$$

as

$$\begin{aligned} f_\gamma(\gamma; r) &= \sum_s \sum_i \int_0^\infty z a_s (z \gamma)^{b_s} e^{-c_s (z \gamma)} a_i z^{b_i} e^{-c_i z} dz \\ &= \sum_s \sum_i a_s a_i \gamma^{b_s} (c_i + c_s \gamma)^{-i-b_s-b_i} \Gamma(i + b_s + b_i). \end{aligned} \quad (4.13)$$

□

The spectral efficiency is defined by the well known expression  $\tau(\gamma(\delta)) = \log_2(1 + \gamma(\delta))$ . Its distribution is straightforwardly obtained by a non-linear, monotone transformation of RVs applied on Eq. (4.9) as

$$f_\tau(\tau; \delta) = \ln(2)2^\tau f_\gamma(2^\tau - 1; r). \quad (4.14)$$

Since the length of the train is typically in the same order of magnitude as the inter-RRU distance, it is not reasonable to represent all passengers by a single point. I apply the following procedure for performance evaluation. First, I determine the average spectral efficiency at each user position between  $\text{RRU}_0$  and  $\text{RRU}_1$ . Then, I assume the users to be uniformly distributed within the train. Intuitively, the train thus acts as a *sliding window* for the moving average over the single users' performances. The result is an average spectral efficiency value for each train position, also referred to as *train average spectral efficiency* in the remainder of this chapter.

For numerical evaluation, I consider a setup as illustrated in Fig. 4.13 with  $d_B = 1\,000$  m. The train has a length of 200.84 m, corresponding to a German "ICE 3" train. Each RRU employs two transmit antennas and each user is equipped with one receive antenna. Results in terms of train average spectral efficiency for each RRU collaboration scheme are provided in Fig. 4.14, represented by the dashed curves.

It is observed that

- Cooperation universally yields the best performance. Note that this scheme completely avoids handovers in the region of interest.
- Coordination shows a slightly lower performance than cooperation, particularly when approaching the middle between two RRUs. In practical systems coordination is typically far less complex than cooperation since only control data has to be exchanged between the BSs. Moreover, it is less prone to the impairments of codebook based precoding (CBP), as detailed in Section 4.3.3. The kink at  $\delta = 0.5$  stems from the RRU switching.
- The baseline scheme yields the worst performance even when the train is close to one of the RRUs, as  $\text{RRU}_0$  and  $\text{RRU}_1$  severely interfere each other. Again, the kink at  $\delta = 0.5$  results from switching the association of all users from  $\text{RRU}_0$  to  $\text{RRU}_1$ .

These results are obtained under the assumption that each RRU chooses its MRT beamformer independently. However, more realistic setups, such as a current LTE-A system only offer codebooks with a limited number of precoders, which typically distribute the available transmit power uniformly over all transmit antennas.

The resulting train average spectral efficiency from the simulations is indicated by the solid curves in Fig. 4.14 and is discussed in the following.

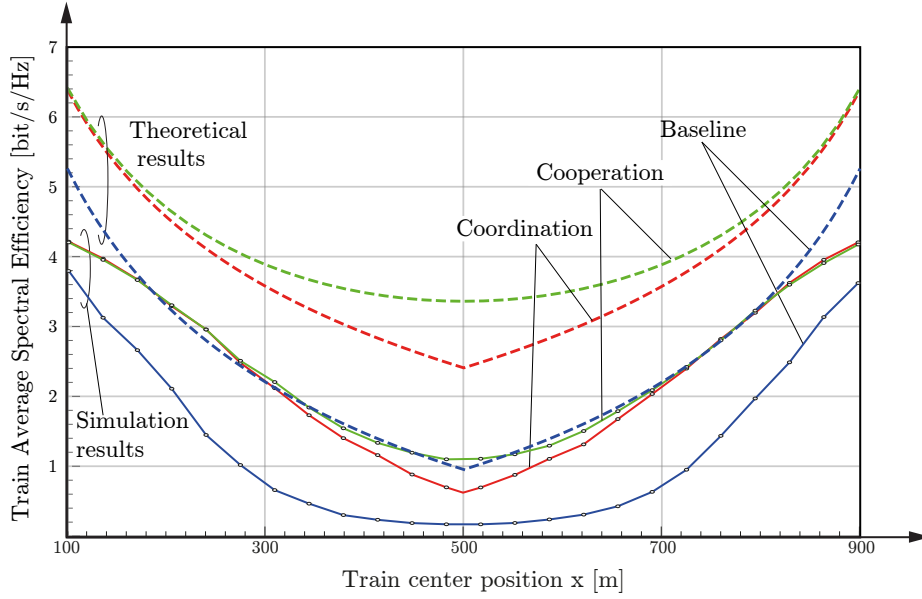


**Figure 4.14.:** Train average spectral efficiency in [bit/s/Hz] over train center position. Blue-, red- and green curves correspond to baseline-, coordination- and cooperation scheme, dashed- and solid curves refer to results of theoretical model and simulation, respectively. ©2015 IEEE, [69].

#### 4.3.3. Simulation Results and Necessary Approximations

##### Simulation Setup

For simulations I consider a German ICE 3 train of length 200.84 m, width 2.95 m and 460 seats in total. I assume 230 active users and employ a full-buffer traffic model. The users are distributed within the train according to a uniform random distribution.

RRUs dynamically assign to BSs, according to the collaboration scheme. Each BS has a total transmit power of  $P_T = 40$  W. The signal between BS and user experiences path loss, small scale fading and penetration loss. I employ the *rural* path loss model of the TS 36.942 specification [4], representing the typical propagation environment for a train traveling through the countryside. The small scale fading is modeled by an ITU 'Vehicular A' channel [56], which is designated for receivers inside moving metal objects. Although other literature on high speed train scenarios commonly employs a variation of the Winner Phase II model [74], it is not applicable in my case, since it was designed for moving objects with relay-units. Finally, I account for the penetration loss into the carriage by a constant of 30 dB [62]. Further simulation parameters are provided in Table 4.1.

**Table 4.1.:** Simulation Parameters. ©2015 IEEE, [69].

Parameter	Value
System bandwidth	20 MHz
Carrier frequency	2.14 GHz
Inter-RRU distance	1 000 m
BS transmit power $P_T$	40 W
Antennas per RRU	2
MIMO mode	CLSM
Path loss model	TS 36.942 'rural' [4]
Channel model	ITU-R Vehicular A [56]
Train speed	200 km/h
Receiver type	zero forcing
Noise power spectral density	- 174 dBm/Hz
Receiver noise figure	9 dB
Train length	200.84 m
Active users	230
user distribution within train	uniform
Antennas per user	1
Traffic model	full buffer
Scheduler	proportional fair
Channel knowledge	perfect
Feedback	MCS: CQI; MIMO: PMI and RI
RRU backhaul connection	radio over fiber, no delay



## Simulation Results

The simulation results are provided in Fig. 4.14 in terms of train average spectral efficiency together with the 95%- confidence intervals. Note that the figure is symmetrical as is the setup. The simulation has been performed over the full range of train positions to capture possible inaccuracies. It is observed that similar to the theoretical model, the cooperation scheme universally yields the highest performance. This finding has also been obtained in comparable studies, which assumed the trains to be equipped with relay nodes [74]. However, the coordination scheme is less complex in its installation and only grants a slightly reduced performance. On the other hand, handovers occur more often, which might pose a problem for high speeds. Concretely, for a train, traveling at 200 km/h and an inter RRU distance of 1 000 m, this would be the case every  $1\,000\text{ m} / 55.5\text{ m/s} = 18\text{ s}$ . While theoretically supported by the standard, such frequent handovers would cause considerable overhead on the air-interface and the backhaul. The cooperation scheme has the advantage of avoiding handovers, since  $\text{RRU}_0$  and  $\text{RRU}_1$  are assigned to the same BS. If interpreted as a system with a moving cell [38], handovers can be reduced to one per 50 km. This comes at the price of higher complexity in terms of synchronization.

The lowest performance is obtained with the baseline scheme, which also exhibits the fastest deterioration over distance. However, as opposed to the results from theory, it does not show a kink in the middle between two RRUs. This is caused by the fact that in the simulator, users are assigned to the BS with the highest receive power. Consequently, for train center positions between 400 m and 600 m, one fraction of the users will associate with  $\text{RRU}_0$ , while the rest will be assigned to  $\text{RRU}_1$ , respectively. If the users were forced to stay attached to one of the RRUs, the performance would even decrease in this region.

The kink for the result of the coordination scheme however is still present, because this result has been merged from two simulation runs - one assuming  $\text{RRU}_0$  to be active and  $\text{RRU}_1$  to be inactive and one vice versa.

## Adaptation due to Precoding Loss

Comparing the simulation results with the results of the theoretical model in Fig. 4.14, we recognize that the theoretical model accurately captures the performance trends of the different collaboration schemes. However, it is observed that it also grants a higher spectral efficiency than obtained with the simulations. I claim that this behavior mainly stems from the limited choice of precoders in the LTE-A codebook as opposed to MRT in the theoretical model. Moreover, the cooperation scheme has to select a single uniform-power precoder for all four transmit antennas of the cooperating RRUs. Hence, power is wasted when the train is close to one of the RRUs, and would better be served by only a single RRU.

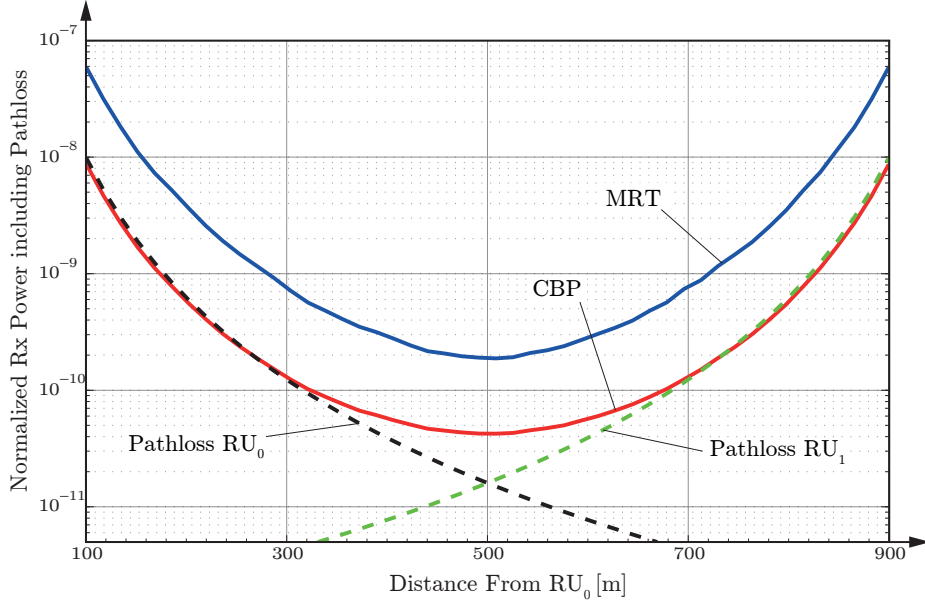


**Figure 4.15.:** Average receive power for MRT and CBP and inverted pathloss for RRU<sub>0</sub> and RRU<sub>1</sub>. ©2015 IEEE, [69].

To quantify the degradation due to the suboptimal precoder choice, I compare the performance of MRT and CBP at a single user and all positions between RRU<sub>0</sub> and RRU<sub>1</sub>. Referring to Eq. (4.7), define  $S_{MRT}$  and  $S_{CBP}$  as the corresponding combined received powers. The channel has dimension  $2 \times 1$  for baseline- and coordination scheme, and  $4 \times 1$  for cooperation, respectively. The resulting received powers are averaged over 2000 channel realizations per user location and are shown in Fig. 4.15 together with the corresponding path loss values from each RRU. Between 300 m and 700 m a considerable deviation from the pathloss is observed, as both RRUs significantly contribute to the received signal in this range.

I denote the ratio  $S_{MRT} / S_{CBP}$  as *precoding loss*, and plot it in Fig. 4.16. Interestingly, the values are almost invariable over all user locations and roughly differ by a factor of two. This result is valid for arbitrary exponential path loss laws. Note that the precoding loss acts on the receive power and thus is not directly applicable on the train average spectral efficiency.

Finally, I adjust the transmit powers of my theoretical model. According to Fig. 4.16, I assume a constant precoding loss of 6.75 for cooperation and 3.52 for baseline and coordination, respectively. The results are depicted by the dashed curves in Fig. 4.17 together with the same simulations results as in Fig. 4.14. It is observed that the results show a considerable improvement in accordance. The remaining gap is caused by various practical design constraints of an LTE system such as Adaptive Modulation and Coding and scheduling (see [80]), which are not incorporated in the theoretical model. Thus, my theory reasonably predicts the throughput performance of passengers in high speed trains and validates results in a highly elaborated simulation environment.

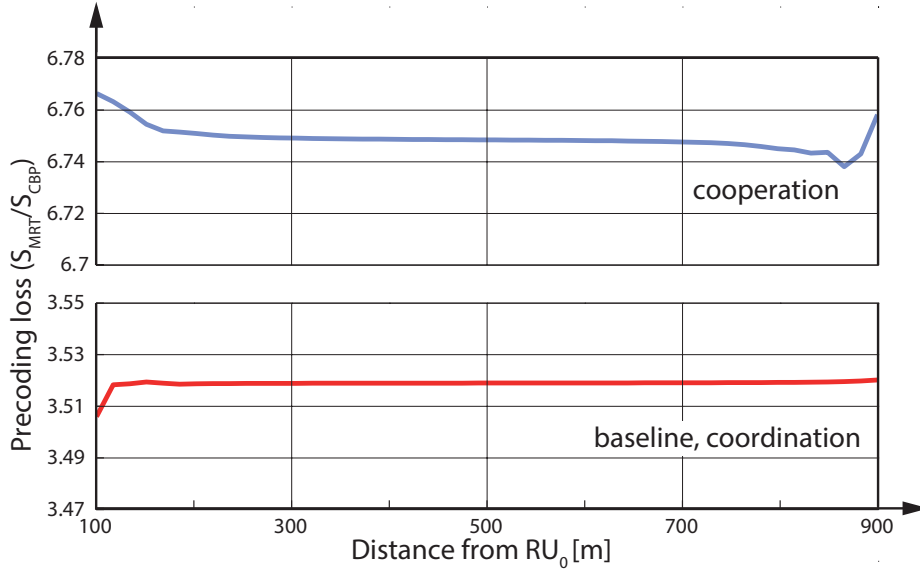


**Figure 4.16.:** Precoding loss calculated as the ratio between the average receive powers of MRT and CBP. Lower curve corresponds to loss for baseline- and coordination scheme, upper curve refers to cooperation, respectively. Note the almost flat curve despite the small scale. ©2015 IEEE, [69].

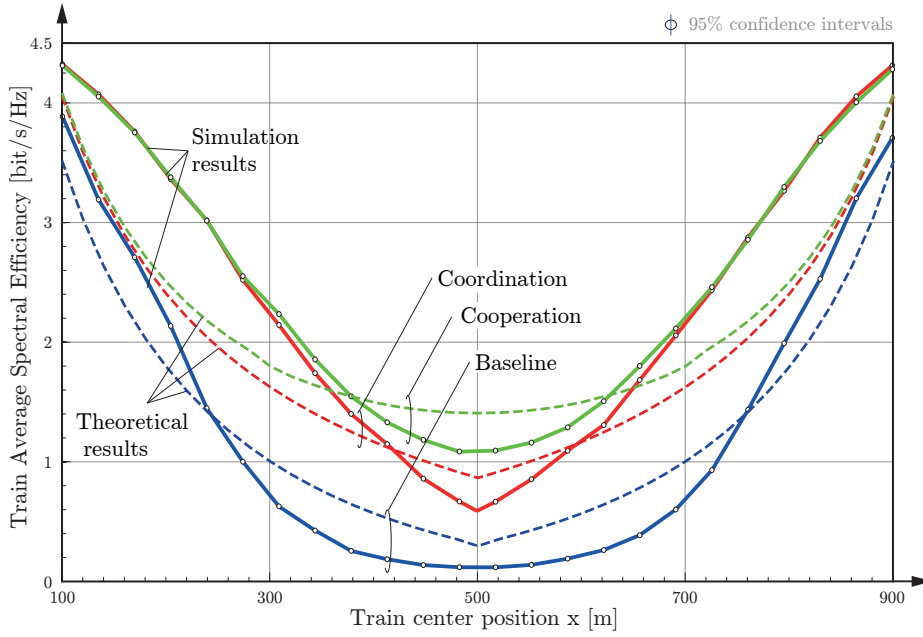


**Figure 4.17.:** Train average spectral efficiency in [bit/s/Hz] over train position in [m]. Solid curves correspond to simulations, dashed curves refer to the theoretical model with incorporated precoding loss, respectively. ©2015 IEEE, [69].

**Table 4.2.:** Simulation parameters for comparison.

Parameter	Value
Train speed	250 km/h
Active users	46
Penetration loss	30 dB

#### 4.3.4. Simulation Results for Relay and Direct Link Setup

In order to compare the relay- and the direct link setup, LTE-A system level simulations are carried out. The system model is similar to the one of the previous section with only a few changes. I consider the baseline scenario and the cooperation scheme. A fully occupied German ICE-train with 460 passengers is regarded, 10% of them are having an active wireless connection. For the direct-link setup a penetration loss of 30 dB is applied referring to the mean value of the aforementioned penetration losses. For the relay setup, no penetration loss is considered, but the whole train is accumulated in a single user. The simulation parameters are the same as in Table 4.1, divergent parameters are summarized in Table 4.2. Simulations are again performed with the Vienna LTE-A SLS.

Simulation results are shown in Fig. 4.18 in terms of average user throughput over center position of the train. Since the throughput at the relay represents the cumulative throughput of all active users, the results for the relay-setup were normalized to 46 (users) for a fair comparison. Dashed lines represent the baseline scheme, solid lines the cooperation scheme. Comparing the performance of relay (circular marks) and direct-link setup (triangular markers), employing relays improves the performance roughly by a factor of two. This gain is surprisingly low, considering that the UEs in the direct setup experience a penetration loss of 30 dB, and the relays are operating under ideal conditions (e.g., no processing delays, no overhead). The direct link approach comes with the advantage of providing a scheduling gain, since the BS can choose from a larger pool of users, and not only a single relay. Taking into account further aspects as discussed in Section 4.1.4, makes the direct-link approach a notable alternative. The results also demonstrate that the performance can be improved by advanced collaboration schemes. The throughput peaks in the vicinity of the base stations can be exploited by a sophisticated scheduler scheme. In regard of the traffic-type, users with delay sensitive data could be assigned resources such that their requirements are fulfilled. Users with best-effort traffic models could mostly be served when the train is closer to an RRU and a higher total data rate is available (cf. [67]).

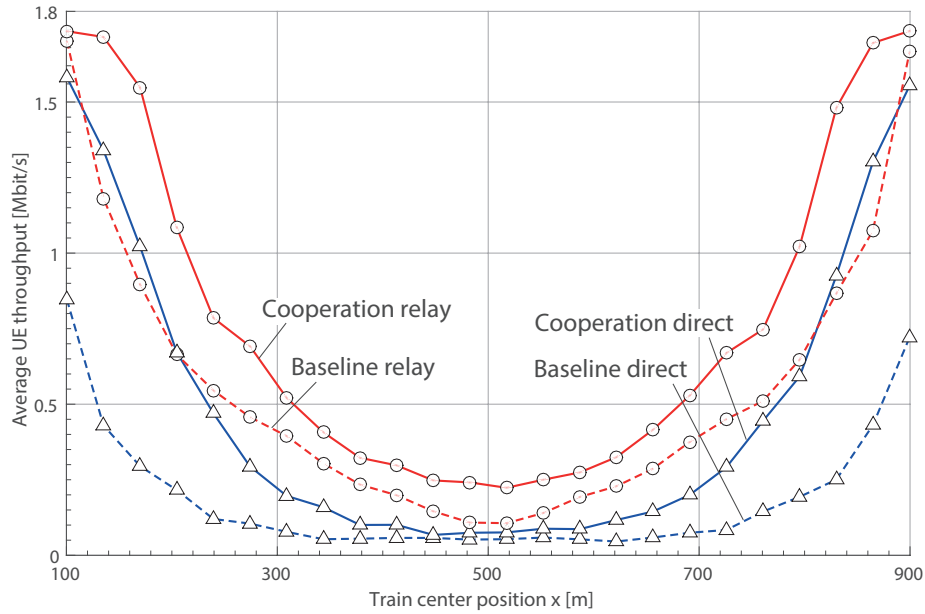


**Figure 4.18.:** Train average throughput [Mbit/s] versus train center position [m]. Curves refer to results for baseline- and cooperation scheme among RRUs for relay- and direct-link setup. ©2015 IEEE, [70].

## 4.4. Summary

This chapter deals with HST scenarios and their particularities and discusses ideas and results for how to improve the supply of passengers with mobile broadband access. Next to a discussion of new concepts I verify my simulation approach by comparing LL and SL simulations based on measured channel traces and show the potential of RRU collaboration schemes based on an analytical model and simulation results.

In Section 4.1, I discuss the critical issues of HST scenarios such as propagation effects (e.g., high doppler due to high speeds) and high user densities. The comparison of utilizing relays on the train versus direct communication between RRUs and users is presented in detail from several points of view - not only technical but also regarding preferences of railway and network operators. Additionally, I introduce ways of alleviating the problem of frequent handovers.

Section 4.2 contains a comparison of performance results obtained “directly” via LL simulations, utilizing actually measured channels for transmitting a signal equivalent to the LTE frame structure with results from extensively abstracted SL simulations. It can be said that even though several simplifications are included in the SL simulations, the performance results show good accordance when the simulations are initialized with the corresponding parameters (around 5% difference in average throughput). SL simulations furthermore allow for the inclusion of further effects such as feedback delay and only take a fraction of computing time.

Finally, in Section 4.3, I study the potential of collaboration among RRUs. The main focus here is on the description of the SIR, for which I define an analytical model based on the network geometry and Gamma distributed small scale fading. It turns out that assuming MRT in the analytical model leads to a large discrepancy with the simulation results, which stems mostly from the fact that CBP is used in the simulator. When adjusting for this offset, the results lie in the same range and display similar trends.

In critical retrospective, there are some aspects that could be revised. The path loss considerations for the LL vs. SL comparison do not account for the antenna pattern in the SL simulations, which does not reflect the distinguishable propagation effects of the real setup. Even though challenging to incorporate separately, including the antenna pattern would enhance the agreement of simulation and reality. The assumptions for the analytical model in Section 4.3 are rather simplistic and the accordance between analytical results and simulation results could be improved with further additions to the analytical framework.

Several interesting aspects remain to be investigated. The obtained shape of the throughput curve could be combined with a traffic aware scheduler, e.g., as I described in [67]. Thus, users with delay-sensitive traffic would be served rather consistently, while best-effort user can make use of the excess throughput when the train is closer to a RRU. When the placement of RRUs is considered off the tracks, the possible incidence angles of the signal on the glass windows have a wide range. In combination with an angular dependent penetration loss characteristic, it might be possible to identify an optimal distance from the tracks. The addition of the feedback delay in SL simulations (cf. Fig. 4.10) leads to a jitter in the packet arrival, which is particularly harmful for services that demand high reliability. One possible solution could be to use an adapted CQI decision table that is more conservative and leads to less failed transmissions.

## Chapter 5.

# Performance Evaluation of Indoor Cellular Networks

As counterpart to the previous chapter, where the focus was on the mobility of users (as train passengers), I now present performance results for indoor wireless cellular networks. This scenario is in so far interesting because for one, a massive increase of demand for indoor users is expected (cf. [23]) and secondly, compared to "classical" cellular networks, the propagation is heavily influenced by blockages in the form of walls. Therefore, I focus in this chapter on methods for including this effect in the performance investigation of indoor cellular networks and leverage techniques from random shape theory and stochastic geometry (as partially already introduced in Chapter 2) to include wall blockages in the system model.

Based on my work in [68, 71–73], the contributions presented in this chapter are:

- Section 5.1 discusses similar approaches to the one in my thesis and gives a short overview on related work.
- In Section 5.2, I investigate the influence of wall generation methods on the performance of an indoor wireless cellular network. These methods vary in terms of mathematical tractability and realism (i.e., how well do the created scenarios resemble the layout of a real-world building). I vary the placement and orientation of walls and investigate the performance in terms of signal to interference ratio (SIR) and signal to interference and noise ratio (SINR) based on a theoretical model as well as on system level simulations. Here, I choose a regular base station (BS) placement with a fixed inter-BS distance.
- In Section 5.3, I then move from SIR performance and fixed BS placement, to a more flexible scenario with random and regular BS placement with varying density. Thus, I answer the question, how the area spectral efficiency (ASE) depends on the wall volume in the scenario and the number of BSs per area. This metric is especially interesting for a network operator who wants to assure a certain performance or who wants to estimate how many users can be served by a given number of BSs.

## 5.1. Introduction

There are various ways how to assess the network performance in indoor scenarios, when including the effect of blockages. One option is to use ray-tracing [47, 48, 60]. This approach however comes with the drawback, that results are only obtained for a specific environment and the amount of necessary a priori knowledge about the scenario is extensive<sup>1</sup>. These aspects prohibit an analytical study, where a certain degree of abstraction is necessary. Well known models for shadowing effects, such as log-normal shadowing [42] entail the problem of ignoring the distance dependency of the blockage attenuation. Considering blockages as concentrated objects avoids this issue and has been done, e.g., in [17] by using a Manhattan line process (MLP) to model a wireless network, thus including distance dependency as well as spatial correlation among blockages. Further work on blockages in urban scenarios focuses on placing simplified buildings within the region of interest (ROI) [18, 86, 87]. While already part of the mentioned work, the important effect of blockages on the distinction between line of sight (LOS) and non line of sight (NLOS) is studied in detail in [36, 76].

In [61], authors include the correlation among blockages, but only a rather regular building structure is assumed and the derived expressions become quite involved. Since most of the further existing work concentrates on urban environments, indoor cellular networks are not thoroughly explored in terms of system level performance. Therefore, I focus in this chapter on the impact of wall blockages on the network performance and do so by proposing various wall placement methods in Section 5.2, and on the BS placement in Section 5.3.

## 5.2. Impact of Wall Generation Methods on Indoor Network Performance

### 5.2.1. System Model

#### Transmitter and Receiver Constellation

I consider a finite square-grid of transmitters (Tx) with spacing  $R$ , as shown in Fig. 5.1a, and denote this arrangement as [square]. I also scrutinize a second setup, where the Tx constellation is rotated (around the central Tx) by an angle of  $\pi/4$ . It is depicted in Fig. 5.1b and referred to as [rhomboid]. The impact of this rotation is not obvious a priori. It will become evident when the Tx are interacting with the wall objects. These fixed transmitter arrangements are chosen, in order to simplify the analysis by knowing the actual relative positions of all transmitters for all receiver positions.

---

<sup>1</sup> Additionally, specific parameters have to be known precisely, such as the wall material or absorption values - when changing these input parameters only slightly, results may already vary significantly.



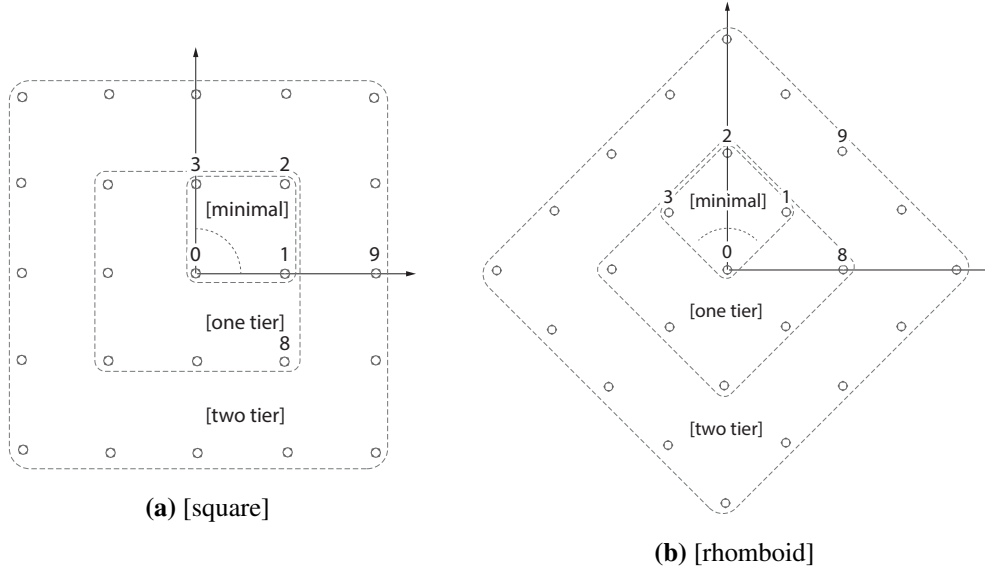


**Figure 5.1.:** Transmitter arrangements and tier setups. Dotted circular line denotes receiver locations. ©2016 IEEE, [71].

The receiver (Rx) is considered to be located at distance  $d_0 = R/2$  away from the origin. For tractability, it is assumed to be associated with its *closest* Tx, which I denote as desired transmitter (dTx). The surrounding Txs are denoted as interfering transmitter (iTx) and are labeled as  $iTx_i$ . Thus, Rx represents a user at the cell-edge. Due to the constant radius, I simply denote the Rx position by the angle  $\Phi$  between the lines Rx-dTx and dTx- $iTx_1$  (cf. Fig. 5.2). In polar coordinates, the positions are given as  $(R/2, \Phi)$ , with  $0 \leq \Phi \leq \pi/2$ . Due to symmetry, results for the whole angular range are periodically repeated.

I examine three different Tx tier setups: The [minimal] setup only contains the three closest interferers  $iTx_1$ ,  $iTx_2$  and  $iTx_3$ . For the [one tier] setup I include all iTxs for  $1 \leq i \leq 8$  (the first tier of interferers). Consequently for the [two tier] setup I consider all 24 interferers depicted in Fig. 5.1. Comparing these three setups, I later show the impact of including different numbers of tiers on the network performance (cf. Section 5.2.7, Fig. 5.11).

### Signal Propagation

I focus on downlink transmissions and assume that the signal from a Tx to the Rx experiences distance-dependent path loss, penetration loss due to wall blockage and small-scale fading. The path loss is abstracted by a log-distance dependent law:  $\ell(d) = 1/c d^{-\alpha}$ . The attenuation due to the walls is determined by aggregating the attenuation values of the individual walls. For future work, more sophisticated attenuation models will be included [99]. Rayleigh fading is applied on each

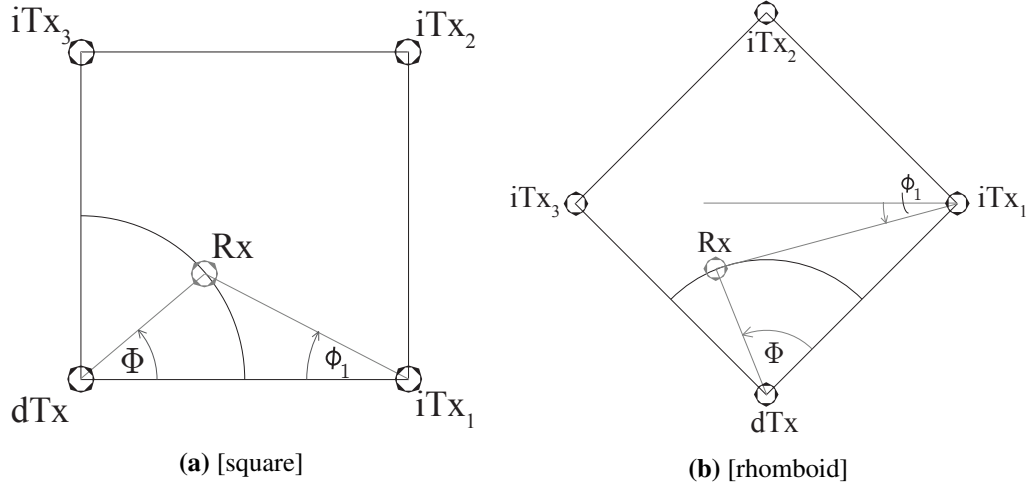


**Figure 5.2.:** Illustration of the angle for Rx position  $\Phi$  and the relative angle for  $iT_x_i$ ,  $\phi_i$ . Note the differences between the [square] and [rhomboid] transmitter arrangement. ©2016 IEEE, [71].

link independently to account for the multi-path propagation effects. It is denoted by  $h_i$  for link  $i$ . The channel gain is then exponentially distributed according to  $h_i \sim \exp(\mu)$ , where  $\mu = \mathbb{E}[h_i]$ . The scenario including the blockages is assumed to be *two-dimensional*. Furthermore, the scrutinized network is considered to be interference limited, also since we consider the frequency range below 6 GHz with corresponding penetration loss values. Therefore, interference is not completely blocked by walls and still has a significant influence on the SINR (which might no longer be the case for transmissions in the mmWave band). This assumption will be verified by extensive Monte Carlo simulations in Section 5.2.7.

Wall blockages are combined with equal weight in the total wall attenuation of a link. When defining  $w_l$  with  $0 \leq w_l \leq 1$  as multiplicative factor, representing the wall loss of the  $l$ -th wall, then the total attenuation added by walls on a particular link  $i$  connecting Rx and  $Tx_i$  is

$$\hat{\omega}_i = \prod_{l=1}^{K_i} w_l, \quad (5.1)$$

where  $K_i$  corresponds to the total number of walls blocking the link. According to this definition, all walls can thus have different attenuation values. For the sake of simplicity, I set all individual wall attenuation values to  $w_l = w$  for the remainder of this work. Consequently, Eq. (5.1) can be reformulated as

$$\hat{\omega}_i = w^{K_i}. \quad (5.2)$$

Note that  $K_i$  is a *discrete* random variable (RV) and, hence,  $\hat{\omega}_i$  is also a *discrete* RV.

### 5.2.2. Wall Generation Methods

For generating an indoor environment comprising of wall blockages, I employ several methods ranging from conveniently tractable Boolean schemes to a practical floor plan generator. My goal is to evaluate the applicability of the tractable models, which are commonly specified by a small set of parameters. Examples for the respective methods can be found in Fig. 5.3.

#### Random 2D Wall Placement

For generating walls with 2D random center positions, I utilize a Boolean schema that was already introduced in Section 2.3.3. Each wall can thus be described by the triple  $\{\mathbf{C}_i, L_i, \theta_i\}$ . Here,  $\mathbf{C}_i$  describes the center location, which is scrutinized from a homogeneous Poisson point process (PPP). The individual length of each wall  $L_i$  is independently chosen from an arbitrary distribution  $f_L(l)$  with mean  $\mathbb{E}[L]$ . Also the wall orientation angle  $\theta_i$  is independently sampled from the wall angle distribution  $f_\Theta(\theta)$ . I consider two possible angular ranges, from which  $\theta$  is sampled. For one, I choose  $\theta$  from a uniform distribution on the interval  $[0, \pi)$ . The second option is a binary choice from the set  $\{0, \pi/2\}$  with equal probability. I denote these two models as [uniform] and [binary] (cf. Figs. 5.3a and 5.3b). While not realistic by appearance, the [uniform] method represents the most random wall placement, while for [binary] all walls are either parallel or perpendicular, which is closer to a real floor plan than completely random wall orientations.

#### Random 1D Wall Placement (Manhattan Grid)

For the third method, I assume the walls to have infinite length<sup>2</sup> and to be oriented perpendicularly to the coordinate axes. Their centers are considered to be distributed according to one-dimensional PPPs along each axis, with density  $\lambda'$ . Hence, I obtain two independent MLPs, one for each dimension. Their superposition, combining all walls together, is denoted as [MLP] (cf. Fig. 5.3c).

#### Regular Wall Placement

The fourth method is realized by fixing the distance between two parallel walls in the MLP to a certain value  $\Delta$ , yielding a regular grid of walls. For achieving random realizations with this model, I introduce a random shift of the whole grid by  $\delta_x$  and  $\delta_y$  in x- and y direction, with  $\delta_x \sim \mathcal{U}[-\Delta/2, \Delta/2]$  and  $\delta_y \sim \mathcal{U}[-\Delta/2, \Delta/2]$ . I denote this method as [regular] (cf. Fig. 5.3d).

---

<sup>2</sup>for simulations with a finite ROI, I assume walls to span the whole length of the x- or y-dimension.

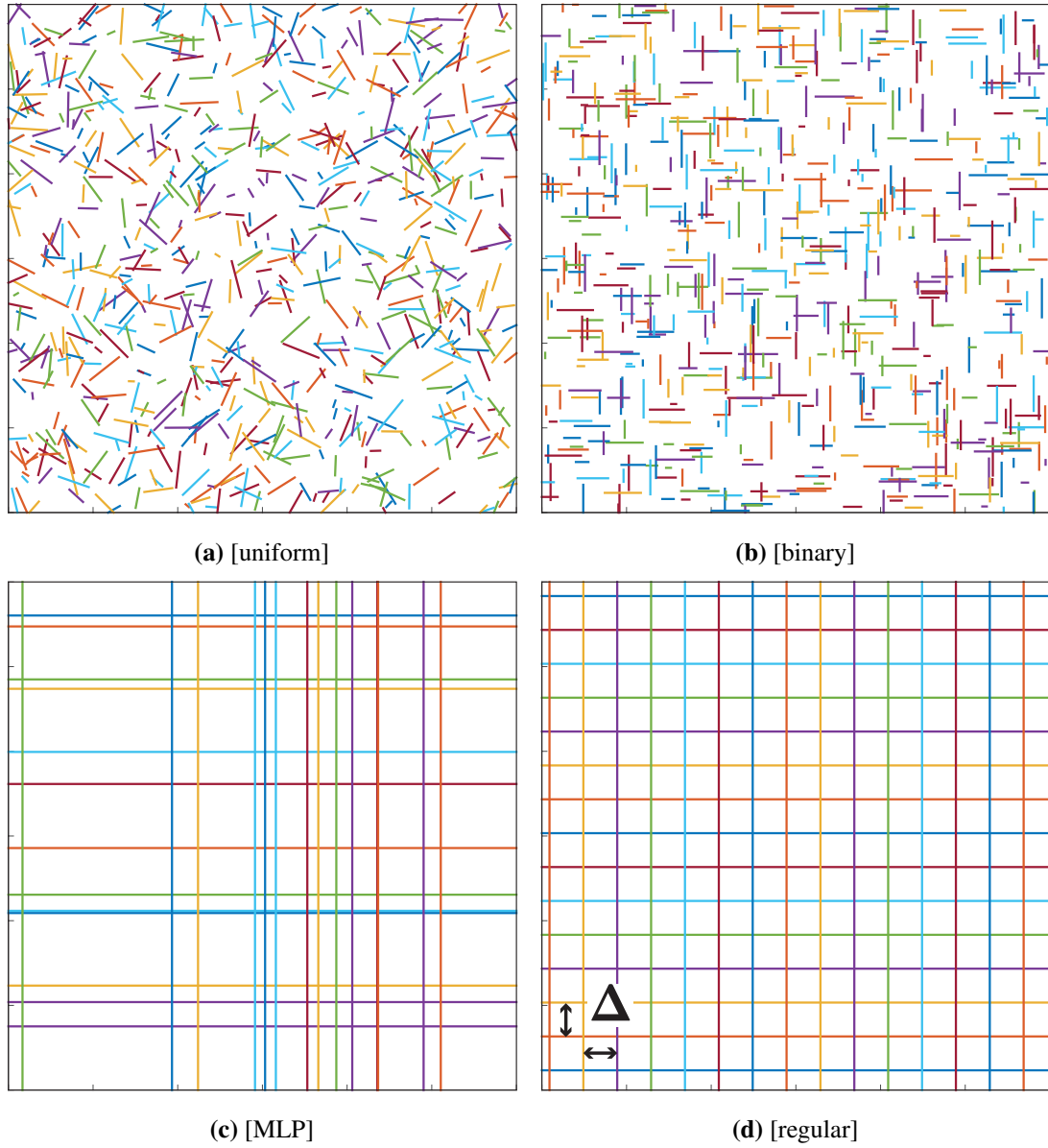


**Figure 5.3.:** Examples for scenarios created with (a) [uniform], (b) [binary], (c) [MLP], (d) [regular] wall generation method; scenarios were created with parameters that lead to same average wall volume. In (d), the random shift of the regular grid by  $\Delta$  is indicated. ©2016 IEEE, [71].

### Wall Placement through Floor Plan Generator

With the fifth method, I aim at generating *realistic*, yet reproducible indoor scenarios. One option would be to resort to algorithms for generating floor plans as they are used in architecture, e.g., in [20]. The drawback of these algorithms is however, that they generally require specific pre-knowledge (e.g., correlation of room positions for different room types) or the resulting floor plans introduce a non-homogeneous wall density based on the room placement. Therefore, I employ a generic algorithm, that divides the ROI in rectangles of arbitrary size which do not overlap and cover the whole area. Thus, in contrast to [MLP], also shorter walls can occur, but in contrast du [binary], cannot overlap. To achieve this, the ROI is iteratively separated in smaller and smaller rectangles. This algorithm is described in detail in Algorithm 1. There, the variable  $n$  specifies the number of global iterations and mainly defines the number of rooms in the ROI. Without any constraints, this algorithm leads to  $4^n$  rooms of arbitrary size. To avoid a very large discrepancy between the biggest and the smallest room and also rooms with a large ratio of longer to shorter side, several limitations are introduced for each recursion:

- The position of the separator point  $(x_r, y_r)$  is forced to be within the central area of the rectangle, relative to its dimensions  $x_s$  and  $y_s$ , such that  $\mu x_r < x_s < (1 - \mu)x_r$ , with  $\mu$  representing the relative *boundary distance* and  $0 < \mu < 1$ . A similar condition is introduced for  $y_s$ .
- The absolute size of  $x_s$  and  $y_s$  is limited to arbitrary values  $x_{\min}$  and  $y_{\min}$ . If the dimension of any of the newly generated rectangles is smaller than these values, this separator point is discarded and the rectangle is not divided anymore.
- To avoid that very large rectangles remain, there are  $n_{\text{rep}}$  possible repetitions to find a suitable separator point that does not violate the minimal dimensions. Thus, the second condition will not stop the division immediately when a separator is chosen close to the border of the considered rectangle.

As discussed later, the number of rooms is calibrated heuristically. It turned out, that a convenient way of fine-tuning the average attenuation is not to change the already mentioned parameters, but for a constant set of  $\mu$ ,  $x_{\text{lim}}/y_{\text{lim}}$  and  $n_{\text{rep}}$  to change the dimensions of the ROI,  $X \times Y$ . The same number of rooms is then distributed on a smaller or larger area. An example for a floor plan generated according to this algorithm can be found in Fig. 5.4. I refer to this generation method as [practical].

#### 5.2.3. Comparability of Scenarios in Terms of Wall Volume

Since I compare the performance for several different wall generation methods, I need to ensure that they remain comparable regarding their initializing parameters. In order to do so, I define a *wall*

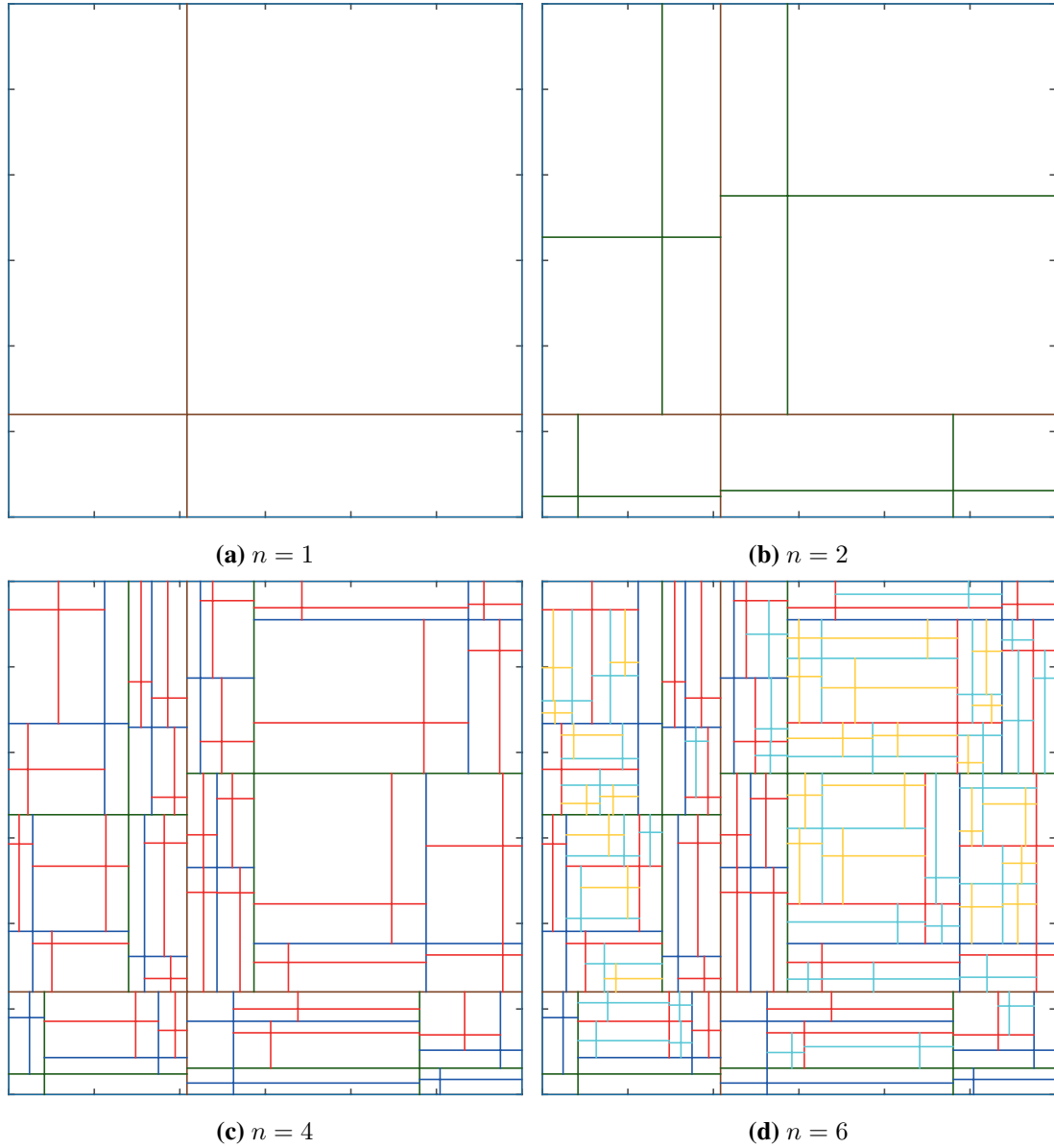


**Figure 5.4.:** Example for generating floor plans for the [practical] wall generation method; displayed are step 1, 2, 4 and 6 of the algorithm. It can be observed that some of the rectangles are not further divided due to the limitation of the minimal room dimensions. ©2016 IEEE, [71].

---

**Algorithm 1:** Floor plan generation algorithm
 

---

```

for  $n$  do
     $n_r = 4^n$ ;
    for  $n_r$  do
        while  $t < n_{\text{rep}}$  do
            generate separator point;
            if  $x_s > x_{\min} \wedge y_s > y_{\min}$  then
                store new rooms;
                 $t = n_{\text{rep}}$ 
            else
                 $t = t + 1$ 
            end
        end
    end
end
    
```

---

volume  $V^{(w)}$ , which is defined as the sum of the length of all walls within the ROI. It is thus defined by

$$V^{(w)} = \sum_i l_i \quad (5.3)$$

where  $l_i$  is the length of the  $i$ -th wall. Under the premise that the average wall volume  $\mathbb{E}[V^{(w)}]$  has to be constant for every wall generation method (not for each individual spatial realization though), the initialization parameters become interconnected among all methods. I do not consider further statistical parameters for generating different spatial realizations and limit myself on this first-order matching.

#### 5.2.4. Average Number of Wall Blockages

The wall volume  $V^{(w)}$  that I defined in Eq. (5.3) is used to parametrize all wall generation methods to obtain comparable scenarios. As a baseline, I utilize the [uniform]- and the [binary]-approaches<sup>3</sup>. In these models, the wall volume is calculated as the product of the wall density  $\lambda$ , the average wall length  $\mathbb{E}[L]$  and the area of the ROI  $A^{\text{ROI}}$ , i.e.,

$$V^{(w)} = \mathbb{E} \left[ \sum_i l_i \right] = \mathbb{E}[L] \lambda A^{(\text{ROI})} = \mathbb{E}[L] \lambda XY. \quad (5.4)$$

---

<sup>3</sup>The orientation does not affect the wall volume and thus the calculation for [uniform] and [binary] is the same

In order to achieve the same wall volume in the [MLP], the one dimensional density  $\lambda'$  is set to  $\lambda' = \lambda/2 \mathbb{E}[L]$ , such that the same wall volume results:

$$V^{(w)} = \mathbb{E}[N_x]Y + \mathbb{E}[N_y]X = \lambda'XY + \lambda'XY = \mathbb{E}[L]\lambda XY, \quad (5.5)$$

where  $N_x$  and  $N_y$  represent the number of walls created for each dimension.

To achieve the same goal in the [regular] case, I set the fixed distance between two walls to  $\Delta = 2/(\lambda\mathbb{E}[L])$  (for walls in x as well as in y direction). Thus, the wall volume results as

$$V^{(w)} = N_xY + N_yX = \frac{X}{\Delta}Y + \frac{Y}{\Delta}X = \mathbb{E}[L]\lambda XY. \quad (5.6)$$

Due to the fixed distances between walls, I have to ensure that the dimensions of the ROI are an integer multiple of  $\Delta$ , such that  $N_x$  and  $N_y$  are integers and the wall volumes is exactly equal to the ones of the other methods.

Along the lines of [18, Theorem 1], the number of walls that obstruct a path of length  $d$  for [uniform], [binary] and [MLP] is a Poisson RV with mean  $\mathbb{E}[K]$ . In general,  $\mathbb{E}[K]$  formulates as

$$\mathbb{E}[K] = \beta d \quad (5.7)$$

where  $d$  is the Euclidean distance between transmitter and receiver and the *blockage factor*  $\beta$  that is specific for each wall generation method. For the [uniform] model, i.e., two dimensional wall center distribution and  $\theta \sim \mathcal{U}[0, \pi)$ , it is calculated as

$$\beta = \lambda \mathbb{E}[L] \frac{2}{\pi} \quad (5.8)$$

For binary wall orientations  $\theta \in \{0, \pi/2\}$ , it is obtained as

$$\beta = \lambda \mathbb{E}[L] \frac{|\sin(\phi)| + |\cos(\phi)|}{2} \quad (5.9)$$

where  $\phi$  corresponds to the absolute angle between the connection of transmitter and receiver and the x-axis.

*Proof.* We begin at the same point as for the uniform wall orientation distribution in [18, Theorem 1], but introduce the relative angle<sup>4</sup> between the connecting line of Tx and Rx and the wall  $\theta' = \theta - \phi$ . The binary distribution of wall angles is given by the probability mass function (pmf)  $f_{\Theta}(\theta)$ :

$$f_{\Theta}(\theta) = 1/2(\delta(\theta) + \delta(\theta - \pi/2)), \quad (5.10)$$

where  $\delta(x)$  represents a Dirac delta distribution.

---

<sup>4</sup>This is not necessary for uniformly distributed wall orientation angles, due to rotational invariance.



The average number of walls, blocking a link of length  $d$  then follows as

$$\begin{aligned}
 \mathbb{E}[K] &= \int_{\Theta} \int_L \lambda d |\sin(\theta')| f_L(l) dl f_{\Theta}(\theta) d\theta \\
 &= \lambda d \mathbb{E}[L]^{1/2} (|\sin(-\phi)| + |\sin(\pi/2 - \phi)|) \\
 &= \lambda \mathbb{E}[L] \frac{|\sin(\phi)| + |\cos(\phi)|}{2} d = \beta d.
 \end{aligned} \tag{5.11}$$

□

This equation can also be interpreted as splitting the wall process into two processes with half the density and one with all walls with orientation  $\theta = 0$  and one with  $\theta = \pi/2$ . The terms  $|\sin(\phi)|d$  and  $|\cos(\phi)|d$  then represent the respective proportion of the length of the connecting line between Tx and Rx in x- and y-direction.

For the MLP, the blockage factor results as

$$\beta = \lambda' (|\sin(\phi)| + |\cos(\phi)|) = \lambda \mathbb{E}[L] \frac{|\sin(\phi)| + |\cos(\phi)|}{2}, \tag{5.12}$$

where  $\lambda' = 1/2 \lambda \mathbb{E}[L]$ . Here, the contribution of two wall processes is already obvious from the construction of the scenario. Note that [binary] and [MLP] have the same blockage factor, but nevertheless, they yield a distinct SIR distribution, as later shown in Section 5.2.7.

For the [regular] method,  $K$  can be interpreted as a sum of two independent, uniformly-distributed RVs with a certain bias. The bias is determined by the relative Tx-Rx positions, as explained in the following. I start out by considering only a single spatial dimension. The number of walls without random shift is determined as  $n_x = \lfloor (d_x - \Delta/2)/\Delta \rfloor + 1$ , where  $d_x = d |\cos(\phi)|$ , respectively. Applying the random shift  $\delta_x$ , the link may experience one wall more or less. For  $\hat{d}_x < \Delta/2$ , where  $\hat{d}_x = \text{mod}(d_x - \Delta/2, \Delta)$ , the probability to experience one wall less is  $(\Delta/2 - \hat{d}_x)/\Delta$ . At the same time, this probability corresponds to the likelihood that the link is blocked by an additional wall for  $\hat{d}_x > \Delta/2$ . Hence, the expected number of additional walls is obtained as  $p_x = (\hat{d}_x - \Delta/2)/\Delta$ . Note that  $-1/2 \leq p_x \leq 1/2$ . Analogously, the additional number of walls  $p_y$  in the y-dimension is determined by applying the above mentioned steps and using  $d_y = d |\sin(\phi)|$ . Then,

$$\mathbb{E}[K] = n_x + n_y + p_x + p_y. \tag{5.13}$$

Due to the nonlinear floor and modulo operator, this expression cannot be simplified. When it is evaluated numerically however, it turns out that  $\mathbb{E}[K]$  for [regular] yields the same result as for [binary] and [MLP] (cf. Eqs. (5.9) and (5.12)). This is later explained in Section 5.2.7 and shown in Fig. 5.8.

The average number of walls for [practical] cannot be determined analytically. To obtain comparable results, the average attenuation (which corresponds to the average number of walls) is heuristically adjusted to be similar to [binary]. This is shown in Section 5.2.7.

### 5.2.5. Performance Evaluation

In this section, I derive expressions for the performance of an indoor Rx for various blockage scenarios. In particular, I scrutinize the SIR as a figure of merit, as it constitutes a basis for further important metrics in the wireless communication context, such as coverage and rate.

#### Instantaneous SIR

Assume an Rx to be located at distance  $d_0$  from its dTx at the origin. Then, for an individual snapshot of an indoor scenario, its *instantaneous* SIR formulates as

$$\gamma = \frac{P_0 h_0 \ell(d_0) \hat{\omega}_0}{\sum_{i=1}^N P_i h_i \ell(d_i) \hat{\omega}_i}, \quad (5.14)$$

where  $P_i$  is the transmit power of  $\text{Tx}_i$ ,  $h_i$  denotes the small-scale fading,  $\ell(d_i)$  is the path loss as specified in Section 5.2.1, and  $N$  is the number of iTxs, with  $N = 3$ ,  $N = 8$  and  $N = 24$  in the [minimal]-, [one tier]- and [two tier] scenario, respectively. For simplicity, I assume that  $P_i = P$ . The terms  $\hat{\omega}_0$  and  $\hat{\omega}_i$  correspond to the instantaneous, total wall attenuation of each link, as defined in Eq. (5.2).

#### SIR Coverage Probability

In the next step, I evaluate the SIR-coverage probability, which represents the likelihood that the instantaneous SIR exceeds a certain threshold  $\delta$ . Eq. (5.14) contains two sources of randomness: (i) the small-scale fading and (ii) the aggregate attenuation due to wall blockages. Given  $K_i$  for  $i = \{0, \dots, N\}$ , I obtain

$$\mathbb{P}[\gamma > \delta | \{K_0, \dots, K_N\}] = \prod_{i=1}^N \frac{1}{1 + \delta \frac{\hat{\omega}_i \ell(d_i)}{\hat{\omega}_0 \ell(d_0)}}, \quad (5.15)$$

*Proof.* For a given wall realization  $\{K_0, \dots, K_N\}$ , it follows

$$\begin{aligned}
 \mathbb{P}[\gamma > \delta | \{K_0, \dots, K_N\}] &= \mathbb{P} \left[ \frac{h_0 \ell(d_0) \hat{\omega}_0}{\sum_{i=1}^N h_i \ell(d_i) \hat{\omega}_i} > \delta \right] \\
 &= \mathbb{P} \left[ h_0 > \frac{\delta}{\hat{\omega}_0 \ell(d_0)} \sum_{i=1}^N h_i \ell(d_i) \hat{\omega}_i \right] \\
 &= \mathbb{E}_{h_i} \left[ \exp \left( -\mu \frac{\delta}{\hat{\omega}_0 \ell(d_0)} \sum_{i=1}^N h_i \ell(d_i) \hat{\omega}_i \right) \right] \\
 &= \prod_{i=1}^N \mathbb{E}_{h_i} \left[ \exp \left( -\mu \frac{\delta}{\hat{\omega}_0 \ell(d_0)} h_i \ell(d_i) \hat{\omega}_i \right) \right] \\
 &= \prod_{i=1}^N \frac{1}{1 + \delta \frac{\hat{\omega}_i \ell(d_i)}{\hat{\omega}_0 \ell(d_0)}}. \tag{5.16}
 \end{aligned}$$

□

Then, the unconditional SIR-coverage probability is obtained as

$$\begin{aligned}
 \mathbb{P}[\gamma > \delta] &= \sum_{k_0=0}^{\infty} \cdots \sum_{k_N=0}^{\infty} \left( \prod_{i=1}^N \frac{1}{1 + \delta \frac{w^{k_i} \ell(d_i)}{w^{k_0} \ell(d_0)}} \right) \\
 &\quad \times p_{K_0}(k_0) \cdots p_{K_N}(k_N), \tag{5.17}
 \end{aligned}$$

where  $p_{K_i}(K_i)$  denotes the pmf of  $K_i$ , with  $i = 1, \dots, N$ . Note that  $1 - \mathbb{P}[\gamma > \delta]$  can be interpreted as the cumulative distribution function (cdf) of the SIR.

For qualitative statements, I further introduce the *average SIR*, which is expressed as

$$\mathbb{E}[\gamma] = \int_{-\infty}^{\infty} \left( -\frac{d\mathbb{P}[\gamma > \delta]}{d\delta} \Big|_{\delta=t} \right) t dt. \tag{5.18}$$

Note that in the following Eq. (5.15) I will employ  $10^{\delta/10}$  instead of  $\delta$  for the following reason. We recall that the instantaneous attenuation  $\hat{\omega}_i$  is found by an exponential function with an RV in the exponent. Such functions occur in both the numerator as well as the denominator of Eq. (5.14). Consequently, a small variation in the exponents will lead to substantial variations in the SIR statistics and thus will dominate the empirical arithmetic mean to an inadequate extent. Hence, when

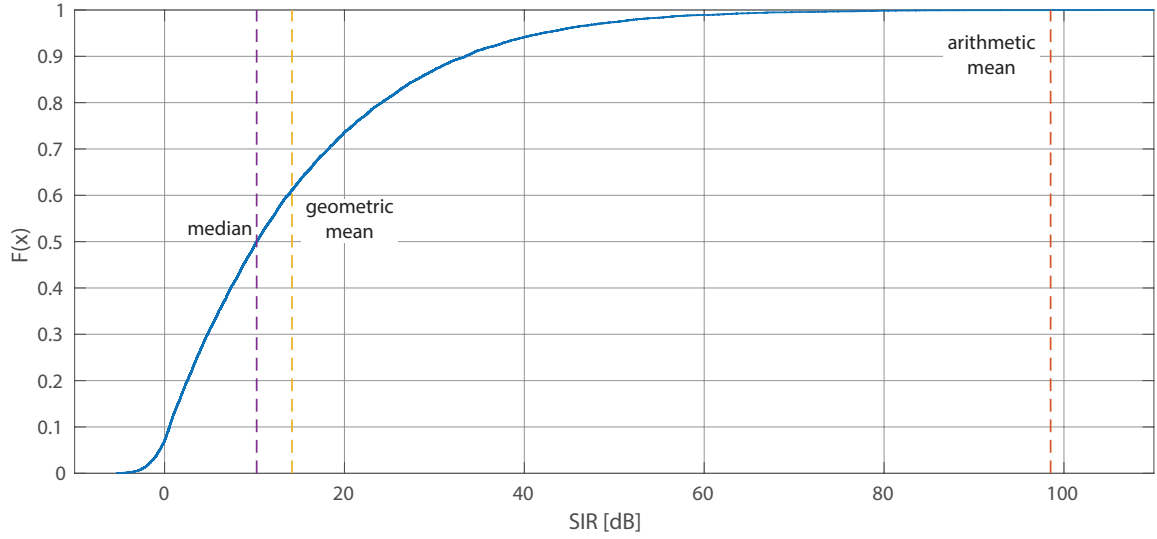


**Figure 5.5.:** This figure shows an example of a ecdf of SIR samples for  $10^4$  spatial realizations. While the arithmetic mean is dominated by large values, the geometric mean is very close to the median of the ecdf. These samples result from simulations with [uniform] wall generation and random BS placement, which leads to a wide spread of SIR values. For all other scenario generation methods however, it was also found that the geometric mean is always closer to the median than the arithmetic mean.

performing *simulations*, I equivalently utilize the empirical geometric mean, in order to eliminate this effect which is defined as

$$\text{geomean}(\{x_0, x_1, \dots, x_n\}) = \left( \prod_{i=1}^n x_i \right)^{\frac{1}{n}} = 10^{\left[ \frac{1}{n} \sum_{i=1}^n \log_{10} x_i \right]}, \quad (5.19)$$

which also shows that the geometric mean corresponds to the arithmetic mean in the logarithmic domain, i.e., taking the arithmetic mean of logarithmic values yields the same result as calculating the geometric mean of linear values and transforming it into the logarithmic domain. An example of the behavior of arithmetic and geometric mean of SIR samples for many spatial realizations can be found in Fig. 5.5. The figure illustrates clearly that the arithmetic mean is dominated by the very large samples and that the geometric mean is much closer to the median of the empirical cumulative distribution function (ecdf).

Now applying the geometric mean to calculate the ensemble average SIR, it formulates as<sup>5</sup>

$$\begin{aligned} \text{geomean}(\gamma) &= \text{geomean} \left( \frac{P_0 h_0 \ell(d_0) \hat{\omega}_0}{\sum_{i=1}^N P_i h_i \ell(d_i) \hat{\omega}_i} \right) \\ &= \frac{\text{geomean}(P_0 h_0 \ell(d_0) \hat{\omega}_0)}{\text{geomean}(\sum_{i=1}^N P_i h_i \ell(d_i) \hat{\omega}_i)}. \end{aligned} \quad (5.20)$$

In order to draw meaningful comparisons with my analytical results, I thus replace  $\delta$  by  $10^{\delta/10}$  in Eq. (5.15) and following. In the following, I present approximations for the average attenuation using different wall generation methods.

### 5.2.6. SIR Approximations by Utilizing the Average Wall Attenuation

#### Approximations for [binary]

The unconditional expression for the SIR in Eq. (5.17) becomes rather involved especially for larger numbers of interferers. Therefore, the initial idea is to replace the instantaneous accumulated wall loss  $\hat{\omega}_i$  with its average. This can be calculated following [18, Theorem 4] by

$$\omega_i = \mathbb{E}[\hat{\omega}_i] = e^{-\mathbb{E}[K_i](1-w)} = e^{-\lambda \mathbb{E}[L] d \beta_i d_i (1-w)}, \quad (5.21)$$

thus eliminating this source of randomness and simplifying the analysis. Due to the introduction of the geometric mean however, I do not use  $\omega_i$ , but  $\tilde{\omega}_i = w^{\mathbb{E}[K_i]}$  instead. Plugging this into Eq. (5.15) together with replacing  $\delta$  by  $10^{\frac{\delta}{10}}$  results in

$$\mathbb{P}[\gamma > \delta] = \prod_{i=1}^N \frac{1}{1 + 10^{\frac{\delta}{10}} \frac{\tilde{\omega}_i \ell(d_i)}{\tilde{\omega}_0 \ell(d_0)}}, \quad (5.22)$$

eliminates the random number of walls and thus omits the de-conditioning in Eq. (5.17), *but* leads to considerable deviations from Eq. (5.20). The discrepancy mainly arises from the fact that

$$\frac{w^{\mathbb{E}[K_0]}}{\sum_i w^{\mathbb{E}[K_i]}} \not\approx \mathbb{E} \left( \frac{w^{K_0}}{\sum_i w^{K_i}} \right). \quad (5.23)$$

In other words, when only assuming a deterministic wall attenuation based solely on the link length, the interference is also determined by the distance of the interferers, which leads to an overestimation of the SIR. To alleviate this issue, I introduce the concept of *effective wall attenuation* to better approximate Eq. (5.18). The expressions are provided for an arbitrary number of iTxs.

<sup>5</sup>Note that the set notation for the argument of the  $\text{geomean}(\cdot)$  is omitted here; the set contains one value per spatial realization (of walls).

I start by calculating the probability that for iTx<sub>i</sub>, none of the other iTxs experience a smaller attenuation by walls

$$\begin{aligned}\mathbb{P}\left[\bigcap_{i \neq j} K_i \leq K_j\right] &= \sum_{x=0}^{\infty} \prod_{i \neq j} \mathbb{P}[K_i \leq K_j | K_i] \text{pmf}_{K_i}(x) \\ &= \sum_{x=0}^{\infty} \prod_{i \neq j} \left( \sum_{y=x}^{\infty} \frac{e^{-\mu_j} \mu_j^y}{y!} \right) \frac{e^{-\mu_i} \mu_i^x}{x!}.\end{aligned}\quad (5.24)$$

The altered pmf for  $K_i$  from iTx<sub>i</sub> is calculated as

$$\text{pmf}_{K'_i}(x) = \frac{\prod_{i \neq j} \left( \sum_{y=x}^{\infty} \frac{e^{-\mu_j} \mu_j^y}{y!} \right) \frac{e^{-\mu_i} \mu_i^x}{x!}}{\mathbb{P}\left[\bigcap_{i \neq j} K_i \leq K_j\right]}.\quad (5.25)$$

Then, the *effective number of walls* formulates as

$$\mathbb{E}[K'_i] = \sum_{x=0}^{\infty} x \text{pmf}_{K'_i}(x)\quad (5.26)$$

and the corresponding effective wall attenuation is found as

$$\tilde{\omega}'_i = \mathbb{P}\left[\bigcap_{i \neq j} K_i \leq K_j\right] w^{\mathbb{E}[K'_i]}.\quad (5.27)$$

Thus, the realizations in which iTx<sub>i</sub> is one of the dominant interferers are emphasized. Replacing  $\tilde{\omega}_i$  by  $\tilde{\omega}'_i$  in Eq. (5.22) then leads to a close approximation of Eq. (5.20), as demonstrated in Section 5.2.7.

### Approximations for [MLP]

For the [MLP]- and the [regular] wall generation method, I have to deal with *another source of discrepancy*. In these approaches, the walls stretch out infinitely long, and, hence, the wall processes as experienced by the Txs are strongly correlated with each other (see Figs. 5.3c and 5.3d). It should be noted that also in the [uniform] and the [binary] approach, it can happen that two links are blocked by the same wall. In Fig. 5.10 I show that this case has a very low likelihood and I therefore neglect it.

In order to account for the correlations, I reformulate Eq. (5.14), by splitting the line-processes into the *horizontal*- and the *vertical* process. Then, I account for the Txs that experience the same walls in one dimension, as indicated in Fig. 5.6. For a [minimal][square] setup, I obtain

$$\gamma = \frac{h_0 d_0^{-\alpha} w^{K_v + K_h}}{h_1 d_1^{-\alpha} w^{K'_v + K_h} + h_2 d_2^{-\alpha} w^{K'_v + K'_h} + h_3 d_3^{-\alpha} w^{K_v + K'_h}},\quad (5.28)$$

and

$$\begin{aligned}\gamma^{-1} &= \frac{h_1 d_1^{-\alpha} w^{K'_v+K_h}}{h_0 d_0^{-\alpha} w^{K_v+K_h}} + \frac{h_2 d_2^{-\alpha} w^{K'_v+K'_h}}{h_0 d_0^{-\alpha} w^{K_v+K_h}} + \frac{h_3 d_3^{-\alpha} w^{K_v+K'_h}}{h_0 d_0^{-\alpha} w^{K_v+K_h}} \\ &= \frac{h_1 d_1^{-\alpha} w^{K'_v}}{h_0 d_0^{-\alpha} w^{K_v}} + \frac{h_2 d_2^{-\alpha} w^{K'_v+K'_h}}{h_0 d_0^{-\alpha} w^{K_v+K_h}} + \frac{h_3 d_3^{-\alpha} w^{K'_h}}{h_0 d_0^{-\alpha} w^{K_h}},\end{aligned}\quad (5.29)$$

where  $K_v$  and  $K_h$  are the wall counts that are experienced between the user and the dTx. They are Poisson RVs with  $\mathbb{E}[K_h] = \lambda' d_0 |\sin(\phi_0)|$ ,  $\mathbb{E}[K_v] = \lambda' d_0 |\cos(\phi_0)|$  and  $\lambda' = 1/2 \lambda \mathbb{E}[L]$  (cf. Section 5.2.4). The terms  $K'_v$  and  $K'_h$  are the amounts of walls that are experienced from the iTxs and that are not shared with the dTx. They are also Poisson distributed, with  $\mathbb{E}[K'_v] = \lambda' d_2 |\cos(\phi_2)|$  and  $\mathbb{E}[K'_h] = \lambda' d_2 |\sin(\phi_2)|$ , as indicated in Fig. 5.6a. It should be noted that  $K_v$  walls are also blocking the link of iTx<sub>3</sub>, while  $K_h$  is also seen by iTx<sub>1</sub>. Finally, along the lines of Eq. (5.15) I calculate the conditional probability  $\mathbb{P}[\gamma > \delta | K_v, K'_v, K_h, K'_h]$ , and then de-condition on  $\{K_v, K'_v, K_h, K'_h\}$  according to Eq. (5.17).

In a similar manner, I obtain the instantaneous SIR in the [minimal][rhomboid] case as

$$\gamma = \frac{h_0 d_0^{-\alpha} w^{K_v+K_h}}{h_1 d_1^{-\alpha} w^{K'_v+S(-\cos(\phi))K_v+K'_h} + h_2 d_2^{-\alpha} w^{K_v+K'_h+K''_h} + h_3 d_3^{-\alpha} w^{K''_v+S(\cos(\phi))K_v+K'_h}} \quad (5.30)$$

and

$$\begin{aligned}\gamma^{-1} &= \frac{h_1 d_1^{-\alpha} w^{K'_v+S(-\cos(\phi))K_v+K'_h}}{h_0 d_0^{-\alpha} w^{K_v+K_h}} + \frac{h_2 d_2^{-\alpha} w^{K_v+K'_h+K''_h}}{h_0 d_0^{-\alpha} w^{K_v+K_h}} + \frac{h_3 d_3^{-\alpha} w^{K''_v+S(\cos(\phi))K_v+K'_h}}{h_0 d_0^{-\alpha} w^{K_v+K_h}} \\ &= \frac{d_1^{-\alpha} w^{K'_v+K'_h}}{h_0 d_0^{-\alpha} w^{K_v(1-S(-\cos(\phi)))+K_h}} + \frac{h_2 d_2^{-\alpha} w^{K'_h+K''_h}}{h_0 d_0^{-\alpha} w^{K_h}} + \frac{h_3 d_3^{-\alpha} w^{K''_v+K'_h}}{h_0 d_0^{-\alpha} w^{K_v(1-S(\cos(\phi)))+K_h}},\end{aligned}\quad (5.31)$$

where

$$S(x) = \begin{cases} 1 & , x \geq 0 \\ 0 & , x < 0 \end{cases}, \quad (5.32)$$

with  $K_v$  and  $K_h$  as for the [square] transmitter arrangement. The terms  $K'_v$ ,  $K''_v$ ,  $K'_h$  and  $K''_h$  are Poisson RVs with  $\mathbb{E}[K'_v] = \lambda' \min(d_1 \cos(\phi_1), R/\sqrt{2})$ ,  $\mathbb{E}[K''_v] = \lambda' \min(d_3 \cos(\phi_3), R/\sqrt{2})$ ,  $\mathbb{E}[K'_h] = \lambda' d_1 |\sin(\phi_1)|$  and  $\mathbb{E}[K''_h] = \lambda' R/\sqrt{2}$ , with  $\lambda'$  as in the [square] model, respectively.

I obtain the conditional SIR-coverage probability  $\mathbb{P}[\gamma > \delta | K_v, K'_v, K''_v, K_h, K'_h, K''_h]$  which depends on six variables. Due to the exponentially increasing complexity with each additional variable,

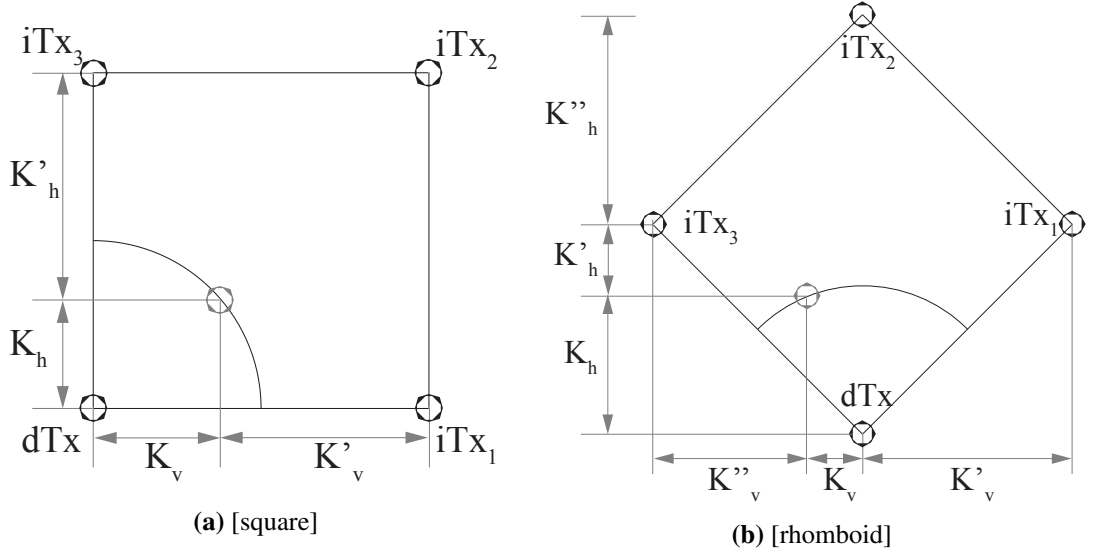


**Figure 5.6.:** Illustration of parts in the arrangement, for which dTx and iTxs are blocked by the same walls, in  $x$  and  $y$  direction respectively. ©2016 IEEE, [71].

the simulation time becomes infeasible and results can no longer be obtained within a reasonable amount of time. Hence, I propose to replace  $K'_h$  and  $K''_h$  by  $\mathbb{E}[K'_h]$  and  $\mathbb{E}[K''_h]$ . The accuracy of this approximation is discussed in Section 5.2.7 and exemplified in Fig. 5.10.

Note that the generalization to [one tier] and [two tier] is tedious but straightforward. As shown in Section 5.2.7, results for [minimal] do not deviate significantly (least not qualitatively) from the results for [one tier] and [two tier].

### Approximations for [regular]

Similarly, the Txs in the [regular]- model experience correlated wall objects. Since, according to Eq. (5.13), the uncorrelated random part in this model concerns only one wall in the horizontal- and one wall in the vertical direction, neglecting this correlation still yields a good approximation, as verified in Section 5.2.7.

### 5.2.7. Numerical Evaluation

In this section, I numerically evaluate my analytical results with a realistic set of parameters. In order to verify their accuracy, I compare them against results from extensive Monte Carlo simulations. Due to the large number of possible combinations of transmitter arrangement, tier setup and wall generation method, I do not present results for all of them, but scrutinize the most representative



**Table 5.1.:** Parameters for numerical evaluation. ©2016 IEEE, [71].

Parameter	Value
inter transmitter distance	$R = 40$ m
number of interferers	$\{3, 8, 24\}$
Rx radius	$R/2 = 20$ m
Rx positions	25
wall density	$\lambda = 0.05 \text{ m}^{-2}$
average wall length	$\mathbb{E}[L] = 5$ m
wall loss	$w = 10$ dB [2]
scenario realizations	$10^5$
path loss law	$l(d) = 10^{-38.46/10} d^{-2}$ [2]
transmitter power	$P = 1$ W
noise power	$N_0 = -174$ dBm + $10 \log_{10}(10^7)$

combinations. In particular, I do not include results for [uniform] because it lacks the angular dependency of the average wall attenuation and I focus on wall generation methods with perpendicular walls.

### Parameters for Numerical Evaluation

I employ the transmitter and receiver setup as introduced in Section 5.2.1, and depicted in Fig. 5.1. The different transmitter constellations [minimal], [one tier] and [two tier] correspond to 3, 8 and 24 iTxS. I set the inter-Tx distance to 40 m, and the Rx radius to 20 m, corresponding to the cell-edge. The performance is evaluated at 25 equidistantly spaced Rx positions, corresponding to 25 different values of  $\Phi$ . For [binary], I define a wall density of  $\lambda = 0.05 \text{ m}^{-2}$  and an average wall length of  $\mathbb{E}[L] = 5$  m. The wall generation parameters for [MLP] and [regular] are derived as specified in Section 5.2.1. With these parameters, the room size for [regular] is 4 m x 4 m. A constant wall loss of  $w = 10$  dB is assumed [2]. This value is at the higher end of penetration loss values at the considered carrier frequency and corresponds to inner walls necessary for structural integrity. It also leads to a more pronounced influence of the wall attenuation on the network performance. All TxS are considered to radiate with a constant transmit power of  $P = 1$  W. The path loss law of [2] is applied, which specifies a path loss exponent of  $\alpha = 2$  and a path loss constant of  $c = 38.46$  dB. The parameters are summarized in Table 5.1.

For comparison, I carry out extensive Monte Carlos simulations, applying the same set of parameters. The results for each angle-position  $\Phi$  are obtained by averaging over  $10^5$  spatial realizations.

### Average Wall Attenuation

First, I discuss the average wall attenuation with respect to the individual Tx's. In the interest of clarity, a [minimal] setup with four Tx's is considered. Conclusions for the additional Tx's positions in the [one tier]- and [two tier] setup are straightforward and do not lead to any further insights. As explained in Section 5.2.4, the *geometric mean of the wall attenuation* is used to compare different scenarios. It directly relates to the average number of blockages obstructing a path between a Tx and the Rx.

**Comparison of Analytical and Simulated Results:** Based on the analytical expressions for the average number of blockages in Section 5.2.4, I compare  $w^{\mathbb{E}[K_i]}$  to  $\text{geomean}(\hat{\omega}_i) = w^{\overline{K_i}}$  from simulations. The results for the dTx and the three closest iTx over the Rx positions  $\Phi$  are shown in Fig. 5.7. In Fig. 5.7a, results for the [square] arrangement are depicted, in Fig. 5.7b results for the [rhomboid] arrangement, respectively. The evaluation of the analytical expressions is represented by solid lines. In Section 5.2.4, it was already discussed that the analytically obtained average number of blockages for [binary], [MLP] and [regular] are the same. Therefore, the results for all three wall generation methods are exactly overlapping. These results are compared to the simulation results for [binary], which are denoted by 'o'. My first observation is that analysis and simulations perfectly overlap for all Tx's. Furthermore, the angular dependency of the attenuation, as present in Eqs. (5.7) and (5.9), becomes evident. The influence of the Tx arrangement can be seen by the different positions  $\Phi$ , where the attenuation takes on minima and maxima in Figs. 5.7a and 5.7b. This is due to the change of the relative position  $\Phi$  and the absolute angle  $\phi$ , as introduced in Section 5.2.1. Thus, for the same Rx position  $\Phi$ , different angles  $\phi_i$  are observed when comparing the [square] and [rhomboid] arrangement.

**Comparison of [binary], [MLP] and [regular]:** So far I showed that the analytically obtained average number of blockages for [binary], [MLP] and [regular] are the same and coincide with the simulation results for [binary]. In Fig. 5.8 I show that this is also true for the simulation results of [MLP] and [regular]. The results for [binary] are represented by 'o', results for [MLP] by '+' and results for [regular] by 'x'. It should be noted that since the [binary], [MLP] and [regular] case exactly overlap, this also means that analytical results and simulation results for [MLP] and [regular] perfectly overlap. Also the results from analysis, already presented in Fig. 5.7, are shown in the figure as solid lines and perfectly overlap with the simulation results.

**Comparison of [binary] and [practical]:** The parameters of the [practical] scenario, as summarized in Table 5.2, are calibrated heuristically, such that the average attenuation matches my reference [binary]. The matching of the wall densities was carried out by changing the size of the ROI, while keeping all other generation parameters constant. As of this writing, no analytical relation between

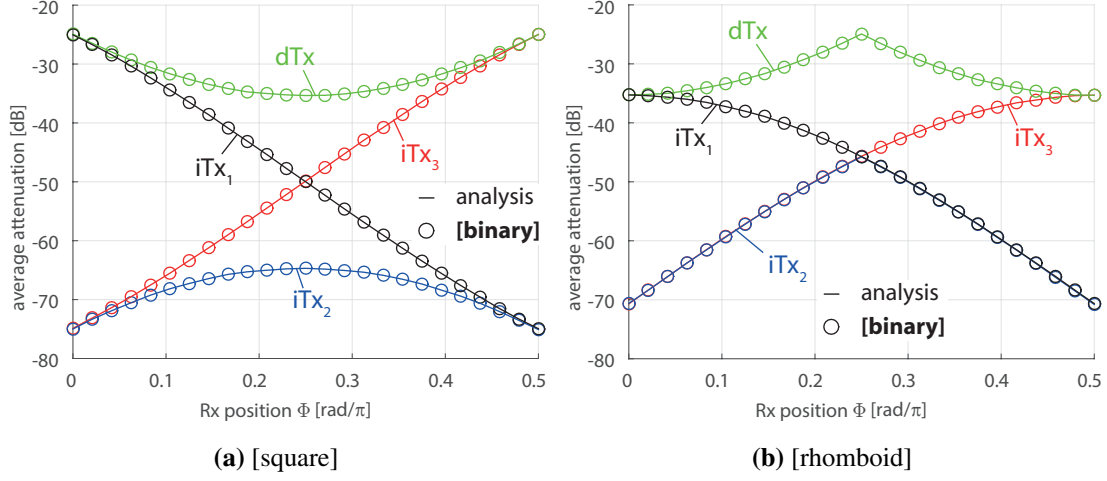


**Figure 5.7.:** Average attenuation for dTx and  $iTx_i$ ,  $i = \{1, 2, 3\}$  over Rx position  $\Phi$ . Comparison of analysis and simulation for [binary]. ©2016 IEEE, [71].

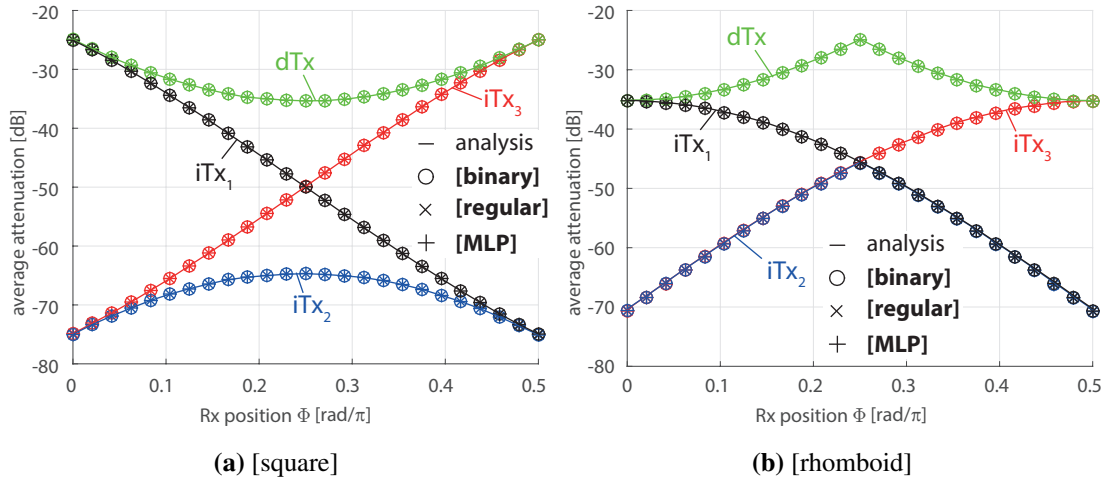


**Figure 5.8.:** Average attenuation over Rx position  $\Phi$ , comparison of [binary], [regular] and [MLP]; simulation results represented by markers, analytical results by solid lines. ©2016 IEEE, [71].

**Table 5.2.:** Floor plan parameters. ©2016 IEEE, [71].

Parameter	Value
number of total recursions	$n = 6$
boundary distance	$\mu = 0.2$
minimal room dimensions	$y_{\min} = x_{\min} = 0.02 x_{\text{ROI}}$
separator placement repetition	$n_{\text{rep}} = 5$
ROI dimensions	$x_{\text{ROI}} = y_{\text{ROI}} = 168 \text{ m}$

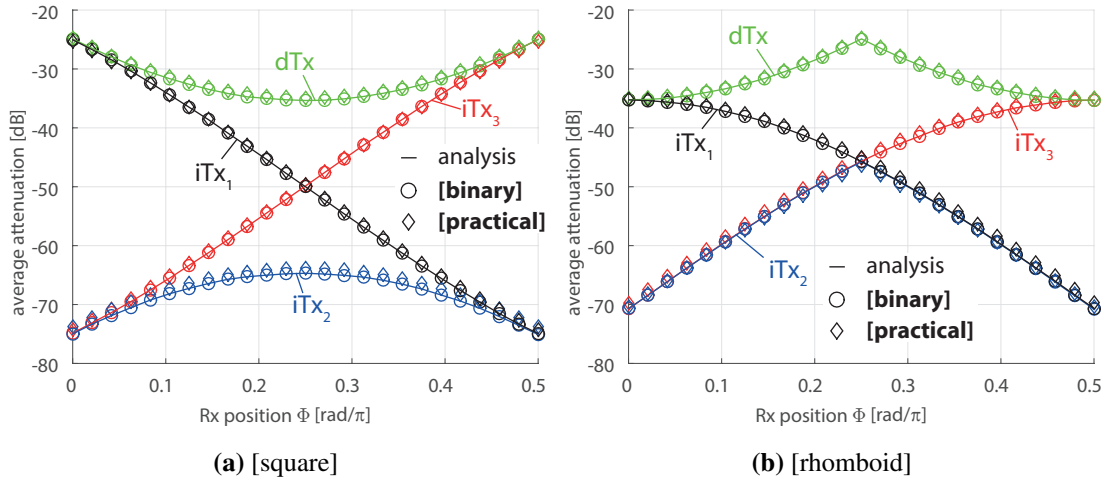


**Figure 5.9.:** Average attenuation over Rx position  $\Phi$ , comparison of [binary] and [practical]; parameters for [practical] were heuristically adapted to fit the attenuation of [binary]. The same qualitative trend stems from the fact, that it is mostly determined by the transmitter-receiver distance and the angular dependency (due to binary wall orientation angles), which is similar for [binary] and [practical]. ©2016 IEEE, [71].

this set of parameters and the average attenuation has been found. The corresponding results are shown in Fig. 5.9. Results for [binary] are represented by 'o', results for [practical] by '◇'. It can be seen that the results of the [practical] scenario show the same trend. Even though the parameters were only adapted heuristically, there is a surprisingly low deviation from the analytical results (depicted by solid lines in the figure).

### SIR Performance Comparison

In this section, I investigate SIR performance (for analytical results) and SINR performance (for simulation results) for various representative scenarios. Note that the noise is only incorporated in the simulations.

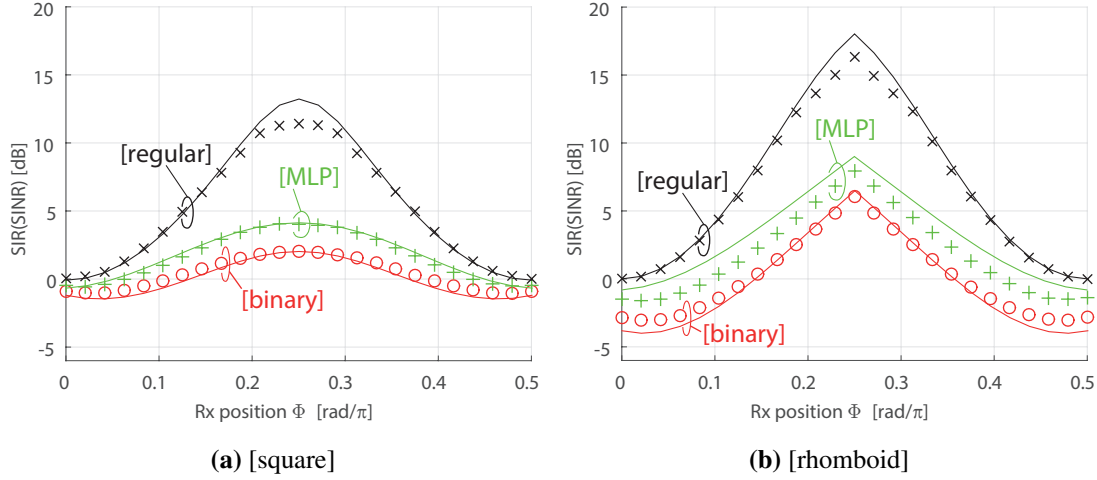


**Figure 5.10.:** Average SIR (analysis) and SINR (simulations) over Rx position  $\Phi$ ; comparison of analysis and simulations for [binary], [regular] and [MLP]; results obtained for [minimal] tier setup. ©2016 IEEE, [71].

**Comparison of analysis and simulations:** In order to validate the analytical framework and the approximations in Section 5.2.5, I compare them against results from Monte Carlo simulations. The comparison is carried out by considering a [minimal] setup and the results are shown in Fig. 5.10. The markers in the figure represent simulation results, while solid lines refer to the theoretical results. The results for [regular] show a good accordance, they only deviate for Rx positions around  $\Phi = \pi/4$ . This is observed, because at this position all three iTxs have equally strong impact on the sum interference, which results in larger differences in the instantaneous SINR as for  $\Phi = 0$  and  $\Phi = \pi/2$ . For [MLP], the results almost completely match for [square] in the left figure. For [rhomboid] in the right figure I observe an offset, that stems from the approximation introduced in Section 5.2.5. If  $K'_h$  and  $K''_h$  were not replaced by  $\mathbb{E}[K'_h]$  and  $\mathbb{E}[K''_h]$  in (5.31), the results would also match for [rhomboid]. The results for [binary] display a slight deviation for  $\Phi = 0$  and  $\Phi = \pi/2$ , but otherwise show good accordance. This is in particular interesting, because the correlation between blockages was not considered in the approximation of [binary].

From this comparison, it can also be concluded that the considered indoor systems (for the specified carrier frequency and resulting wall penetration losses) are not noise limited. The variations between analytical results and simulations are remarkably minor, even though the simulations take additive noise into account.

**Comparison of [minimal], [one tier] and [two tier]:** I introduced three different tier setups in Section 5.2.1. The analytical results for the SIR in Section 5.2.5 were derived for [minimal], as well as the results presented in Fig. 5.10. I now compare simulation results for all three tier setups to investigate the error that is introduced by neglecting respective interferers. The accumulated

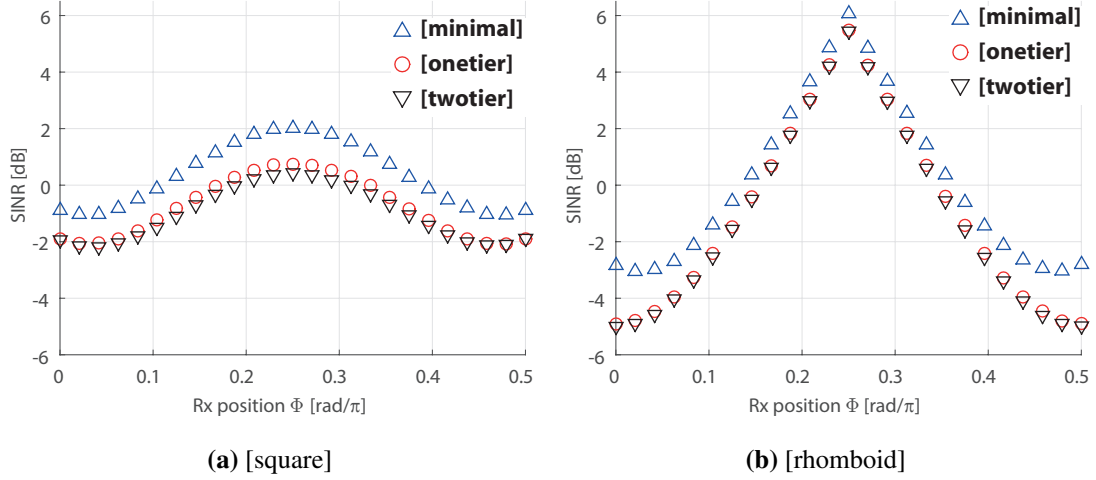


**Figure 5.11.:** Average SINR over Rx position  $\Phi$ ; comparison of tier setups [minimal], [one tier] and [two tier] for [binary]. Same characteristics of results for all tier setups visible; No significant difference between [minimal] and [one tier] negligible deviation of [one tier] from [two tier]. ©2016 IEEE, [71].

interference depends mostly on the closest interferers. Comparing the simulation results for the [minimal] setup with the [one tier] and the [two tier] setup shows up to which extent further interferers influence the SINR. Simulation results for [binary] and all three setups are presented in Fig. 5.11. Results for [minimal] are represented by ' $\triangle$ ', results for [one tier] by ' $\circ$ ' and results for [two tier] by ' $\nabla$ '. As the curves show, all three results follow the same characteristic. As expected, the SINR is lower, when more interferers are present. The difference is not so significant however, since the additional wall loss considerably attenuates interferers at higher distances. While there is a gap of 1-2 dB between the results for [minimal] and [one tier], there is no significant discrepancy between the results for [one tier] and [two tier]. On the one hand, this justifies the application of the [minimal] setup, since it captures the general trends. On the other hand, it dismisses the need to simulate the full-blown [two tier] scenario. A similar behavior is observed for the other wall-generation methods.

**Comparison of all wall arrangement methods:** Finally, I compare SINR results for a [one tier] setup in Fig. 5.12. Results for all four wall generation methods are compared, now also including [practical], which is represented by ' $\diamond$ '. Considering the almost similar attenuation characteristics in Fig. 5.9, the SINR results for [practical] is higher than in the [MLP] but worse than in the [regular] arrangement. This identifies [binary] as the wall generation method that yields the worst performance and [regular] the best performance. Considering [practical], it is the most realistic wall generation method but also the only one that cannot be treated mathematically. At least for [rhomboid] results for [MLP] are a tight lower bound for the performance of [practical]. For [square], the performance lies between the results of [MLP] and [regular]. Even though [binary] is most convenient to treat

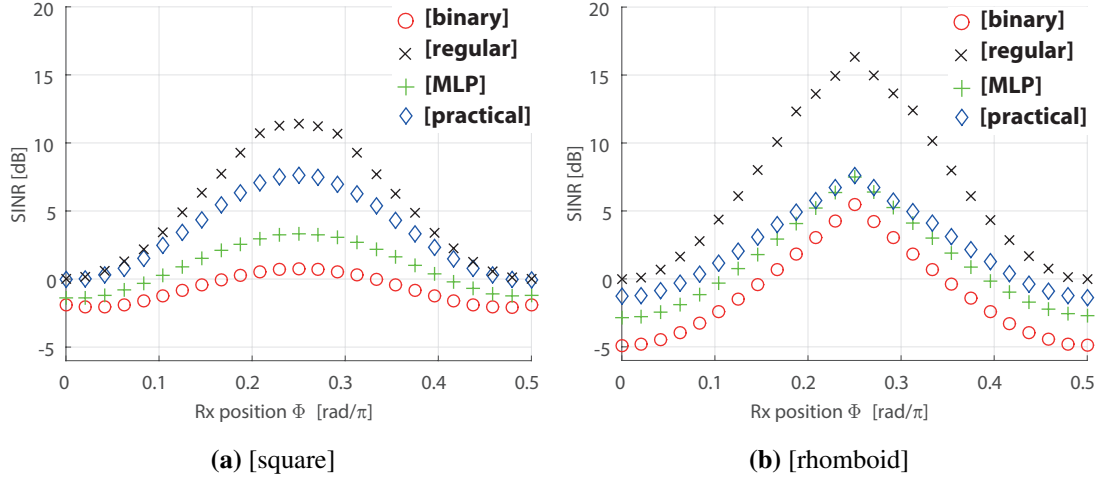


**Figure 5.12.:** Average SINR over Rx position  $\Phi$ ; comparison of all four wall generation methods - [binary], [regular], [MLP] and [practical]; results obtained for [one tier] setup. ©2016 IEEE, [71].

mathematically, it only yields a loose lower bound.

### Discussion of Results

Next to the already discussed aspects, some general conclusions can be drawn from the presented results. Most importantly, I showed that a similar average attenuation (conf. Figs. 5.7 to 5.9) does not result in similar SIR performances (conf. Figs. 5.10 to 5.12). This is due to different correlations of the blockages for the dTx and iTxs (cf. Section 5.2.5), which alter the SINR distribution. An example for the ecdf of the SINR at two Rx positions for [rhomboid] can be found in Fig. 5.13. There, this again shows that the results for [practical] lie between the results of the mathematically tractable methods.

Another general observation is the difference between the [square] and the [rhomboid] arrangement. Only in the [uniform] case, the SIR results are indifferent of the Tx arrangement. This follows from the independence of the average wall attenuation from the angle between the Tx and the Rx (cf. Eq. (5.8)). For all presented results, all wall generation methods experience angular-dependent average attenuations. Therefore, the SIR results for all considered scenarios are different for [square] and [rhomboid]. An intuitive explanation is the that for Rx position  $\Phi = \pi/4$  for [square], walls with orientation  $\theta = 0$  and  $\theta = \pi/2$  are “visible”, while for [rhomboid] and the same Rx position only walls with orientation  $\theta = 0$  have an impact on the total wall attenuation.

For all considered scenarios, I could identify the [binary] wall generation method to result in the worst SIR performance. On the opposite side, the best performance is yielded by [regular]. I deduce that for constant wall volume, the performance becomes worse, the more randomness is introduced

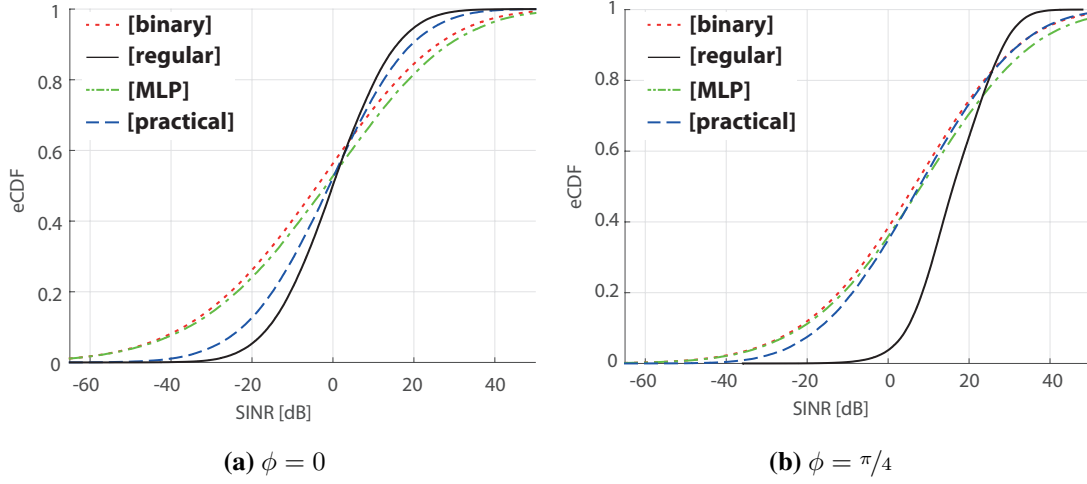


**Figure 5.13.:** SINR meta distributions for [one tier], [rhomboid], user angles  $\phi = \{0, \pi/4\}$  and all four wall distribution methods; dotted lines for [binary], solid lines for [regular], dash-dotted lines for [MLP] and dashed lines for [practical]. ©2016 IEEE, [71].

in the wall generation, since there is no guaranteed attenuation of the interference, as it is the case for [regular]. This yields an interesting duality with random and regular Tx arrangements, where similar trends were observed [12].

### 5.3. Sector Size and Area Spectral Efficiency

While the focus of the previous section was on the impact of wall generation methods for fixed BS locations with regular arrangement and constant distances, I now shift the attention to the impact of the BS placement. Therefore, I focus on the least restrictive wall generation method, i.e., [uniform], which is also the easiest to deal with analytically. Additionally, when a non-regular BS placement is used, the angular dependency in the performance results vanishes. For randomly placed BSs, I derive expressions for coverage probability and spectral efficiency and subsequently also ASE, dependent on the wall attenuation value and wall density. I then compare these analytical results to performance results from simulations, where I also include results for the regular arrangement as defined in Section 5.2.1.



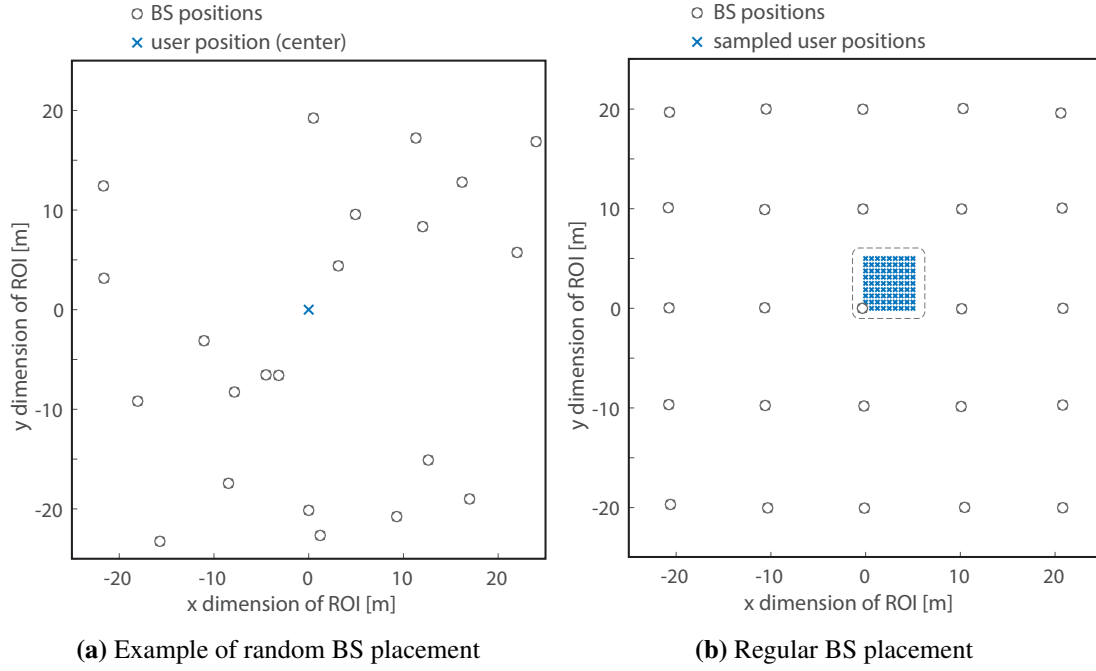


**Figure 5.14.:** An example for a realization for random BS placement with BS density  $\rho$  corresponding to an inter-BS distance  $R = 10$  m; user always located in center of ROI. Regular BS placement for inter-BS distance  $R = 10$  m with sampled user positions. ©2018 IEEE, [68].

### 5.3.1. System Model Adaptations

#### Transmitter and Receiver Placement

I investigate two kinds of BS placement, namely random and regular placement. The random placement is user-centric and all performance metrics are evaluated for a user in the center of the ROI. The BSs are placed according to a homogeneous PPP  $\Psi$  with density  $\rho$ . For my analytical performance evaluation, I will consider association of the user to the *closest* BS, while in simulations, I will compare association to the *closest* and the *strongest* BS (cf. Section 5.3.2).

When I compare random and regular BS placement, I assure that the average number of BSs in a given area for random placement of BS with density  $\rho$  is the same for a regular grid of BSs with a constant inter-site distance  $R$ . The BS density is the inverse of the sector size, which is thus related by

$$\rho^{-1} = R^2. \quad (5.33)$$

I consider a [two tier] setup, which amounts to 25 BSs in total. For [uniform] wall placement, it is irrelevant to choose [square] or [rhomboid] transmitter arrangement. Since I am interested now in the

average performance in the whole sector, I no longer assume circularly arranged Rx locations, but I sample user positions in the whole sector. Due to symmetry, it is sufficient to sample user positions in one quadrant with side-length  $R/2$  and evaluate the average performance for all positions. I choose the density of samples within the quadrant large enough to provide statistically accurate results. Since analytical results for the regular BS placement with a large number of user positions is no longer feasible to be treated analytically, I only investigate it by means of simulations.

### Signal Propagation

The general assumptions from Section 5.2.4 also hold for the following. As before, I also focus on downlink transmissions in this section. I consider a log-distance dependent path loss described as  $l(d) = d^{-\alpha}$ . Note that this model is a slight simplification w.r.t. the previous section. This is done for simpler analytical expressions and except of the missing factor  $1/c$ , the obtained results are the same. Again I assume that the signal experiences small-scale fading to account for multi-path propagation effects. As before, I assume Rayleigh fading for all links, such that the channel gain between BS and user follows an exponential distribution. In this section, I distinguish between the channel gain w.r.t. the desired BS and denote it by  $h \sim \exp(\mu)$ , while the channel gain for links with interfering BS<sup>6</sup>  $i$  is denoted by  $g_i$ . I additionally assume that  $h$  and  $g_i \forall i$  to be independent and identically distributed (i.i.d.). In the following, I always assume  $\mu = 1$  for all links. As it could be observed from the comparison of SIR and SINR in Fig. 5.10, the addition of noise has no significant influence. Therefore, I presume the network to be interference limited and thus will neglect the influence of noise. Wall attenuation is treated as defined in Eq. (5.2).

### Wall Placement Method

I use the [uniform] wall placement method (cf. Section 5.2.2), since it is the easiest to handle analytically and since the average wall attenuation is not angular dependent. For the random BS placement, this effect would anyways vanish. The average number of walls, blocking a link then follows Eq. (5.7) in combination with Eq. (5.8).

#### 5.3.2. Analytical Description

In this chapter, I derive analytically the performance of an indoor user, in terms of coverage probability and average achievable rate and consequently ASE. For these considerations, correlation among

---

<sup>6</sup>Note that in contrast to the previous subsection, I separate the small scale fading of desired and interfering transmitters, which simplifies notation in the following derivations.

blockages on multiple links (i.e., one wall blocking two links at the same time) is ignored. As starting point, I am using the SIR and ignore the influence of noise.

For all considered propagation effects defined in Section 5.2.1, the *instantaneous* SIR  $\gamma'$  for a given realization of BSs, walls and fading is described by

$$\gamma' = \frac{P_0 h r^{-\alpha} \hat{\omega}_0}{\sum_{i \in \Psi \setminus b_0} P_i g_i d_i^{-\alpha} \omega_i} = \frac{h r^{-\alpha} w^{K_0}}{\sum_{i \in \Psi \setminus b_0} g_i d_i^{-\alpha} w^{K_i}}, \quad (5.34)$$

where  $r$  denotes the distance of the user from the BS the user is associated with and  $d_i$  the distance from interfering BS  $i$ . The transmit power  $P_i$  is assumed to be equal for all BSs and therefore cancels out. I denote the desired BS by  $b_0$  and distinguish association to the *closest* BS, which I denote by  $b_0^{(c)}$ , and association to the *strongest* BS, denoted by  $b_0^{(s)}$  accordingly. In a scenario without walls,  $b_0^{(c)}$  also corresponds to the strongest BS in the long term average, thus eliminating the influence of the small scale fading. This leads to a slightly different term as in Eq. (5.14), since now the considered number and placement of BSs is random and the association is not fixed. Thus the sum of interferers is indicated by  $i \in \Psi \setminus b_0$ , excluding the tagged BS.

In Eq. (5.34), the fading, the distance from the user, as well as the number of walls (which in turn is dependent on the distance) are RVs. In order to be able to obtain analytical results, I do not use the actual number of walls  $K_i$ , but replace it with its average for a given distance  $\mathbb{E}[K_i]$ . This is equivalent to assuming a continuous and deterministic wall attenuation along the propagation path, that then only depends on the distance and not on the discrete distribution of walls in the scenario. Thus, I eliminate the combinations of discrete wall attenuation values on all BS-user links and simplify the analysis considerably. Consequently,  $b_0^{(c)}$  corresponds again to the strongest BS without fading. In the rest of my thesis I therefore always assume an association to  $b_0^{(c)}$  when using a continuous distribution of walls and an association to  $b_0^{(s)}$  when the discrete realization of walls is considered.

Substituting the instantaneous number of walls  $K_i$  with the average  $\mathbb{E}[K_i]$  leads to

$$\gamma = \frac{S}{I_r} = \frac{h r^{-\alpha} w^{\mathbb{E}[K_0]}}{\sum_{i \in \Psi \setminus b_0} g_i d_i^{-\alpha} w^{\mathbb{E}[K_i]}} = \frac{h r^{-\alpha} w^{\beta r}}{\sum_{i \in \Psi \setminus b_0} g_i d_i^{-\alpha} w^{\beta d_i}} \quad (5.35)$$

with  $\beta$  as already defined in Eq. (5.8).

### Coverage Probability

In the following, I will derive expressions for the coverage probability with the underlying assumptions. The derivation is similar to [12], but with the addition of blockages.

The coverage probability is generally defined as

$$p_c(\delta, \rho, \alpha) \triangleq \mathbb{P}[\gamma > \delta], \quad (5.36)$$

where  $\delta$  is the SIR threshold, above which the user is assumed to be in coverage. Since I defined the distance between the user to its closest/associated BS by  $r$ , this also means that the distance  $d_i$  of all interfering BSs is *larger* than  $r$  and thus there is no BS located in a circle around the user with radius  $r$ . Thus, I condition on the distance of the closest BS and average over all possible values of  $r$  and additionally apply the probability density function (pdf) of the void probability  $f_r(r) = 2\pi\rho r e^{-\rho\pi r^2}$ , which represents the probability for no BS being located closer than  $r$ . This results in

$$\begin{aligned} p_c(\delta, \rho, \alpha) &= \mathbb{E}_r [\mathbb{P}[\gamma > \delta | r]] \\ &= \int_{r>0} \mathbb{P}[\gamma > \delta | r] f_r(r) dr \\ &= \int_{r>0} \mathbb{P}[\gamma > \delta | r] e^{-\pi\rho r^2} 2\pi\rho r dr. \end{aligned} \quad (5.37)$$

Plugging in Eq. (5.35) leads to

$$\begin{aligned} p_c(\delta, \rho, \alpha) &= \int_{r>0} \mathbb{P} \left[ \frac{hr^{-\alpha}w^{\beta r}}{I_r} > \delta \middle| r \right] e^{-\pi\rho r^2} 2\pi\rho r dr \\ &= \int_{r>0} \mathbb{P} \left[ h > \delta r^\alpha w^{-\beta r} I_r \middle| r \right] e^{-\pi\rho r^2} 2\pi\rho r dr. \end{aligned} \quad (5.38)$$

where  $I_r$  is the resulting accumulated interference for a single spatial realization of BSs.

Next I utilize that  $h$  is exponentially distributed. It follows

$$\begin{aligned} \mathbb{P} \left[ h > \delta r^\alpha w^{-\beta r} I_r \middle| r \right] &= \mathbb{E}_{I_r} \left[ \exp(-\delta r^\alpha w^{-\beta r} I_r) \middle| r \right] \\ &= \mathcal{L}_{I_r}(\delta r^\alpha w^{-\beta r}) \end{aligned} \quad (5.39)$$

where  $\mathcal{L}_{I_r}(s)$  is the Laplace transform of the RV  $I_r$ .

Plugging this back in Eq. (5.38) yields

$$p_c(\delta, \rho, \alpha) = \int_{r>0} \mathcal{L}_{I_r}(\delta r^\alpha w^{-\beta r}) e^{-\pi\rho r^2} 2\pi\rho r dr, \quad (5.40)$$

with

$$\begin{aligned}
 \mathcal{L}_{I_r}(\delta r^\alpha w^{-\beta r}) &= \mathbb{E}_{\Psi, g_i} \left[ \exp \left( -\delta r^\alpha w^{-\beta r} \sum_{i \in \Psi \setminus b_0} g_i d_i^{-\alpha} w^{\beta d_i} \right) \right] \\
 &\stackrel{(a)}{=} \mathbb{E}_{\Psi} \left[ \prod_{i \in \Psi \setminus b_0} \mathbb{E}_g [\exp(-\delta r^\alpha w^{-\beta r} g d_i^{-\alpha} w^{\beta d_i})] \right] \\
 &\stackrel{(b)}{=} \mathbb{E}_{\Psi} \left[ \prod_{i \in \Psi \setminus b_0} \frac{1}{1 + (r/d_i)^\alpha w^{\beta(d_i-r)} \delta} \right] \\
 &\stackrel{(c)}{=} \exp \left( -2\pi\rho \int_r^\infty \left( 1 - \frac{1}{1 + (\frac{r}{v})^\alpha w^{\beta(v-r)} \delta} \right) v dv \right), \tag{5.41}
 \end{aligned}$$

where (a) follows from all  $g_i$  being i.i.d., (b) follows from the exponential distribution of  $g_i$  and the last step (c) from the probability generating functional (PGFL) of the PPP (cf. Section 2.4). The integral over  $v$  corresponds to averaging over the interferer locations for a given  $r$ .

### Area Spectral Efficiency

First I will derive an expression for the spectral efficiency. I assume therefore, that the considered user can reach the (noiseless) Shannon bound  $\log_2(1 + \gamma)$  by using an adaptive modulation and coding scheme (MCS) and treating interference as noise. For the considered scenario, the spectral efficiency is given by (cf. [12, Appendix C])

$$\begin{aligned}
 \tau(\rho, \alpha) &= \mathbb{E}[\log_2(1 + \gamma)] \\
 &= \int_{r>0} e^{-\pi\rho r^2} 2\pi\rho r \int_{t>0} \mathbb{P} \left[ \log_2 \left( 1 + \frac{hr^{-\alpha} w^{\beta r}}{I_r} \right) > t \right] dt dr \\
 &= \int_{r>0} e^{-\pi\rho r^2} 2\pi\rho r \int_{t>0} \mathbb{P} \left[ h > (2^t - 1) r^\alpha w^{-\beta r} I_r \right] dt dr \\
 &= \int_{r>0} e^{-\pi\rho r^2} 2\pi\rho r \int_{t>0} \mathcal{L}_{I_r}(r^\alpha w^{\beta r} (2^t - 1)) dt dr, \tag{5.42}
 \end{aligned}$$

with

$$\mathcal{L}_{I_r}(r^\alpha w^{\beta r} (2^t - 1)) = \exp \left( -2\pi\rho \int_r^\infty \left( 1 - \frac{1}{1 + (\frac{r}{v})^\alpha w^{\beta(v-r)} (2^t - 1)} \right) v dv \right), \tag{5.43}$$

where I performed the same steps as in Eqs. (5.38) to (5.41).

Next I introduce the ASE denoted by  $\kappa$ . This metric better reflects the average cell capacity than the user-centric metrics introduced up to this point. By normalizing the spectral efficiency by the average cell area (which is simply  $1/\rho$ ), I arrive at the average throughput per Hz per unit area. Thus, it can be described by

$$\kappa(\rho, \alpha) = \frac{\tau(\rho, \alpha)}{\mathbb{E}[A^{(cell)}]} = \rho\tau(\rho, \alpha). \quad (5.44)$$

The ASE is an indicator for the average cell capacity that the given network can support. Especially from an operator point of view this is interesting, since it is important to know, e.g., how the cell capacity increases when the total number of installed BSs is increased for a given building or floor.

How the ASE and the aforementioned performance metrics depend quantitatively on the scenario parameters and how the simplifying assumptions for my analytical approach compare against simulation results is discussed in detail in the following section.

### 5.3.3. Results for Coverage Probability and Area Spectral Efficiency

In this section, I present results for the coverage probability  $p_c$  and the ASE  $\kappa$ . I compare the (numerically evaluated) resulting values from Eq. (5.40) and Eq. (5.44) with the results of Monte-Carlo simulations. One simulation run for a parameter set is equivalent to one spatial realization of BS locations, one placement of walls including their random orientation and fading realizations. I assume random BS placement for the analytical results, while I simulate both, random and regular BS placement (cf. Figs. 5.14a and 5.14b). For the given wall density  $\lambda$  and the average wall length  $\mathbb{E}[L]$ , the average room size<sup>7</sup> is  $16 \text{ m}^2$ . I consider the case with no walls (0 dB penetration loss) and 3 dB, 6 dB and 10 dB. (In [2], inner walls are assumed to have 5 dB penetration loss - thus I cover values with similar magnitude.) The applied parameters are summarized in Table 5.1.

#### Coverage Probability

First, I present results for the random BS placement. The coverage probability for all three considered values of  $\rho$  are shown in Fig. 5.15. For each BS density, I show results for all four values of wall attenuation. The results from numerically evaluating Eq. (5.40) are represented by circular markers. Solid lines represent the coverage probability resulting from simulations, based on Eq. (5.35). Additionally, I show results from simulations based on Eq. (5.34) as dashed lines.

---

<sup>7</sup>This value results from assuming a [regular] wall placement, where  $\Delta = 4 \text{ m}$  for the given parameters and same wall volume (cf. Eq. (5.6)).

**Table 5.3.:** Parameters for numerical evaluation. ©2018 IEEE, [68].

Parameter	Value
path loss exponent	$\alpha = 4$
wall density	$\lambda = 0.05 \text{ m}^{-2}$
average wall length	$\mathbb{E}[L] = 10 \text{ m}$
wall attenuation	$w_{dB} = \{0, 3, 6, 10\} \text{ dB}$
inter BS distance	$R = \{10, 30, 60\} \text{ m}$
resulting BS density	$\rho \approx \{10^{-2}, 10^{-3}, 3 \cdot 10^{-4}\} \text{ m}^{-2}$
# of BSs (for regular)	25 BSs $\Rightarrow$ 2 rings
spatial realizations	$10^5$

Several conclusions can be drawn from these results. Firstly, while  $p_c$  in Eq. (5.40) still depends on  $\rho$ , this dependency vanishes for  $w = 1$  and  $\alpha = 4$  (cf. [12]) and thus, the values are constant for varying densities. The coverage probability improves however for larger wall attenuation values. The improvement is larger for smaller values of  $\rho$ , since the attenuation is (exponentially) distance dependent and thus by moving the interferers further away, blockages provide a better protection.

Regarding the comparison of analytical results from evaluating Eq. (5.40) and simulations assuming a continuous wall distribution, we find an almost perfect agreement. Small deviations are visible for larger values of  $\rho$  - these are mostly due to the lack of further interferers when simulating a finite ROI.

Finally, comparing an association to  $b_0^{(c)}$  and continuous wall attenuation values with association to  $b_0^{(s)}$  and discrete wall realizations, I find that the first setup is only strictly worse for the scenario without blockages (the different here only stems from the small scale fading). For  $w > 0$ , this is only true for small values of  $\delta$ . For larger SIR thresholds, this is no longer the case. Assuming a continuous function for the wall attenuation, parameterized by the link-length, leads to a guaranteed attenuation of the interference, while in case of random and discrete walls a dominant interferer can result from a very low number of walls (even as small as for the associated BS) for an unfavorable wall realization.

### Area spectral efficiency

In Fig. 5.16, ASE-results for the same acquisition of performance values as in the previous subsection are presented, namely analytical evaluation of Eq. (5.44) (represented by circular markers), simulation results with association to  $b_0^{(c)}$  and continuous wall attenuation (represented by solid lines) and simulation results with association to  $b_0^{(s)}$  and discrete wall realizations (represented by dashed lines).

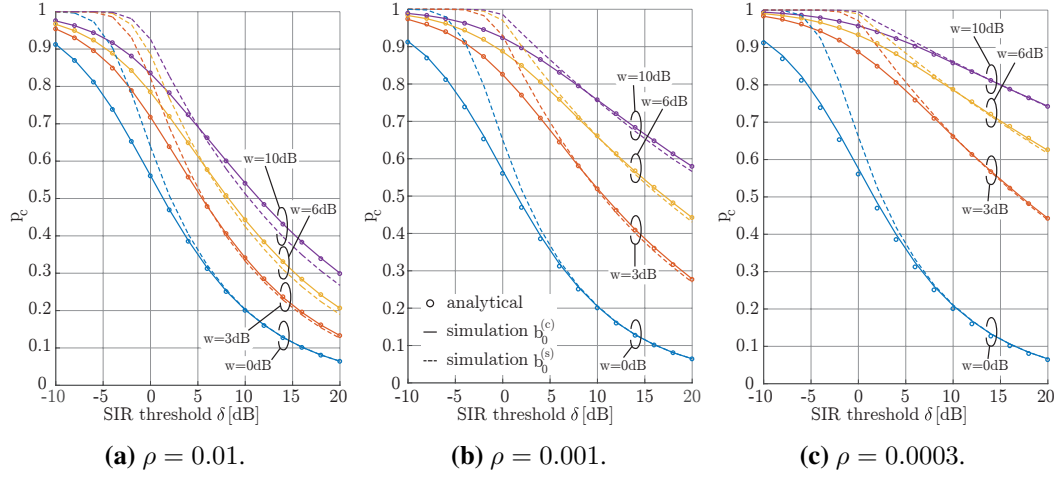


**Figure 5.15.:** Coverage probability  $p_c$  for various BS densities - association to  $b_0^{(c)}$ : solid lines represent simulation results, circular markers result from evaluating Eq. (5.40); association to  $b_0^{(s)}$  represented by dashed lines (simulation results only). ©2018 IEEE, [68].

Once again the analytical results and the corresponding results from simulations coincide almost perfectly with a small gap due to the finite simulation area. The simulation results for association to  $b_0^{(s)}$  are also almost identical, which fits to the similar behavior of the coverage probability results.

For the comparison of regular and random BS placement, I show simulation results in Fig. 5.17. Only three penetration loss values are considered, in order to keep the figure readable. Per penetration loss value, results for four configurations are displayed, namely the combinations of random and regular BS placement with association to  $b_0^{(c)}$  with continuous wall distribution and association to  $b_0^{(s)}$  with discrete wall distribution.

As the results show, the regular BS placement yields a strictly better ASE performance than the random BS placement for all values of  $w$ . The slope also remains the same, only a shift is introduced by the regular BS placement.

#### 5.3.4. Discussion of Results

Regarding the presented results, there are some interesting conclusions to draw. The influence of the wall parameters ( $w$ ,  $\lambda$  and  $\mathbb{E}[L]$ ) is given by their combination  $w^{2/\pi\lambda\mathbb{E}[L]} = w^\beta$ . As long as this combined factor is not changed, the analytical results stay the same<sup>8</sup>. For all considered scenarios, the addition of walls improves the coverage probability as well as the ASE. This improvement is better for larger sector sizes, since the added attenuation grows faster for the interferers at a larger

<sup>8</sup>This is only true in a range of wall lengths, where the correlation among blockage of links is negligible.



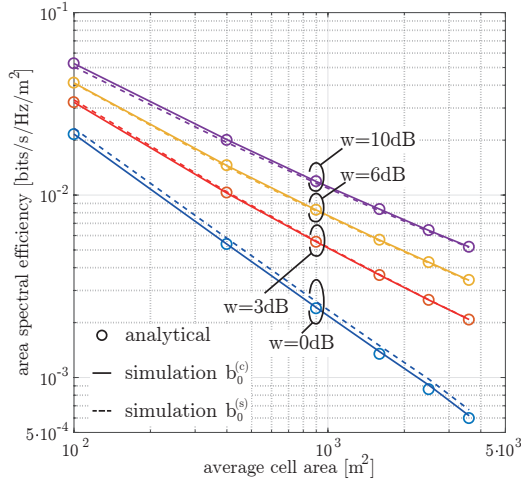


**Figure 5.16.:** ASE for different wall attenuations - association to  $b_0^{(c)}$ : solid lines represent simulation results, circular markers result from evaluating Eq. (5.44); association to  $b_0^{(s)}$  represented by dashed lines. ©2018 IEEE, [68].

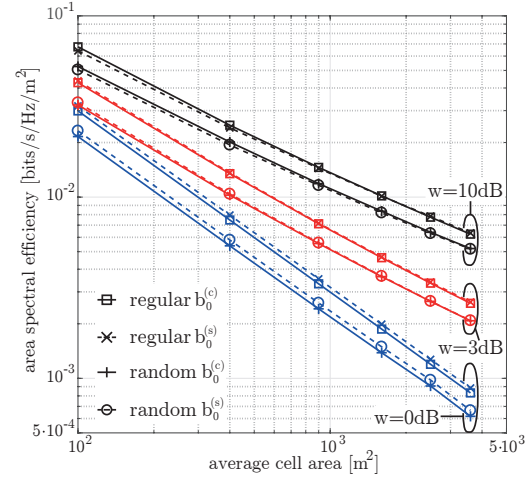


**Figure 5.17.:** Comparison of ASE for regular and random BS placement and for different wall attenuations - association to  $b_0^{(c)}$  represented by solid lines, to  $b_0^{(s)}$  by dashed lines. ©2018 IEEE, [68].

distance. As it was already shown in [12] for the wall-less scenario, a regular BS placement yields better performance results as a random placement. This remains true for a scenario with walls. Even though I made the simplifying assumption for the analytical derivation to connect to the closest BS and a continuous wall distribution, the averaged performance results in terms of ASE show almost no difference when compared to simulation results where an association to  $b_0^{(s)}$  and discrete wall realizations is considered.

## 5.4. Summary

In this chapter, I investigate the performance of indoor cellular networks where I assume a system with indoor transmitters. The effects of the signal blockage of indoor walls is included in the system model by applying tools from stochastic geometry and random shape theory, which allow a mathematical description of the wall attenuation in the system model.

In Section 5.2, I define various mathematically tractable wall generation methods with perpendicular wall orientation. It is made sure that all such created scenarios remain comparable by setting the parameters of each method to yield the same average wall volume over spatial realizations. This also leads to the same average accumulated wall attenuation on a link of a given length for all methods. Due to the perpendicular wall orientations, the distribution of walls blocking a link is found to be angular dependent. The network performance is investigated for a regular transmitter placement and

user positions at the cell edge. To obtain analytical SIR expressions, suitable approximations are derived. It turns out that the SIR results are different for all investigated wall generation methods, even though the distance dependent average wall attenuation is the same. Due to the angular dependency of the wall attenuation, also the transmitter arrangement (for similar inter-transmitter distances) has an impact on the SIR. Generally it can be said, that a more random wall placement, i.e., 2D placement according to a PPP with random and relatively short wall length, yields the worst performance results, while scenarios with a completely regular wall placement exhibit the best performance. This is mostly due to the added correlation among blockages for desired and interfering link, which adds some *guaranteed* attenuation of interference. Results obtained for scenarios produced with a generic floor plan generator lie between these worst and best case results.

Consecutively, in Section 5.3, in addition to the SIR, also the ASE is investigated as an indicator for the network capacity. In contrast to the previous considerations, a uniform, continuous wall orientation distribution is assumed, to reduce the complexity of the analytical expressions. Additionally, results are averaged over the complete sector area and no longer limited to the sector boundary. Analytical results are obtained for a random transmitter placement. It turns out that the coverage probability (and thus the average SIR) as well as the ASE is improved for increasing wall penetration loss values (within realistic values for the considered carrier frequency). Considering the average sector size, which is the inverse of the BS density, it results that larger sector sizes lead to a better coverage probability, due to larger attenuation of interferers at larger distances. Conversely, the ASE improves with smaller sector size, since more BSs are placed per area. When comparing association to the closest BS and association to the strongest BS, the performance difference almost vanishes for the global network average. Also when including walls in the system model, random BS placement can be identified as worst case and regular BS placement as best case for network performance.

When judged critically, some aspects of the system model are debatable. The major weakness is the omission of reflections, that are at best only implicitly represented through the path loss exponent and channel model. The wall volume in scenarios produced by the floor plan generator is not connected to the wall volume of other wall generation methods. This aspect still needs to be included. The analytical investigation focuses on average performance values, based on the average accumulated wall attenuation, which neglects the meta distribution of, e.g., the SIR. This could be incorporated in future work by a similar approach as described in [44].

Considering the propagation modeling, the realism of the system model could be improved by more sophisticated models for the accumulated wall penetration. Further planned extensions of the investigations include the consideration of impenetrable walls. This is more realistic for upcoming mmWave networks and emphasizes the necessity of LOS for the desired link [76]. Also the combination of Section 5.2 and Section 5.3 might lead to further insights (i.e., perpendicular walls and variable BS placement). Up to now only quasi static users were considered. For varying load requirements, variable configurations of transmitters into one or several sectors allows the adjustment of sector

size and interference. The investigation of this aspect would yield interesting results for practical deployments.



## Chapter 6.

### Conclusions

Cellular networks have come a long way from first deployments to today's sophisticated networks with vast available data rates. This ongoing trend in increased capacity is not only happening alongside applications and services with growing demands, but also expectations of users are increasing constantly. Additionally, due to the ongoing trend of urbanization, the majority of users in future networks are expected to be mostly highly mobile (in cars or trains) or in indoor environments. To quench the need for high data rates in these environments, traditional outdoor base stations (BSs) are not sufficient and specifically designed solutions have to be found for this task.

Following this reasoning, I focus in my thesis on aspects of exactly these particular use-cases of cellular networks. The main contribution of my work lies in defining analytical models for performance evaluation in high speed train (HST) and indoor scenarios. Instead of only providing results for single links or single realizations of a particular network setting, my models allow to gain insights in *trends of average network efficiency*. These models are always cross-checked with simulations, that contain more details than can be included in the mathematical model. Thus, their accuracy is verified or correction terms can be introduced to improve upon necessary abstractions.

#### 6.1. Summary of Contributions

In Chapter 4, I discuss cellular networks in HST scenarios. In the first part, I introduce important concepts and discuss advantages and drawbacks of different technical solutions. Especially the comparison of direct passenger-BS communication and relay aided communication is discussed thoroughly. In summary, the relay approach grants the benefit of avoiding the penetration loss of the carriage, but faces the problem of two way propagation<sup>1</sup> (once directly from the BS and once from the relay), if the penetration loss is not high enough. Additionally, relays mean increased investment and maintenance cost as well as potential legal issues. Therefore, direct communication yields the

---

<sup>1</sup>This is true, when simple amplify and forward is assumed.

simpler solution, but needs to deal with the penetration loss. This can potentially be overcome with special types of windows or electromagnetic apertures in the chassis.

In the next part, I provide a comparison between link level (LL) and system level (SL) simulations, utilizing channel measurement results as input. This serves as justification why a SL approach is viable in such scenarios, even though it introduces substantial abstractions on the actual transmission. It turns out that when parameterized correctly, average throughput results are in good accordance (only around 5% discrepancy) and performance trends are preserved (i.e., decreasing throughput with increasing distance). Furthermore, SL simulations allow to easily tune transmission parameters. Thus, I could observe the severe impact of feedback delay, which stems from the quickly changing small-scale fading and results in failed transmissions and increased jitter.

For my investigations on remote unit collaboration schemes, I assume a generic placement of remote radio units (RRUs) along the tracks. Based on an analytical model as well as SL simulations, I obtain results in terms of signal to interference ratio (SIR) and throughput/capacity. Coordinating the closest RRUs to not interfere with each other already improves the performance, while assuming cooperation by combining the RRUs in the same sector yields the best results. Differences among the analytical model and simulations result from assuming maximum ratio transmission (MRT) in the model and codebook based precoding (CBP) in simulations. This difference however is a constant offset, and adjusting for it shifts the results in the same range of values.

Indoor scenarios are discussed in Chapter 5. The focus is on the influence of wall blockages and how they alter the system performance. In the first part of this chapter I introduce three mathematically tractable wall generation methods, all of which only allow perpendicular walls (i.e., either  $0^\circ$  or  $90^\circ$  orientation). This leads to an angular dependent average wall attenuation and makes the performance also dependent on the orientation of the transmitter grid. In order to obtain comparable wall realizations, generation parameters are chosen such that the average wall volume in a given area is constant among all three methods. It turns out that for the derived expression for the average walls blocking a link with given length, the values are exactly the same when initialized accordingly. The fourth wall generation method is based on a generic algorithm to fill a given area with non-overlapping squares without gaps. This yields more realistic wall constellations, but is no longer mathematically tractable. To be comparable to the other methods, the algorithm parameters are tuned to result in the same average wall values. For the first three wall generation methods, also expressions for the SIR performance are derived. In order to simplify the analysis, only the *average* accumulated wall attenuation is used in the SIR expression and not the *instantaneous* one. This leads to deviations between results from the analytical model and from simulations. Therefore, this has to be mitigated by appropriate additions in the SIR calculation of the individual models. Consequently, for 2D wall center placements, I introduce the concept of *effective wall attenuation* to account for the random distribution of walls (that was eliminated by only considering the average). For wall placements according to a Manhattan line process, I utilize the correlation of blockages for different links.

From the results it can be observed that the analytically calculated average wall attenuation fits perfectly to simulation results for all wall generation methods and is identical among all methods. The resulting SIR performance however is not identical, which is due to the difference in correlation of blockages among links. From these results, the most regular wall placement method can be identified as best case and the most random one as worst case scenario in terms of SIR performance. Results for the more realistic floor plan generator lie within the results of these two methods.

The second part of the chapter then discusses the difference between random and regular BS placement in indoor environments. Utilizing the coverage probability and the area spectral efficiency (ASE) as performance metric, I investigate the influence of scenario parameters such as individual wall attenuation value and BS density. In the derived mathematical expressions, the same approximation of only using the average number of walls in the SIR terms is used again. It turns out however that differences between analytical results and simulation results for both metrics are not significant. Simulations come with the advantage however, that also association to the strongest BS is possible, while the analytical framework always assumes association to the closest BS. The results show that for the given range of attenuation values, increasing the wall attenuation also increases coverage probability as well as ASE. This means that the interference is attenuated more than the desired signal. Regarding the BS density, it turns out that a decreasing density leads to interferers at larger distances and thus increased coverage probability, while the ASE results exhibit the exact opposite trend, since a larger BS density means more sum capacity that is available in the network.

## 6.2. Open Issues for Future Research

Although the introduced models for the investigation of cellular networks in HST and indoor scenarios already allow for a profound understanding of performance trends, there are still aspects that were not covered in my thesis. I give a short overview on facets that may serve as incipience for future work.

In the context of HST scenarios, when comparing LL and SL simulation results, only utilizing the actually measured channels as direct input into simulations gave comprehensive results. Ideally, channel traces can be generated based on the power delay profile (PDP) (which is available from the measurement results). To do so however, a line of sight (LOS) component has to be included in the channel generation, in order to mimic the conditions in the measurement environment, which is currently not available.

The penetration loss of windows in train carriages is angular dependent. When assuming direct communication without relay, finding the optimal position of the BS then requires the knowledge of the actual relation between incidence angle and penetration loss. This could be an interesting addition to the scenario in order to make it more realistic.

Following the 'U'-shaped throughput results curve, going from one RRU to the next, the available capacity first decreases and then increases again. In combination with traffic models, a traffic aware scheduler, similar to the one discussed in [67], could be employed to adapt the resource distribution in an appropriate way, according to delay-sensitivity of the underlying application. Thus, users with, e.g., voice calls would be served with a constant rate, while best effort users would mostly be scheduled when close to a RRU. Using such a scheduler in the given environment has not been done and could prove to yield interesting results.

Being at the verge of the 5th generation of mobile networks (5G), parts of my presented models will have to be reconsidered. Especially the transmission in the mmWave range makes it necessary to consider different propagation models. The capabilities of massive multiple-input multiple-output (MIMO) may prove useful in HST scenarios, as it was already discussed in [93].

Also in the context of indoor scenarios would it be insightful to consider mmWave transmissions. This has a large influence on the penetration loss values and will lead to a larger isolation among transmitters. Therefore, systems will more likely be noise limited.

The concept of meta-distributions, as introduced in [44], could prove useful in order to avoid the introduced approximations for the calculation of the SIR. In a similar direction goes the idea of not only focusing on average performance values, but also to investigate "disruptive events". A solution to this could be provided by approaches related to large deviations theory [58].

So far only indoor transmitters and users have been considered, completely isolated from the outdoor environment. The influence of macro BSs on indoor users, as well as of indoor transmitters on outdoor users, be it in terms of interference or actually of increased coverage, would give a more complete picture of future cellular networks.

To increase the realism of wall generation methods, the usage of further floor plan generating algorithms, also from the field of architecture, would be beneficial. Such algorithms could help to automatically generate a multitude of spatial realizations, that can be parameterized by, e.g., average room size or average number of rooms per flat and also include hallways and walls with different materials, without falling back to only investigating one particular building.



# Appendix A.

## List of Abbreviations

<b>1G</b>	first generation
<b>2G</b>	second generation
<b>3G</b>	third generation
<b>4G</b>	fourth generation
<b>3GPP</b>	Third Generation Partnership Project
<b>5G</b>	5th generation of mobile networks
<b>ASE</b>	area spectral efficiency
<b>BS</b>	base station
<b>CAPEX</b>	capital expenditure
<b>CBP</b>	codebook based precoding
<b>cdf</b>	cumulative distribution function
<b>CF</b>	characteristic function
<b>CoMP</b>	coordinated multi-point
<b>CQI</b>	channel quality indicator
<b>DAS</b>	distributed antenna system
<b>dTx</b>	desired transmitter
<b>ecdf</b>	empirical cumulative distribution function
<b>EIRP</b>	equivalent isotropically radiated power
<b>FFT</b>	fast Fourier transform
<b>GIG</b>	generalized integer gamma
<b>GSM</b>	Global System for Mobile Communications
<b>GSM-R</b>	GSM - Rail(way)
<b>GTEC</b>	Department of Computer Engineering at the University of A Coruña
<b>HetNet</b>	heterogeneous network
<b>HST</b>	high speed train
<b>ICI</b>	inter carier interference
<b>i.i.d.</b>	independent and identically distributed
<b>ISM</b>	Industrial, Scientific and Medical

<b>iTx</b>	interfering transmitter
<b>KP</b>	kilometric point
<b>LL</b>	link level
<b>LOS</b>	line of sight
<b>LT</b>	Laplace transform
<b>LTE</b>	Long Term Evolution
<b>LTE-A</b>	LTE advanced
<b>LTE-R</b>	LTE for Railway
<b>MCS</b>	modulation and coding scheme
<b>MGF</b>	moment generating function
<b>MIMO</b>	multiple-input multiple-output
<b>MRT</b>	maximum ratio transmission
<b>NLOS</b>	non line of sight
<b>OFDM</b>	orthogonal frequency division multiplexing
<b>OPEX</b>	operational expenditure
<b>pdf</b>	probability density function
<b>PDP</b>	power delay profile
<b>PGFL</b>	probability generating functional
<b>pmf</b>	probability mass function
<b>PP</b>	point process
<b>PPP</b>	Poisson point process
<b>RB</b>	resource block
<b>RoF</b>	radio over fiber
<b>ROP</b>	random object process
<b>RRU</b>	remote radio unit
<b>RV</b>	random variable
<b>Rx</b>	receiver
<b>SINR</b>	signal to interference and noise ratio
<b>SIR</b>	signal to interference ratio
<b>SISO</b>	single-input single-output
<b>SL</b>	system level
<b>SLS</b>	System Level Simulator
<b>SNR</b>	signal to noise ratio
<b>Tx</b>	transmitter

# Bibliography

- [1] 3rd Generation Partnership Project (3GPP), “Technical Specification Group Radio Access Networks; Deployment aspects (Release 8)”, 3GPP, TR 25.943, Dec. 2008.
- [2] —, “Evolved Universal Terrestrial Radio Access (E-UTRA); Further advancements for E-UTRA physical layer aspects”, 3rd Generation Partnership Project (3GPP), TR 36.814, Mar. 2010.
- [3] —, “Evolved Universal Terrestrial Radio Access (E-UTRA); mobility enhancements in heterogeneous networks”, 3GPP, TR 36.839, Jan. 2013.
- [4] —, “Evolved universal terrestrial radio access (E-UTRA); radio frequency (RF) system scenarios”, 3GPP, TR 36.942, Oct. 2014.
- [5] —, “Evolved Universal Terrestrial Radio Access (E-UTRA) physical channels and modulation”, 3GPP, TS 36.211, Jan. 2015.
- [6] —, “Study on 3D channel model for LTE”, 3GPP, TR 36.873, Jun. 2015.
- [7] F. Ademaj, M. K. Mueller, S. Schwarz, and M. Rupp, “Modeling of spatially correlated geometry-based stochastic channels”, in *2017 IEEE 86th Vehicular Technology Conference (VTC-Fall)*, Sep. 2017, pp. 1–6.
- [8] B. Ai, X. Cheng, T. Kurner, Z.-D. Zhong, K. Guan, R.-S. He, L. Xiong, D. Matolak, D. Michelson, and C. Briso-Rodriguez, “Challenges Toward Wireless Communications for High-Speed Railway”, *IEEE Transactions on Intelligent Transportation Systems*, vol. 15, no. 5, pp. 2143–2158, Oct. 2014.
- [9] M. Aljuaid and H. Yanikomeroglu, “Investigating the Gaussian convergence of the distribution of the aggregate interference power in large wireless networks”, *IEEE Trans. Veh. Technol.*, vol. 59, no. 9, pp. 4418–4424, Aug. 2010.
- [10] J. Andersen, T. Rappaport, and S. Yoshida, “Propagation measurements and models for wireless communications channels”, *IEEE Commun. Mag.*, vol. 33, no. 1, pp. 42–49, Jan. 1995.
- [11] J. Andrews, “Seven ways that HetNets are a cellular paradigm shift”, *IEEE Commun. Mag.*, vol. 51, no. 3, pp. 136–144, Mar. 2013.
- [12] J. Andrews, F. Baccelli, and R. Ganti, “A tractable approach to coverage and rate in cellular networks”, *IEEE Trans. Commun.*, vol. 59, no. 11, pp. 3122–3134, Nov. 2011.

- [13] J. Andrews, H. Claussen, M. Dohler, S. Rangan, and M. Reed, “Femtocells: Past, present, and future”, *IEEE J. Sel. Areas Commun.*, vol. 30, no. 3, pp. 497–508, Apr. 2012.
- [14] F. Baccelli, M. Klein, M. Lebourges, and S. Zuyev, “Stochastic geometry and architecture of communication networks”, *Telecommun. Syst.*, vol. 7, pp. 209–227, Jun. 1997.
- [15] F. Baccelli and S. Zuyev, “Stochastic geometry models of mobile communication networks”, in *Frontiers in queueing: models and applications in science and engineering*, CRC Press, Inc., Boca Raton, FL, USA, 1996, pp. 227–243.
- [16] F. Baccelli and B. Blaszczyzyn, *Stochastic Geometry and Wireless Networks: Volume I Theory*, ser. Foundation and Trends in Networking. Now Publishers, Mar. 2009, pp. 249–449.
- [17] F. Baccelli and X. Zhang, “A correlated shadowing model for urban wireless networks”, in *IEEE Conf. Computer Commun. (INFOCOM)*, IEEE, 2015, pp. 801–809.
- [18] T. Bai, R. Vaze, and R. W. Heath, “Analysis of blockage effects on urban cellular networks”, *IEEE Trans. Wireless Commun.*, vol. 13, no. 9, pp. 5070–5083, Sep. 2014.
- [19] T. Berisha, P. Svoboda, S. Ojak, and C. F. Mecklenbräuker, “Cellular network quality improvements for high speed train passengers by on-board amplify-and-forward relays”, in *2016 International Symposium on Wireless Communication Systems (ISWCS)*, Sep. 2016, pp. 325–329.
- [20] M. Bruls, K. Huizing, and J. J. van Wijk, “Squarified treemaps”, in *Data Visualization 2000: Proceedings of the Joint EUROGRAPHICS and IEEE TCVG Symposium on Visualization in Amsterdam, The Netherlands, May 29–30, 2000*, W. C. de Leeuw and R. van Liere, Eds. Vienna: Springer Vienna, 2000, pp. 33–42.
- [21] N. Campbell, “The study of discontinuous phenomena”, *Proc. Cambridge Philosoph. Soc., Math. and Physical Sci.*, vol. 15, pp. 117–136, 1909.
- [22] S. N. Chiu, D. Stoyan, W. S. Kendall, and J. Mecke, *Stochastic Geometry and Its Applications, 3rd Edition*. John Wiley and Sons, Sep. 2013.
- [23] Cisco, *Cisco visual networking index: Global mobile data traffic forecast update, 2015 - 2020 white paper*, Sep. 2016.
- [24] C. A. Coelho, “The Generalized Integer Gamma Distribution - A Basis for Distributions in Multivariate Statistics”, *Journal of Multivariate Analysis*, vol. 64, no. 1, pp. 86–102, 1998.
- [25] *Council Directive 96/48/EC of 23 July 1996 on the interoperability of the trans-European high-speed rail system*, Council of the European Union, Sep. 1996.
- [26] A. Damnjanovic, J. Montojo, Y. Wei, T. Ji, T. Luo, M. Vajapeyam, T. Yoo, O. Song, and D. Malladi, “A survey on 3gpp heterogeneous networks”, *IEEE Wireless Communications*, vol. 18, no. 3, pp. 10–21, Jun. 2011.

- 
- [27] A. Davidson and C. Hill, "Measurement of building penetration into medium buildings at 900 and 1500 mhz", *IEEE Transactions on Vehicular Technology*, vol. 46, no. 1, pp. 161–168, Feb. 1997.
  - [28] M. Derakhshani and T. Le-Ngoc, "Aggregate interference and capacity-outage analysis in a cognitive radio network", *IEEE Trans. Veh. Technol.*, vol. 61, no. 1, pp. 196–207, Nov. 2012.
  - [29] U. Dersch and E. Zollinger, "Propagation mechanisms in microcell and indoor environments", *IEEE Transactions on Vehicular Technology*, vol. 43, no. 4, pp. 1058–1066, Nov. 1994.
  - [30] H. Dhillon, R. Ganti, F. Baccelli, and J. Andrews, "Coverage and ergodic rate in K-tier downlink heterogeneous cellular networks", in *Allerton Conf. Commun., Control, and Computing 2011 (Allerton)*, Monticello, IL, USA, Sep. 2011, pp. 1627–1632.
  - [31] —, "Modeling and analysis of K-tier downlink heterogeneous cellular networks", *IEEE J. Sel. Areas Commun.*, vol. 30, no. 3, pp. 550–560, Apr. 2012.
  - [32] T. Domínguez-Bolaño, J. Rodríguez-Piñeiro, J. A. García-Naya, and L. Castedo, "The GTEC 5G link-level simulator", in *2016 1st International Workshop on Link- and System Level Simulations (IWSLS)*, Jul. 2016, pp. 1–6.
  - [33] —, "Experimental Characterization of LTE Wireless Links in High-Speed Trains", *Wireless Communications and Mobile Computing*, vol. vol. 2017, 2017.
  - [34] H. ElSawy and E. Hossain, "Two-tier HetNets with cognitive femtocells: Downlink performance modeling and analysis in a multichannel environment", *IEEE Trans. Mobile Comput.*, vol. 13, no. 3, pp. 649–663, Mar. 2014.
  - [35] H. ElSawy, E. Hossain, and M. Haenggi, "Stochastic geometry for modeling, analysis, and design of multi-tier and cognitive cellular wireless networks: A survey", *IEEE Commun. Surveys & Tutorials*, vol. 15, no. 3, pp. 996–1019, Jun. 2013.
  - [36] C. Galiotto, N. K. Pratas, N. Marchetti, and L. Doyle, "A stochastic geometry framework for los/nlos propagation in dense small cell networks", in *IEEE Int. Conf. Commun (ICC'15)*, Jun. 2015, pp. 2851–2856.
  - [37] L. Gao, Z. Zhong, B. Ai, and L. Xiong, "Estimation of the Ricean factor in K the high speed railway scenarios", in *5th International ICST Conference on Communications and Networking in China (CHINACOM)*, 2010.
  - [38] J. Gavrilovich C.D., "Broadband communication on the highways of tomorrow", *IEEE Communications Magazine*, vol. 39, no. 4, pp. 146–154, Apr. 2001.
  - [39] J. Gertner, *The Idea Factory: Bell Labs and the Great Age of American Innovation*. Penguin Publishing Group, New York, 2012.
  - [40] M. Gholizadeh, H. Amindavar, and J. Ritcey, "On the capacity of MIMO correlated Nakagami-m fading channels using copula", *EURASIP J. Wireless Commun. and Networking*, vol. 2015, no. 1, p. 138, 2015.

- [41] A. Ghosh, N. Mangalvedhe, R. Ratasuk, B. Mondal, M. Cudak, E. Visotsky, T. A. Thomas, J. G. Andrews, P. Xia, H. S. Jo, H. S. Dhillon, and T. D. Novlan, “Heterogeneous cellular networks: From theory to practice”, *IEEE Communications Magazine*, vol. 50, no. 6, pp. 54–64, Jun. 2012.
- [42] A. Goldsmith, *Wireless Communications*. Cambridge University Press, 2005.
- [43] K. Guan, Z. Zhong, J. I. Alonso, and C. Briso-Rodriguez, “Measurement of distributed antenna systems at 2.4 ghz in a realistic subway tunnel environment”, *IEEE Transactions on Vehicular Technology*, vol. 61, no. 2, pp. 834–837, Feb. 2012.
- [44] M. Haenggi, “The Meta Distribution of the SIR in Poisson Bipolar and Cellular Networks”, *IEEE Transactions on Wireless Communications*, vol. 15, no. 4, pp. 2577–2589, Apr. 2016.
- [45] M. Haenggi, J. Andrews, F. Baccelli, O. Dousse, and M. Franceschetti, “Stochastic geometry and random graphs for the analysis and design of wireless networks”, *IEEE J. Sel. Areas Commun.*, vol. 27, no. 7, pp. 1029–1046, Jul. 2009.
- [46] M. Haenggi and R. K. Ganti, *Interference in Large Wireless Networks*, ser. Foundations and Trends in Networking. NoW Publishers, Hanover, MA, USA, Feb. 2009, vol. 3.
- [47] K. Haneda, J. Jarvelainen, A. Khatun, and K. i. Takizawa, “Spatial coexistence of millimeter-wave distributed indoor channels”, in *2015 IEEE 81st Vehicular Technology Conference (VTC Spring)*, May 2015, pp. 1–5.
- [48] T. Hashimoto, Y. Nishioka, Y. Inasawa, and H. Miyashita, “Indoor propagation estimation combining statistical models with ray-tracing”, in *2015 International Symposium on Antennas and Propagation (ISAP)*, Sep. 2015, pp. 1–3.
- [49] R. He, B. Ai, G. Wang, K. Guan, Z. Zhong, A. F. Molisch, C. Briso-Rodriguez, and C. P. Oestges, “High-Speed Railway Communications: From GSM-R to LTE-R”, *IEEE Vehicular Technology Magazine*, vol. 11, no. 3, pp. 49–58, Sep. 2016.
- [50] R. He, Z. Zhong, B. Ai, and J. Ding, “Measurements and analysis of short-term fading behavior for high-speed rail viaduct scenario”, in *2012 IEEE International Conference on Communications (ICC)*, Jun. 2012, pp. 4563–4567.
- [51] R. He, Z. Zhong, B. Ai, G. Wang, J. Ding, and A. F. Molisch, “Measurements and analysis of propagation channels in high-speed railway viaducts”, *IEEE Transactions on Wireless Communications*, vol. 12, no. 2, pp. 794–805, 2013.
- [52] R. W. Heath, M. Kountouris, and T. Bai, “Modeling heterogeneous network interference using Poisson point processes”, *IEEE Transactions on Signal Processing*, vol. 61, no. 16, pp. 4114–4126, 2013.
- [53] L. Hentilä, P. Kyösti, M. Käske, M. Narandzic, and M. Alatossava, *MATLAB implementation of the WINNER Phase II Channel Model ver1.1*, [https://www.ist-winner.org/phase\\_2\\_model.html](https://www.ist-winner.org/phase_2_model.html), Dec. 2007.

- 
- [54] J. Hu and N. C. Beaulieu, "Accurate simple closed-form approximations to Rayleigh sum distributions and densities", *IEEE Commun. Lett.*, vol. 9, no. 2, pp. 109–111, Feb. 2005.
- [55] Huawei, *Five Trends to Small Cell 2020*, Feb. 2016.
- [56] ITU, "Recommendation ITU-R M.1225: Guidelines for Evaluation of Radio Transmission Technologies for IMT-2000", ITU, Tech. Rep., 1997.
- [57] *K-Bow - Micro C-RAN Capacity Solution*, Kathrein AG, 2015.
- [58] H. P. Keeler, B. Jahnel, O. Maye, D. Aschenbach, and M. Brzozowski, "Disruptive events in high-density cellular networks", in *2018 16th International Symposium on Modeling and Optimization in Mobile, Ad Hoc, and Wireless Networks (WiOpt)*, May 2018, pp. 1–8.
- [59] K. J. Kerpez, "A radio access system with distributed antennas", *IEEE Transactions on Vehicular Technology*, vol. 45, no. 2, pp. 265–275, May 1996.
- [60] S. R. Lamas, D. G. G. and J. Hamalainen, "Indoor planning optimization of ultra-dense cellular networks at high carrier frequencies", in *2015 IEEE Wireless Communications and Networking Conference Workshops (WCNCW)*, Mar. 2015, pp. 23–28.
- [61] J. Lee, X. Zhang, and F. Baccelli, "A 3-D spatial model for in-building wireless networks with correlated shadowing", *IEEE Transactions on Wireless Communications*, vol. 15, no. 11, pp. 7778–7793, Nov. 2016.
- [62] C. Li and B. Li, "An analysis on high speed train coverage solutions", *Communication World*, vol. 33, 2008.
- [63] D. Li, J. Wang, M. Chen, Z. Zhang, and Z. Li, "Base-band involved integrative modeling for studying the transmission characteristics of wireless link in railway environment", *EURASIP J. Wireless Commun. and Networking*, vol. 2015, no. 1, p. 81, 2015.
- [64] S.-H. Liao, C.-H. Chen, C.-C. Chiu, M.-H. Ho, T. Wysocki, and B. Wysocki, "Optimal receiver antenna location in indoor environment using dynamic differential evolution and genetic algorithm", *EURASIP J. Wireless Commun. and Networking*, vol. 2013, no. 1, p. 235, 2013.
- [65] Z. Liu and P. Fan, "An effective handover scheme based on antenna selection in ground-train distributed antenna systems", *IEEE Transactions on Vehicular Technology*, vol. 63, no. 7, pp. 3342–3350, Sep. 2014.
- [66] A. Mesodiakaki, F. Adelantado, L. Alonso, and C. Verikoukis, "Energy-efficient context-aware user association for outdoor small cell heterogeneous networks", in *2014 IEEE International Conference on Communications (ICC)*, Jun. 2014, pp. 1614–1619.
- [67] M. K. Müller, S. Schwarz, and M. Rupp, "QoS investigation of proportional fair scheduling in LTE networks", in *Proc. of the Wireless Days Conference*, Valencia, Spain, Nov. 2013.

- [68] —, “Investigation of area spectral efficiency in indoor wireless communications by blockage models”, in *Workshop on Spatial Stochastic Models for Wireless Networks (SpaWiN)*, May 2018, pp. 1–6.
- [69] M. K. Müller, M. Taranetz, and M. Rupp, “Performance of remote unit collaboration schemes in high speed train scenarios”, in *Proc. of the 82nd Vehicular Technology Conference (VTC2015-Fall)*, Boston, US, Sep. 2015.
- [70] —, “Providing current and future cellular services to high speed trains”, *IEEE Communications Magazine*, Oct. 2015.
- [71] —, “Analyzing wireless indoor communications by blockage models”, *IEEE Access*, vol. 5, pp. 2172–2186, Dec. 2016.
- [72] —, “Effects of wall-angle distributions in indoor wireless communications”, in *IEEE 17th International Workshop on Signal Processing Advances in Wireless Communications (SPAWC 2016)*, Jul. 2016, pp. 1–5.
- [73] M. K. Müller, M. Taranetz, V. Stojnov, and M. Rupp, “Abstracting indoor signal propagations: Stochastic vs. regular”, in *International Symposium ELMAR 2016*, Sep. 2016, pp. 249–252.
- [74] Y. Qiu, H. Liu, and P. Fan, “Capacity enhancement using cooperative distributed antenna system under LOS MIMO channels in high speed train scenario”, in *International Workshop on Signal Design and Its Applications in Communications*, IEEE, 2013, pp. 103–106.
- [75] T. Rappaport, *Wireless Communications: Principles and Practice*, 2nd. Upper Saddle River, NJ, USA: Prentice Hall PTR, 2002.
- [76] M. D. Renzo, “Stochastic geometry modeling and analysis of multi-tier millimeter wave cellular networks”, *IEEE Transactions on Wireless Communications*, vol. 14, no. 9, pp. 5038–5057, Sep. 2015.
- [77] M. Rupp, S. Schwarz, and M. Taranetz, *The Vienna LTE-Advanced Simulators: Up and Downlink, Link and System Level Simulation*, 1st ed., ser. Signals and Communication Technology. Springer Singapore, 2016.
- [78] A. A. M. Saleh, A. Rustako, and R. Roman, “Distributed antennas for indoor radio communications”, *IEEE Transactions on Communications*, vol. 35, no. 12, pp. 1245–1251, Dec. 1987.
- [79] W. Schottky, “Über spontane Stromschwankungen in verschiedenen Elektrizitätsleitern”, *Annalen der Physik*, vol. 362, no. 23, pp. 541–567, 1918.
- [80] S. Schwarz, M. Simko, and M. Rupp, “On performance bounds for MIMO OFDM based wireless communication systems”, in *2011 IEEE 12th International Workshop on Signal Processing Advances in Wireless Communications (SPAWC)*, Jun. 2011, pp. 311–315.



- 
- [81] S. Schwarz and M. Rupp, "Society in motion: Challenges for LTE and beyond mobile communications", *IEEE Communications Magazine, Feature Topic: LTE Evolution*, vol. 54, no. 5, pp. 76–83, 2016.
  - [82] S. Scott, J. Leinonen, P. Pirinen, J. Vihriala, V. V. Phan, and M. Latva-aho, "A Cooperative Moving Relay Node System Deployment in a High Speed Train", in *IEEE 77th Vehicular Technology Conference (VTC Spring)*, Jun. 2013, pp. 1–5.
  - [83] *Shift2rail: Driving innovation on railways*, European Commission, 2014.
  - [84] D. Skraparlis, V. Sakarellos, A. Panagopoulos, and J. Kanellopoulos, "Outage performance analysis of cooperative diversity with MRC and SC in correlated lognormal channels", *EURASIP J. Wireless Commun. and Networking*, vol. 2009, no. 1, p. 707 839, 2009.
  - [85] Y. Sui, A. Papadogiannis, and T. Svensson, "The potential of moving relays - a performance analysis", in *IEEE 75th Vehicular Technology Conference (VTC Spring)*, 2012.
  - [86] M. Taranetz, T. Bai, R. W. Heath, and M. Rupp, "Analysis of smallcell partitioning in urban two-tier heterogeneous cellular networks", in *Proc. IEEE 12th Int. Symp. Wireless Commun. Syst. (ISWCS'15)*, Barcelona, Spain, Aug. 2014.
  - [87] M. Taranetz and M. K. Müller, "A survey on modeling interference and blockage in urban heterogeneous cellular networks", *EURASIP Journal on Wireless Communications and Networking*, vol. 2016, no. 1, pp. 1–20, Oct. 2016.
  - [88] M. Taranetz and M. Rupp, "A circular interference model for heterogeneous cellular networks", *IEEE Trans. Wireless Commun.*, pp. 1432–1444, 2 Feb. 2015.
  - [89] L. Tian, V. Degli-Esposti, E. M. Vitucci, and X. Yin, "Semi-deterministic radio channel modeling based on graph theory and ray-tracing", *IEEE Transactions on Antennas and Propagation*, vol. 64, no. 6, pp. 2475–2486, Jun. 2016.
  - [90] G. Tingting and S. Bin, "A high-speed railway mobile communication system based on LTE", in *Electronics and Information Engineering (ICEIE), 2010 International Conference On*, vol. 1, Aug. 2010, pp. 414–417.
  - [91] M. Uhlirz, "Adapting GSM for use in high-speed railway networks", PhD thesis, Institut für Nachrichtentechnik und Hochfrequenztechnik, Technische Universität Wien, 1995.
  - [92] UIC GSM-R Functional Group, "GSM-R functional requirement specification (FRS)", UIC, Paris, France, UIC EIRENE Technology Report, UIC Code 950 version 7.3.0, 2012.
  - [93] V. Va, X. Zhang, and R. W. Heath, "Beam switching for millimeter wave communication to support high speed trains", in *2015 IEEE 82nd Vehicular Technology Conference (VTC2015-Fall)*, Sep. 2015, pp. 1–5.
  - [94] J. Wang, H. Zhu, and N. J. Gomes, "Distributed antenna systems for mobile communications in high speed trains", *IEEE Journal on Selected Areas in Communications*, vol. 30, no. 4, pp. 675–683, May 2012.

- [95] WINNER II WP1, “WINNER II channel models”, *IST-4-027756 WINNER II Deliverable D1.1.2*, Sep. 2007.
- [96] A. Wyner, “Shannon-theoretic approach to a Gaussian cellular multiple-access channel”, *IEEE Trans. Inf. Theory*, vol. 40, no. 6, pp. 1713–1727, Nov. 1994.
- [97] E. Yaacoub, “Enhanced connectivity in railroad networks using LTE relays with directive antennas”, in *7th IEEE GCC Conference and Exhibition (GCC)*, Nov. 2013, pp. 84–88.
- [98] J.-Y. Zhang, Z.-H. Tan, Z.-d. Zhong, and Y. Kong, “A multi-mode multi-band and multi-system-based access architecture for high-speed railways”, in *IEEE 72nd Vehicular Technology Conference Fall (VTC 2010-Fall)*, 2010, Sep. 2010, pp. 1–5.
- [99] X. Zhang and J. G. Andrews, “Downlink cellular network analysis with multi-slope path loss models”, *IEEE Transactions on Communications*, vol. 63, no. 5, pp. 1881–1894, May 2015.
- [100] Y. R. Zheng and C. Xiao, “Simulation models with correct statistical properties for rayleigh fading channels”, *IEEE Transactions on Communications*, vol. 51, no. 6, pp. 920–928, Jun. 2003.
- [101] Y. Zhou, Z. Pan, J. Hu, J. Shi, and X. Mo, “Broadband wireless communications on high speed trains”, in *20th Annual Wireless and Optical Communications Conference (WOCC)*, Apr. 2011.